DEXTRAN-BASED HYDROGELS FOR IN-SITU DELIVERY OF GALLIUM-CONTAINING BIOACTIVE GLASSES

BY

TIMOTHY J. KEENAN

A THESIS
SUBMITTED TO THE FACULTY OF

ALFRED UNIVERSITY

IN PARTIAL FULFILLMENT OF THE REQUIREMENTS
FOR THE DEGREE OF

DOCTOR OF PHILOSOPHY

IN

MATERIALS SCIENCE AND ENGINEERING

ALFRED, NEW YORK

FEBRUARY, 2016

DEXTRAN-BASED HYDROGELS FOR IN-SITU DELIVERY OF GALLIUM-CONTAINING BIOACTIVE GLASSES

BY

TIMOTHY J. KEENAN

B.S. ALFRED UNIVERSITY (2010)

M.S. ALFRED UNIVERSITY (2012)

SIGNATURE OF AUTHOR_____

APPROVED BY_____

MATTHEW HALL, ADVISOR

_____

ANTHONY WREN, ADVISOR

_____

NATHAN MELLOTT, ADVISORY COMMITTEE

_____

ALEXIS CLARE, ADVISORY COMMITTEE

_____

YIQUAN WU, CHAIR, ORAL THESIS DEFENSE

ACCEPTED BY_____

DOREEN D. EDWARDS, DEAN
KAZUO INAMORI SCHOOL OF ENGINEERING

ACCEPTED BY_____

NANCY J. EVANGELISTA, ASSOCIATE PROVOST
FOR GRADUATE AND PROFESSIONAL PROGRAMS
ALFRED UNIVERSITY

ACKNOWLEDGEMENTS

Working towards a degree for nearly 6 years is a feat that is not possible without the help and support of many people, so there are several acknowledgments which need to be made. First and foremost, I would like to thank my two co-advisors, Dr. Matthew Hall and Dr. Anthony Wren. Dr. Hall has been my advisor and mentor for nearly a decade, and his expertise and advice have been instrumental in my development as a materials scientist to this point. Dr. Wren and I began working together while he was a post-doc, and as his career progressed, he not only became a well-liked professor, but also my advisor and mentor. He has taught me a wide range of lab skills, and our daily interactions and discussions have been vital in helping me progress to this point. I would also like to thank Dr. Nathan Mellott and Dr. Alix Clare, who have served as the other 2 members of my Ph.D. committee, and have helped with the organization and execution of my thesis. I would also like to thank Katie Decker for everything she has done for me throughout my time at Alfred. She is an absolutely vital component of the Inamori School of Engineering, and without her, there is no way I could have made it through. In addition to the faculty and staff at Alfred University, I would also like to thank several people in my personal life. First, I would like to thank my fellow Ph.D. candidate Lana Placek, who has been a dear friend and a brilliant co-worker through all my years at Alfred, and whose help I would not have succeeded without. I would also like to thank everyone in my family, including my parents, my siblings, my grandparents, my cousins, and my aunts and uncles, who have all been wonderful supporters throughout these many years of school. Additionally, I would like to thank all of my friends from home, especially Brandon Lindsay, for not only being great supporters and for pretending to be interested in my work, but for also being there whenever I needed to let off some steam and enjoy life outside of math and science. And last but not least, I would like to thank Jill Short for coming along when she did, and helping to inspire me to finish my work and begin my life beyond Alfred University. Her love and support were crucial down the home stretch, and for this I am extremely grateful. Thank you to everyone who has helped me get to this point, I couldn’t have done it without you.

TABLE OF CONTENTS

LIST OF TABLES

LIST OF FIGURES

Page

ABSTRACT

Previously, a series of three Ga_2O_3-Na_2O-CaO-ZnO-SiO_2 bioactive glasses was created in which zinc (Zn) was incrementally replaced by gallium (Ga). The structure and solubility of this glass series was then investigated in order to evaluate the ability of Ga-containing glasses to exhibit bioactive properties, and to determine whether these glasses were eligible candidates for biological studies. The results of this prior work suggested that these Ga-containing glasses exhibited potential as bioactive glasses, thus warranting further study. In the current study, the primary objective was not only to evaluate the biocompatibility of these glasses using cell assays, but to also develop a method of delivery for these glasses into a host system by impregnating these glass particles into a polymer hydrogel matrix, which consisted of functionalized forms of the polysaccharides dextran (Dex) and carboxymethyl cellulose (CMC), which were cross-linked by hydrazone bonds. The structure and solubility of the glass-hydrogel composites were then investigated, and *in vitro* studies were carried out to evaluate their cytocompatibility with healthy fibroblast and osteoblast cells, their anti-bacterial and anti-fungal efficacy, and their cytotoxicity towards cancerous osteosarcoma and myeloma cells.

INTRODUCTION

Biomaterials

1. Evolution and Functionality of Biomaterials

Biomaterials can be defined as materials which have been specifically designed to either elicit no response, or to elicit a specific biological activity upon implantation into a host system.[1] Over time, the design objective of biomaterials engineers has shifted as the application requirements of these materials have evolved. Initially, inertness was a desired trait for implant materials, and this philosophy was embraced all the way from ancient Egypt when molds of precious metals were utilized as inert dental implants[2], until the early 1960's when it was discovered by Branemark that physical bonding could be achieved between bone tissue and titanium implants in rabbit models (osseointegration).[3] Near the end of the 1960's, the focus shifted to developing materials which could form chemical bonds between their surfaces and the surrounding host tissues after Hench *et. al.* formulated a glass composition (45S5), which allowed for the formation of a thin apatite layer on the glass-tissue interface, facilitating a strong chemical bond between the two.[4] This philosophy lasted for several years until it was discovered that some materials could be constructed to resorb over time, which lead to an era of developing materials which could serve some sort of initial function, and then gradually dissolve as the host tissue healed. The first materials to be developed with this intended function were resorbable, synthetic suture materials consisting of poly(α-hydroxyacid)s.[5] This discovery lead to the development of many different types of resorbable materials, and ultimately lead to the creation of implantable drug delivery systems. An example of the advancement from inert to resorbing biomaterials can be seen in Figure 1, with the evolution from amalgum to bioactive glass-containing composite dental fillings.

Figure 1. Bioinert amalgam and bioresorbable composite fillings in teeth.[6]

"Controlled drug delivery" (CDD) devices were first developed to operate on the macroscopic scale, releasing drugs at a constant rate into their respective surrounding environments. The first major breakthroughs utilizing this technology were the ophthalmic insert called Ocusert®, and the intrauterine device called Progestesert®.[5] Later on, Folkman and Langer discovered that it was possible, on a macroscopic scale, to deliver a protein in its active form from a hydrophobic, non-degradable polymer matrix.[7] After this discovery, the philosophy of biomaterials engineers shifted yet again, focusing on not only the design of CDD devices on the macroscopic scale, but to improve these materials to allow for sustained release, and to progress from the use of non-degradable materials as the delivery vehicles, to biodegradable materials. The first clinically-approved, injectable, degradable microparticle drug delivery system called Decapeptyl® was then launched in 1986 as a treatment for prostate cancer.[5]

Throughout the rest of the 1980's, the majority of degradable, drug-delivering microparticle systems were formed by two processes, either by solvent evaporation from emulsions, or by phase separation methods. The number of available techniques for the synthesis of drug-loaded, degradable polymers then began to rapidly expand in the late 1980's and early 1990's. Among these techniques was the Prolease® process for fabricating drug-loaded PLGA microparticles using an ultrasonic sprayer and a liquid

nitrogen/frozen ethanol bath to freeze the particles, and remove the solvent.[8] Other degradable drug-delivery systems were later developed by Sung Wan Kim and Youngro Byun, including thermally-responsive, aqueous solutions of di- and tri-block copolymers of PLGA-PEG.[5]

The latest shift in the field of biomaterials engineering has combined several different concepts, bringing thinking down to the nano-scale, and has begun to involve as much biology as materials science, as this new era of development is much more focused on "targeted" or "site-controlled" drug delivery systems. Over the past several decades, three crucial technological advancements have led to this current shift in focus in the field of biomaterials engineering. The first was the development of polyethylene glycol-conjugated drugs/drug carriers, a technique called "PEGylation". Developed by Frank Davis, this process was conceived in order to simultaneously enhance both the circulation time, and the stability of recombinant protein drugs.[9] The effects of this process are illustrated below in Figure 2.

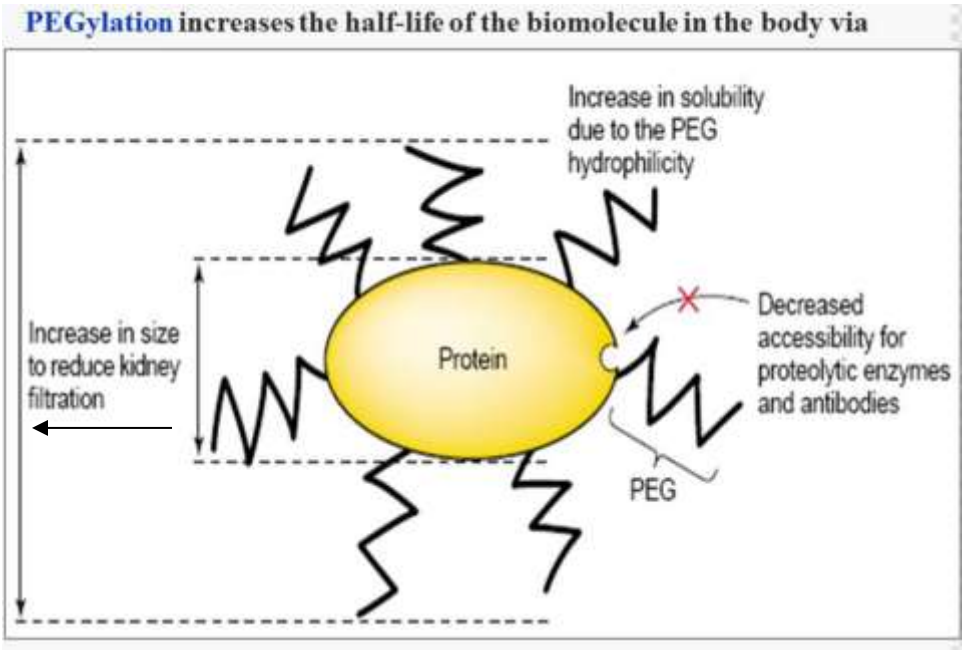

Figure 2. Resulting effects of PEGylation process.[10]

Another technological advancement to influence the current design shift was the development of "active targeting". This concept was established by conjugating either cell membrane receptor antibodies, peptides, or small molecule ligands to the designated

polymer carrier molecule, in order to seek out and deliver nano-therapeutics to specific cells.[11-14] The third technological discovery that helped usher in the current era of biomaterials advancement was the concept of "passive targeting", which is an alternative, complementary concept to "active targeting". Hiroshi Maeda unveiled this method of targeting while observing the "enhanced permeation and retention effect", when defective, leaky blood vessels in rapidly-expanding tumors entrapped nano-scale carriers. He concluded that due to the rapid formation of tumor tissue, the vasculature in the tissue was not fully developed, and as a result, the lymph drainage system was not yet operating efficiently. Hypothetically, the combination of these two effects is what caused the nano-scale drugs he was studying to be trapped within the extra-vascular tissue of the tumor.[15] The current study combines several of the discussed theories and concepts for drug-delivery *in situ*, as the objective is to develop a composite material consisting of a polymeric hydrogel matrix impregnated with finely-ground, Ga-containing bioactive glass particles, in order to achieve a means of effectively delivering and maintaining the glass particles at a desired site, and then allowing the leaching ions to interact with host tissue in the immediate vicinity, in order to elicit specific therapeutic effects.

2. Categorizing Biomaterials

Biomaterials can be broadly classified into three different categories based on how they interact with the body upon implantation, and these categories include bioinert, bioactive, and bioresorbable materials.

Bioinert materials are materials which remain inert upon implantation, meaning that these materials will not induce detrimental effects to the surrounding environment, but they also will not establish any interfacial bonding between the implant and host tissue (e.g. bone). An example of bioinert materials are non-thrombogenic polyurethanes. These materials are polymers used in vascular grafts, which have undergone a process which causes fluorine-containing functional groups to concentrate on their surfaces, in order to lower the surface energy of the implant, and inhibit protein adsorption and platelet adhesion upon implantation.[16] Uncoated metallic implants are also categorized as inert, as they rely solely on a mechanical fit to remain in place, and do not form chemical bonds with host tissue.

Bioactive materials are a type of material which can directly attach to host tissues through chemical bonding with the surface of the material, but the bulk of the implant remains intact indefinitely. An example of bioactive materials are cobalt-based alloy hip implants, which are coated with a hydroxyapatite (HA) layer. The HA layer quickly establishes a strong chemical bond to the bone in which the device was implanted, however, the purpose of this coating is strictly to hold the implant in place, and to help prevent the host tissue from fibrously encapsulating the implant.[17] This particular type of implant is intended to remain intact and undisturbed for as long as possible.

The final category, bioresorbable materials, are materials that directly attach to body tissues through chemical bonds on the surface of the material, and are then gradually resorbed until they are fully replaced by new tissues produced by the host.[18] An example of a bioresorbable material used in clinical practice is poly(lactic acid) (PLA) screws, which are commonly used in corrective jaw surgery to stabilize the jaw while healing after correcting mandible retrusion or mandibular prognathism (over or under bite).[19] Examples of materials from each category are provided in Figure 3.

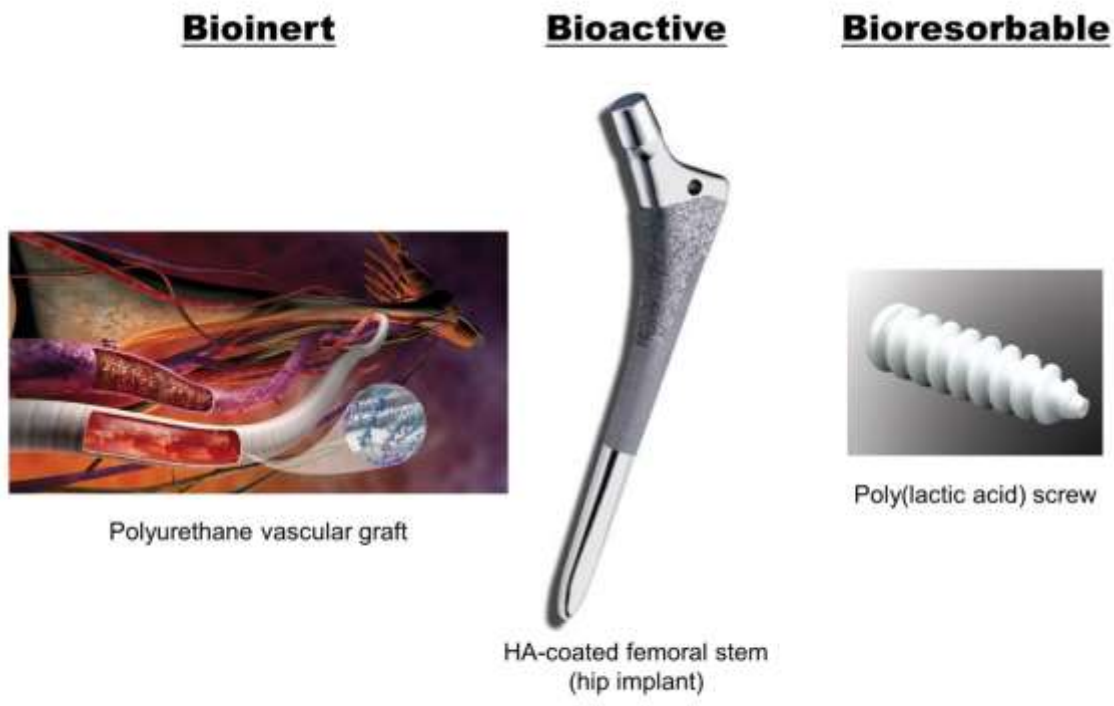

Figure 3. Schematics and images of a polyurethane vascular graft[20], an HA-coated femoral stem[21], and a poly(lactic acid) screw[22].

3. Classes of Biomaterials

Biomaterials can be classified into 5 different classes, including metals, polymers, ceramics, natural materials (derived from plants or animals), and composites of two or more different classes of materials. Each class of material offers different chemistries and different properties, and therefore, offers different advantages and disadvantages for each possible application. This is a brief overview of each class of biomaterial, the properties they exhibit, and a few of their current applications.

Metallic implants provide what are likely the most significant economic and clinical impacts on the field of biomaterials. Although current economic figures are difficult to determine, it was estimated that by the year 2000, the worldwide market for all types of biomaterials was estimated at $20 billion, with an estimated growth of 12 to 20% per year. Of that $20 billion worldwide market in 2000, the United States accounted for approximately $9 billion of that, with an estimated growth rate of about 20% per year.[23] Clinically, four out of ten of the most frequent orthopedic operations performed in the U.S. each year (approximately 3.6 million), involve metallic implant materials. These 4 procedures include the open reduction of a fracture along with internal fixation, placement or removal of an internal fixation device without reduction of a fracture, arthroplasty (procedure where the articular surface of a joint is replaced, remodeled, or realigned) of the knee or ankle, and arthroplasty or total replacement of the hip.[24] The three most common types of metallic implant materials used include stainless steels, cobalt-based alloys, and titanium-based alloys. Stainless steels are commonly used as bone plates and screws, cobalt-based alloys are used in femoral stems for artificial hips and dental partial bridgework, and titanium-based alloys are primarily used in oral and maxillofacial surgeries.[23] An example of the appearance of metallic knee replacement materials is displayed in Figure 4. Metals are selected as the primary materials for these particular applications due to their high yield, ultimate tensile, and fatigue strengths, their high degree of machinability, their corrosion resistance, and, in the case of titanium, for their osseointegration abilities. The major drawbacks associated with metallic implants are the hardness mismatch they can impose, the potential for fibrous encapsulation of the implant by the host tissue, potentially harmful degradation products, and the need for pre-implant fabrication, which can limit host morphological compatibility.

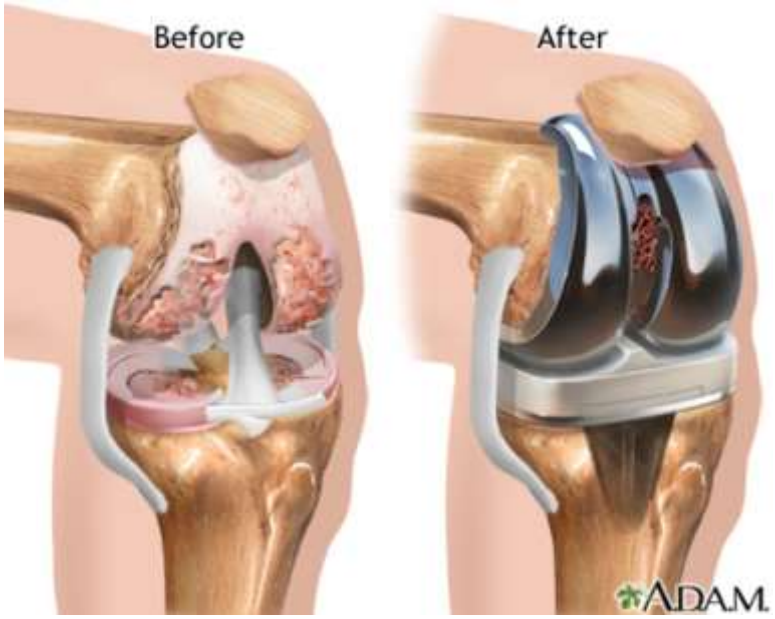

Figure 4. Image of metallic knee replacement materials.[25]

Polymers comprise the widest-ranging class of biomaterials, and can be derived either from natural sources, or from synthetic organic processes. This summary will briefly discuss synthetically-derived polymers, as naturally-derived polymers will be discussed later on. There are many different synthetic polymers used as biomaterials, ranging from hydrophobic, non-swelling materials, to polar materials, to materials which are completely water-soluble. There are also polymers which exhibit drastically different degradation properties, ranging from materials which are hydrolytically unstable and rapidly degrade in a physiological environment, all the way to materials which can remain relatively unchanged for the duration of a patient's life. Polymers are long-chain molecules which are comprised of a large quantity of small repeating units, and in synthetic polymers, the chemistry of the conjoined repeat units slightly differs from the chemistry of the monomers which were used to create the polymer.[26] This difference in chemistry is dependent on the mode of polymerization that was utilized. In the case of polymers, the requirements of the intended application determine the properties which need to be possessed by the final material. The properties of a polymer can be influenced by many different factors, including molecular weight (increased MW translates to increased mechanical properties, decreased processability), method of synthesis (addition

polymerization or condensation polymerization), and degree of crystallinity (increased crystallinity translates to increased mechanical properties, decreased reactivity).[26] A few examples of synthetic polymers and their applications include poly(methyl methacrylate) (PMMA), which is used as the matrix in bone cements and as intraocular lenses, polyethylene (PE), which is used for catheters and as the acetabular component in prosthetic joints, and poly(ethylene terephthalate) (PET), which is used as an arterial woven graft, and as a reinforcing fabric for tissue reconstruction.[23] Synthetic polymers are generally selected as the material of choice for a particular case because of their high degree of tailorability and low manufacturing costs (compared to other classes of biomaterials), and because of the high degree of control the manufacturer has over the chemistry and purity of the final product. However, some of the major drawbacks associated with synthetic polymers include potentially hazardous wastes produced during manufacturing, and the potential elicitation of undesired physiological responses as a result of degradation products after implantation.

The class of ceramics in biomaterials encompasses ceramic, glass, and glass-ceramic materials, and thus includes a vast range of inorganic/non-metallic compositions. This class of materials is most commonly used to either repair or replace skeletal hard connective tissues, and the success of these materials is dependent on the establishment of a stable chemical bond between the host and the implant. However, for materials in the ceramic class, the physiological response upon implantation of a device is particularly sensitive to both the composition, and the degree of crystallinity of the material. There are several categories of materials within this class, including highly crystalline ceramics, porous ceramics, bioactive glasses and glass-ceramics, and calcium phosphates. Highly crystalline ceramics, such as high-density, high-purity alumina (Al_2O_3), are utilized as components in hip prostheses and dental implants due to their excellent corrosion resistance and wear resistance, their high strength, and their acceptable biocompatibility (produces thin capsule formation, allowing for cementless fixation).[23] However, the high degree of crystallinity that provides these materials with their mechanical strength and wear resistance, also prevents the host tissue from chemically bonding to the surface of the implants, which over time, can potentially result in loosening. Porous ceramics, such as Pro Osteon (hydroxyapatite converted from coral), are materials that remain inert upon

implantation, while acting as porous scaffolds for bone re-growth. When these materials possess pore sizes exceeding 100 μm, bone tissue grows within the interconnecting porous network, maintains its vascularity, and remains viable for long periods of time, so long as the scaffold is not used in a load-bearing application.[27] Bioactive glasses and glass-ceramics are materials which exhibit a time-dependent, kinetic modification of the surface, which is initiated immediately upon implantation, and proceeds until a chemical bond is formed between the host tissue and the implant. This ability was first demonstrated by Hench *et al.*, with glasses containing compositions with varying amounts of SiO_2, Na_2O, CaO, and P_2O_5.[28] This group discovered that there are three vital compositional requirements that must be met in order to distinguish a bioactive glass from a traditional soda-lime-silicate glass: (1) must contain <60 mol% SiO2, (2) must contain a relatively high Na_2O and CaO content, and (3) must possess a high CaO/P_2O_5 ratio (≥ 5:1). It was later discovered that compositions could be altered (e.g. substituting 5-15 wt% B_2O_3 for SiO2), and that the bioactive glasses could be heat-treated to form glass-ceramics, and that these changes did not have an effect on the ability of the materials to bond to bone.[23] Bioactive glasses and glass-ceramics have been used as components in bone cements, and in the repair of periodontal defects (Figure 5), and much work is being done to resolve the issues of trying to balance the chemical bonding between host and implant with the matching of implant resorption and host regeneration rates, while still meeting the mechanical requirements for the intended application, which will hopefully allow these materials to be used in many different fields of medicine in the future.

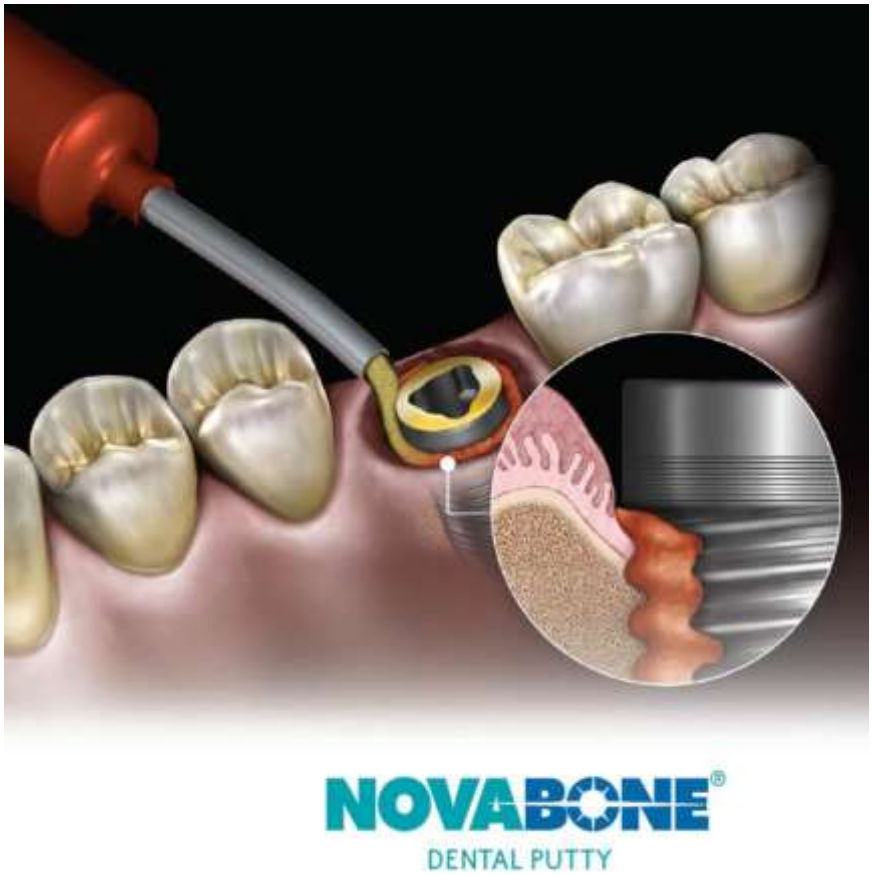

Figure 5. Illustration of action of Novabone® dental putty.[29]

The final category contained in the ceramic class of materials is the calcium phosphates. Since the primary crystalline component of the mineral phase of bone is a calcium-deficient carbonate hydroxyapatite, much effort has been poured into developing synthetic hydroxyapatite which can be utilized as an implant material. As with most ceramic biomaterials, the method and conditions used to synthesize synthetic HA will drastically influence its physical and chemical properties. One of the main stipulations is that the material must possess a Ca/P ratio of at least 1:1, in order to exhibit sufficient resistance to solubility and hydrolysis upon implantation. As the Ca/P ratio increases, so will the material's resistance to solubility and hydrolysis.[30] Other factors that can greatly influence the rate of resorption for synthetic HA include physical features (surface area, crystallite size), chemical factors (atomic and ionic substitutions in the lattice), and biological factors introduced by the host (age, sex, hormone levels). Although development and processing of these materials can be very difficult, calcium phosphates

are used in many different forms for many different applications, some of which include its densified form for alveolar ridge augmentation, as granules for filling bony defects, and as a coating on metal implants for orthopedic and dental surgeries.[31-33]

The fourth class of biomaterial can be described as natural materials, as they are obtained from either plant or animal sources. Although there are examples of directly-sourced, animal-derived materials still used in practice (e.g. bovine-derived heart valves), the majority of naturally-sourced biomaterials are in the form of polymers. Natural polymers are of interest to biomaterials engineers, particularly with the growing interest in tissue engineering and regeneration, due to their ability to be utilized in many different applications, while also possessing many similarities to macromolecular substances that the biological host is metabolically capable of processing.[23] The similarities between naturally-occurring polymers and naturally-occurring substances within the body, provides biomaterials engineers with the ability to design materials which can function at macroscopic level, as well as the molecular level. This is a large advantage over many synthetic polymers which are not easily recognized by immune response cells, and as a result, can elicit either chronic inflammatory or toxic effects.[34] Natural polymers are of such great interest in the field of tissue engineering because of their ability to be broken down by enzymes present within the host, which is ideal when designing a material which is intended to act as a temporary scaffold for cell growth, and then degrade over time. As degradation time is a key factor in the design of bioresorbable materials, choosing the type of cross-linking which is used, and also introducing possible chemical modifications to the polymers, can help the designer control the rate at which the implant dissociates. However, there are still some drawbacks, as natural polymers can still trigger immune responses, and because of their increased structural complexity compared to synthetic polymers, the process of manipulating these materials to exhibit the desired properties is relatively difficult. In addition, any polymers which may be derived from animal sources can exhibit large degrees of variability as many of these polymers are not only species-specific, but also tissue-specific.[23] This requires manufacturers to spend more time and money to stringently control the sourcing of these materials, as continual reproducibility is required. The class of natural polymers is comprised of 3 different types of materials, including proteins, polysaccharides, and polynucleotides. Of these different

forms of natural polymer, collagen is the most commonly used, as it is a key component in connective tissues, allowing it to exhibit desirable mechanical properties while still being deformable.[35] Collagen-based materials are used in a variety of different applications, acting as sutures[36], tendons and ligaments[37], and for use in burn treatment.[38] However, in a previous study in which collagen was used as a matrix material into which bioactive glass particle and microspheres were both attempted to be distributed throughout for use as a drug-delivery mechanism to combat osteomyelitis (bacterial infection of bone), it was observed that uniform distribution of the particles could not be achieved, resulting in either non-uniform or non-existent ion release, and the inhibition of HA deposition on the surface of the materials.[39] This example leads us to the fifth and final class of biomaterials, composites.

The definition of the word composite means "consisting of two or more distinct parts". In the world of biomaterials engineering, this is not a very applicable definition, because on the atomic scale, everything in biological systems is technically a composite, as are implant materials, such as polymers which consist of more than one set of atomic group. In order to avoid confusion, a composite biomaterial should be interpreted on the macro-scale, allowing one to think of composites as materials comprised of two or more components which are chemically distinct, and are separated by an interface.[23] In general, composite biomaterials can be categorized as a mixture of two or more materials of the same class (e.g. hydrogels), or as a mixture of a continuous phase and a discontinuous phase, where the discontinuous phase is the reinforcing material and the continuous phase is the matrix. The properties of the latter type of composite biomaterials are determined by the properties of their components and any interactions between them, meaning that in order to fully describe the composite, one must identify the different components and their inherent properties, as well as the size, concentration, distribution, and orientation of the reinforcing component. Extensive work has been conducted examining different matrix materials (e.g. ultra-high molecular weight polyethylene (UHMWPE), ppolytetrafluoroethylene (PTFE), poly(methyl methacrylate) (PMMA)), containing many different reinforcing materials (e.g. calcium phosphates, bioactive glasses), with several different intended applications (e.g. fracture fixation, implant fixation).[40] After review of the literature it can be estimated that many of the attempts to develop composites for

bone-filling and regeneration applications have been focused on combining synthetic polymers with either HA fibers or particles, with the main focus being on developing implants with sufficient mechanical properties and an ability for bone cells to attach and proliferate across the implant surface and potentially into the bulk.[41-43] Considering these previous attempts, the current study aims to present a novel approach to bone-filling and regeneration by combining two different natural polysaccharides (carboxymethyl cellulose and dextran) via chemical cross-linking to form a hydrogel matrix, which is impregnated with different amounts of Ga-containing bioactive glass particles, to determine if this method might provide a suitable means for in-situ injection and subsequent fixation of bioactive glass particles at a specific location, while also allowing for the release of therapeutic ions from the glass particles which could potentially up-regulate osteoblast and fibroblast activity, while simultaneously inhibiting osteosarcoma, myeloma, bacterial, and fungal viability.

Bioactive Glasses

1. Bioactive Glass/Tissue Interfacial Interactions

1.1. Overview

One of the most interesting types of biomaterials currently available, from a surface chemistry standpoint, are bioactive glasses. First formulated by Hench *et al.*[28], bioactive glasses are glasses which are formulated to possess relatively weak chemical structures (compared to most industrially available glasses), and contain compositional similarities to bone and tissue fluids, such as Na_2O, P_2O_5, CaO, and SiO_2.[44] These analogous compositions contribute to the ability of these glasses to form chemical bonds with surrounding tissue once implanted in the body. Bioactive glasses can be classified as either bioactive (elicits therapeutic response from, and forms chemical bond with host tissue), or bioresorbable (serves initial bioactive function, and then dissolves over time to eventually be replaced by host tissue), but the glasses that are currently of most interest are those that are bioresorbable, as they are intended to first serve as a synthetic graft material, but are eventually resorbed into the host system, ultimately being replaced by healthy tissue. The following is a step-by-step explanation of how bioactive glasses

interfacially interact within the body, starting from implantation into a physiological environment, and progressing all the way to the generation and crystallization of new bone tissue. These steps have also been presented with a time scale in Figure 6.

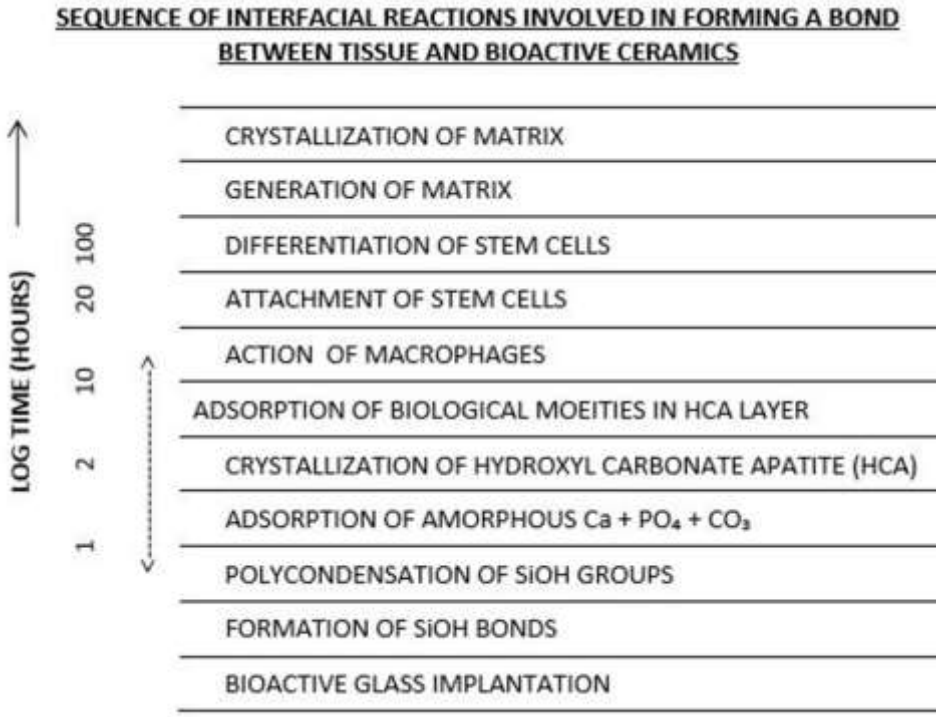

Figure 6. Sequence of interfacial reactions involved in forming a chemical bond between tissue and bioactive ceramics, as described by Hench *et al.*[45]

1.2. Silanol Group Formation

Some of the most important constituents of a bioactive glass are alkali and alkali-earth metals which act as network-modifiers within the glass structure. One of the most prominent network-modifiers is ionic sodium (Na^+). This particular network-modifier is important because immediately upon submergence in a body fluid (e.g. blood), bioactive glass surfaces exchange Na^+ ions with H_3O^+ ions from the body fluid to form silanol groups (Si-OH). At this preliminary stage of interaction between the implant and the body, these silanol groups initially appear as individual groups scattered across the surface of the implant.[46]

1.3. SiO_2-Rich Surface Layer Formation

After the surface of the implant is populated by individual silanol groups, a continuous layer is formed by polycondensation of the silanol groups.[47] This layer of polycondensed silanol groups is very rich in SiO_2. The SiO_2-rich layer exhibits a high surface area and a low isoelectric point, which provides chemisorption sites for calcium and phosphate ions, which will eventually nucleate hydroxyl carbonate apatite (HCA) crystals, and lead to the formation of an initially amorphous calcium phosphate layer, which subsequently proceeds to form a crystalline HCA layer.[45]

1.4. Calcium Adsorption

After polycondensation of the silanol groups occurs, these groups dissociate into negatively charged units. These negative charges then enhance the electrostatic interaction with the positively charged calcium ions in the fluid.[46] This is why the ion concentration of the body fluid is critical in the success of the implant forming strong chemical bonds with the living tissue, because if the body is calcium deficient and results in a deficiency in the body fluid, then the HCA layer cannot be fully formed. Without full formation of the HCA layer, the body will tend to encapsulate the implant with fibrous tissue, inhibiting the successful formation of a bond with the bone.[48]

1.5. Phosphate Adsorption

As calcium ions (Ca^{2+}) are adsorbed by the SiO_2-rich surface layer, phosphate ions (PO_4^{3-}) are simultaneously adsorbed, leading to the formation of amorphous calcium phosphate. Phosphate ions are attracted to the glass surface due to the presence of positively-charged calcium silicate. This step in which PO_4^{3-} ions are being adsorbed will continue until the Ca/P ratio of the layer resembles that of bone (~ 1.65).[46]

1.6. Growth of the Calcium Phosphate ($Ca_3(PO_4)_2$) Layer

As phosphate ions are incorporated into the calcium-rich layer, an amorphous calcium phosphate layer is eventually formed. This amorphous layer forms on top of the SiO_2-rich layer, and steadily grows while incorporating several different ions (such as

Na^+, Mg^{2+}, and Cl-), from the body fluid.[49,50] Incorporation of these other ions helps the forming layer to resemble bone mineral more closely. During this stage, OH^- and CO_3^{2-} ions are also adsorbed from the surrounding solution, and this adsorption initiates crystallization of the layer, at which point the layer stops adsorbing calcium and phosphate ions.[51,52] This step has been shown to not only occur within the body, but also during *in vitro* simulations in which samples are immersed in simulated body fluid (SBF). Santos *et al* observed through SEM analysis that the calcium phosphate layer on a bioactive glass in SBF developed from a layer which contained a Ca/P ratio of about 1.43, which does not resemble bone mineral, to a layer which possessed a Ca/P ratio of 1.65, which closely resembles bone mineral, and the adsorption of PO_4^{3-} dramatically decreased once the Ca/P ratio of the layer neared 1.65.[53] This suggests that the calcium phosphate layers formed on the surfaces of bioactive glass implants possess Ca/P ratios resembling that of bone mineral with or without the presence of biological signalling molecules, further demonstrating their potential as bone void-filling materials.

1.7. HCA Crystallization

After an amorphous calcium phosphate layer which sufficiently resembles the Ca/P ratio present in the mineral phase of bone is formed, the layer will then crystallize.[49] This crystallized HCA layer is a biologically active layer which enhances bone formation by eventually acting as a scaffold upon which osteoblasts will attach and begin the cellular process associated with bone formation. This crystallized HCA layer is also responsible for the formation of a chemical bond between the implant and the surrounding bone tissue.[54] The process from exchange between Na^+ and H_3O^+ ions, to crystallization of the surface HCA layer, is illustrated in Figure 7.

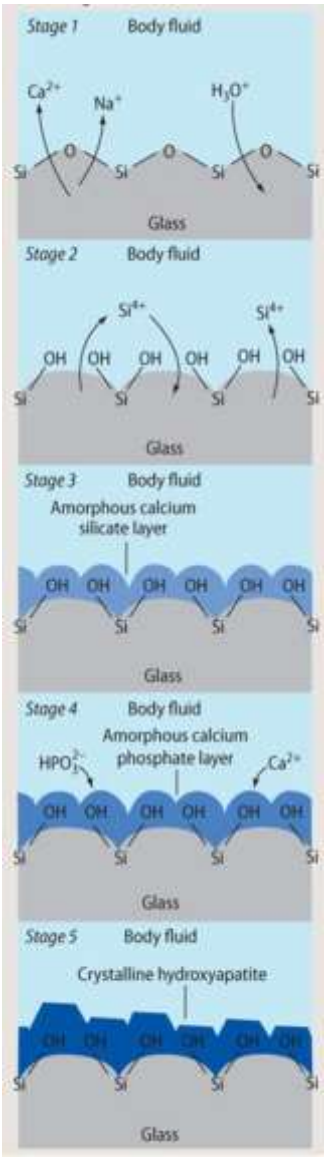

Figure 7. Illustration of the chronological order of reactions which occur to allow for the deposition of a crystalline HA layer on a bioactive glass surface.[55]
(Reproduced by permission of the Royal Society of Chemistry from Nichola J Coleman and John W Nicholson,*Educ.Chem.*, November 2006, 156-160.)

1.8. Osteoprogenitor Cell Attachment, Differentiation, and Bone Matrix Deposition

Once an adequate HCA layer is formed, osteoprogenitor stem cells will begin to attach. A study conducted by Xynos *et al* revealed, through SEM analysis, that cells attached to the HCA layer formed on bioactive glasses will initially demonstrate

morphological changes such as the growth of dorsal membrane ruffles and microvilli, which help regulate the flow of ions into and out of cells.[56] These types of morphological changes are characteristic of cell activation, and as time goes on, the cells will spread across the glass surface to form complete cellular layers and will differentiate, exhibiting 3-dimensional bone nodules. These cells will then begin to deposit the matrix which will act as the backbone of newly formed bone tissue.

2. Bioactive Glass Components

Bioactive glasses have been proven to stimulate the growth of bone upon implantation, and the original formulation was comprised of SiO_2, CaO, Na_2O, and P_2O_5. Since this original composition was discovered, many different formulations have been synthesized. These have included several different components in an attempt to stimulate different therapeutic effects. The glasses used in this study include the traditional compounds SiO_2, CaO, and Na_2O, as well as two non-traditional compounds ZnO and Ga_2O_3. Some of the reasons for the inclusion of the traditional compounds include glass network formation, glass network modification, and ion exchange and HA layer formation upon implantation. However, the reasons for the inclusion of Zn and Ga range beyond simply stimulating bone cells, and include killing bacterial cells and inhibiting the growth of cancer cells. The following is a brief justification for why each constituent was included in the formulation used for this study.

2.1. Silicon (Si)

The chronological process by which bioactive glasses stimulate the growth of new bone has been explained. As the glasses being used in the current study are silicate-based, the main reason for the inclusion of the compound SiO_2 is to form a network which has the ability to hold all of the other compounds within the glass. SiO_2 is also instrumental in forming a functional HA layer along the surface of the glass upon implantation, upon which bone-forming osteoblast cells can attach and begin creating new bone. A key factor in developing silicate-based bioactive glasses is the amount of silica present, as excess content ($\geq$ 60%) can result in the inhibition of dissolution, while deficient content

can result in degradation that proceeds too rapidly for a sufficient bond to form between bone and implant.

2.2. Sodium (Na)

Sodium (Na) is another one of the elements most commonly included in bioactive glasses. As previously discussed, the primary reason for Na-inclusion is the initial exchange of Na^+ ions for H^+/H_3O^+ between the glass surface and physiological solution. This exchange is possible because Na acts as a network modifier which creates disruptive non-bridging oxygens within the silica-based glass structure, thus weakening the structure and ultimately allowing for ion release upon implantation.[57] Na is also included because the cascade of reactions that is initiated by the release of Na^+ ions, which is not only effective for stimulating the deposition of new bone tissue, but also prevents the body from encapsulating the implant upon implantation. Na-content is also tailored according to the intended application of the glass, as a linear correlation has been derived between increased Na-content and an increased thermal expansion coefficient (TEC).[57] This is an important trait when tailoring bioactive glasses for applications such as the coating of a metal prosthesis, as customizing Na-content with the consideration of TEC information can help to prevent interfacial separation between the glass and the metal substrate. Na is also an actively metabolized element within the body, and is involved in numerous metabolic functions, including muscular contraction, nerve impulse transfer, and the balancing of ionic concentration gradients in cells. In the current study, the main purposes for including Na are to weaken the glass network, and to allow for the initiation of the interfacial interactions necessary for the formation of a bond between implant and bone. Figure 8 illustrates the theoretical arrangement of both glass network forming, and modifying ions, in a glass structure.

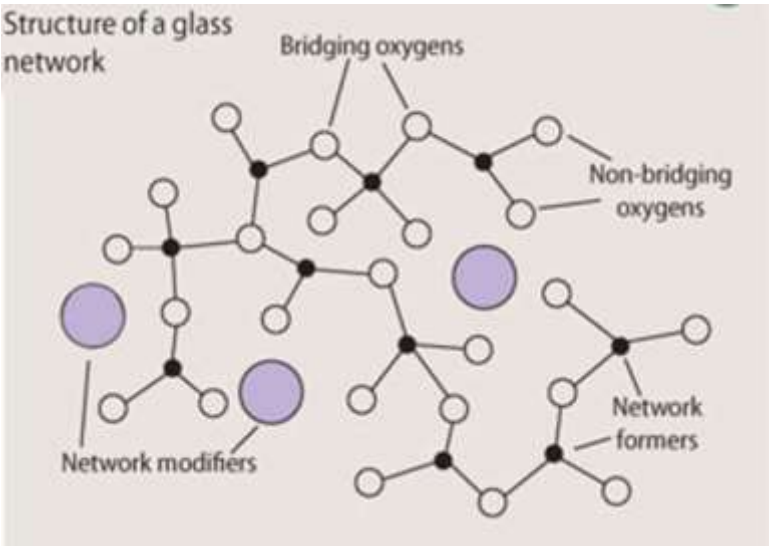

Figure 8. Theorized structure of a glass network containing both glass network forming, and modifying ions.[55] (Reproduced by permission of the Royal Society of Chemistry from Nichola J Coleman and John W Nicholson,*Educ.Chem.*, November 2006, 156-160.)

2.3. Calcium (Ca)

Calcium (Ca) is another element commonly included in bioactive glasses, and is found in concentrations much higher than trace amounts within bones, and throughout the entire body. This element has many different functions within the body, including roles in neurotransmission, muscle contraction, and cellular triggering of exocytosis. However, since most of the body's Ca (~99%) is found in the skeleton, one of the most important functions Ca has is to provide mechanical strength to bones. These important biological functions, along with the properties exhibited when included in bioactive materials, encourage the inclusion of Ca into biodegradable implants.

As previously mentioned, about 99% of the body's Ca can be found within the skeleton. However, since the skeleton is a metabolic organ that continuously undergoes remodeling in order to repair micro-damage, and to allow the body to adapt in order to handle the particular stresses it experiences, the amount of Ca found in the skeleton is not a constant value. The skeleton remodels itself by dissolving old, damaged bone through osteoclasts, and constructing new bone at these sites through osteoblasts. When the osteoclasts release digestive enzymes and remove old bone, those dissolved constituents enter the bloodstream in order to be removed from the body through the circulatory

system. The reason this extra Ca will be removed from the body is because there is a specific amount of Ca that is supposed to be in the bloodstream at any one time. If this amount varies, the skeleton is responsible for maintaining the serum levels. This role of the skeleton is beneficial for people who are able to maintain proper amounts of serum Ca, but for those who struggle to meet the required Ca intake, this role can be detrimental. The reason this process can have negative effects on an individual is that since about two-thirds of bone (wt%) is Ca, the method by which the skeleton compensates for low levels of serum Ca is to increase the rate of bone resorption in order to introduce more into the bloodstream. Since Ca is the main component of bone, and it is a major contributor to the mechanical strengths possessed by bone, resorption of the bone results in weaker bones, which are more likely to fracture. The systematic occurrence of this event over time leads to the disease osteoporosis, and is one of the main disorders that implantable skeletal biomaterials attempt to treat. The role of Ca in the strength and integrity of bones is one of the main reasons why it is included in traditional bioactive glasses, and why it has been included in this study.

One of the properties that a material must possess in order to be used as a bioactive material, is the ability to form a biologically active bond with the host's living tissue upon implantation, through the deposition of an HCA layer. When properly formed, this layer that is mostly composed of Ca and PO_4, closely resembles the composition of bone, and essentially tricks the body into recognizing the implant as normal tissue rather than as a foreign body. It has been discovered that in order for an implant to bond correctly within the body, the ratio of Ca to P in the formed HCA layer must be very close to 1.67. However, designing implantable materials which can obtain surface HCA layers with this ratio can be relatively difficult. In the case of bioactive glasses, it has been observed that the amount of HCA deposited, as well as the composition of the HCA layer deposited upon dissolution of the implant, is dependent on how much Ca was in the glass to begin with, as well as what other compounds were contained in the glass. The amount of Ca present in the glass affects the composition of the deposited layer because when the glass is broken down and ions are released, the forming HCA layer can only include as much Ca is present in the immediate environment, which in this case, is the surface of the dissolving glass. The reason the

overall composition of the bioactive glass affects the HCA layer is that the rate at which the glass physically breaks down and allows ions such as Ca to be released is controlled by the ratio of glass network formers to glass network modifiers present within the structure. Compounds such as calcium oxide (CaO) have been shown to act as network modifiers, meaning they increase the number of non-bridging oxygens present, and therefore lower the structural integrity of the glass. Network modifiers are what allow glasses to exhibit bioactivity, and the ratio of formers to modifiers determines how fast the glass will break down once implanted into the body. This is an extremely temperamental factor in designing bioactive glass implants, as the glass composition needs to be tailored to allow for fast enough degradation that a sufficient HCA layer can form, while not degrading so rapidly that the mechanical properties of the glass are completely compromised and the body is flooded with ionic debris.

Although the presence of sufficient amounts of Ca is necessary to maintain strong, healthy bones, perhaps having an insight into the mechanistic action of this element in bone cells may also help to justify the importance of its inclusion into these glasses. Studies conducted by Turner *et al.*, and by Gu *et al.*, discovered that bone cells behave in a fashion similar to neurons, in that they possess the ability to utilize signaling pathways in order to direct the collective action of neighboring cells.[58,59] These studies unveiled glutamate-signaling pathways in bone cells, which suggests that these pathways are likely responsible for the stress-directed growth and resorption of bone. This is a logical deduction because glutamate has exhibited the ability to act as an almost universal neurotransmitter, possessing the power to determine whether cells survive, differentiate, or die, suggesting that these pathways could be responsible for bone growth or resorption, depending on the loads, or lack thereof, applied to the bone.[59-61] Research focused directly on osteoblasts has revealed that these cells are able to release glutamate, and are able to express various glutamate receptors, just as effectively as neurons.[62] These signaling pathways are of interest in the realm of bioactive glasses because it has been discovered that this process, especially in bone cells, is a Ca^{2+}-dependent process.[58,63] To determine if Ca^{2+} ions released from bioactive glasses could act to alter glutamate pathways in osteoblasts, Valerio *et al.* conducted a study using rat calvaria incubated with a Ca-containing bioactive glass.[64] This study found that an increase in extracellular Ca^{2+}

concentration as a result of bioactive glass dissolution does indeed alter glutamate release, suggesting that different biological responses can be stimulated depending on the amount of Ca^{2+} that is released from the glass. The discovery of the presence of glutamate-signaling pathways in osteoblasts, and the ability to manipulate them using dissolution products of bioactive glasses, further justifies the inclusion of Ca in this glass series.

2.4. Zinc (Zn)

Zinc (Zn) is a trace element that can be incorporated into bioactive glasses, due to its wide range of beneficial effects within the body. It has been extensively proven that Zn is required for the normal growth, development, and maintenance of healthy bones in humans, and in other animals.[65,66] Zn is an essential element for several cellular processes such as cell proliferation and cell differentiation, as well as cellular defense against free radicals.[67,68] It has been shown that Zn acts in a structural role in several proteins such as transcription factors and various cellular signaling proteins.[69] Zn has also been observed as a structural component in critical enzymes, such as DNA repair enzymes[70], and also acts to regulate apoptosis in mammals, but its exact role in apoptosis regulation is extremely cell-specific, and is also extremely complex.[71,72] For example, Franklin *et al*. demonstrated that Zn acts to induce apoptosis in prostate epithelial cells and ovarian epithelial cells, while it also acts to inhibit apoptosis in breast cells, lung epithelial cells, renal cells, and macrophages, thus demonstrating the cell-specific nature of this element's effects.[72] It has also been demonstrated that there is a narrow concentration range in which Zn can induce beneficial effects in cells. Provinciali *et al.* observed that in mouse thymocytes, small doses of zinc induced apoptosis, while large doses actually inhibited apoptosis.[73]

Considering the wide range of biochemical processes this element is involved in, as well as the fact that the skeleton contains the majority of the total body burden of Zn[74], it is evident that this element is crucial for proper bone metabolism. This is why a Zn-deficiency can lead to such a wide range of bone-growth disorders, and this deficiency has been shown to cause defects in the skeletons of several species including chicks, pigs, cows, rhesus monkeys, mice, and most importantly, humans.[75] Zn-deficiency has been

shown to cause disorders such as the abnormal development of the ribs and vertebrae, as well as agenesis (failure to develop during embryonic growth) of long bones. It has also been shown to be responsible for bone-growth disorders such as club foot, cleft palate, and micrognathia (incomplete growth of the jaw) in rats.[75] It was also demonstrated in a 1989 study, that like their parents, the offspring of Zn-deficient rats also exhibit impaired ossification (ability to construct new bone).[76] Most importantly, Zn-deficiencies can also be associated with osteoporosis in humans, and the effects of this disease on bone mineral density can be seen in Figure 9. Reginster *et al*. observed that lower levels of skeletal Zn were exhibited by osteoporotic patients than by healthy controls.[77] This finding supports the hypothesis that Zn may help to improve the crystallinity of apatite, which is a characteristic of mature bone.[78] Additionally, Zn is also useful as a marker of bone resorption, as osteoporotic women have been shown to excrete much higher levels of the element in their urine than healthy controls.[74]

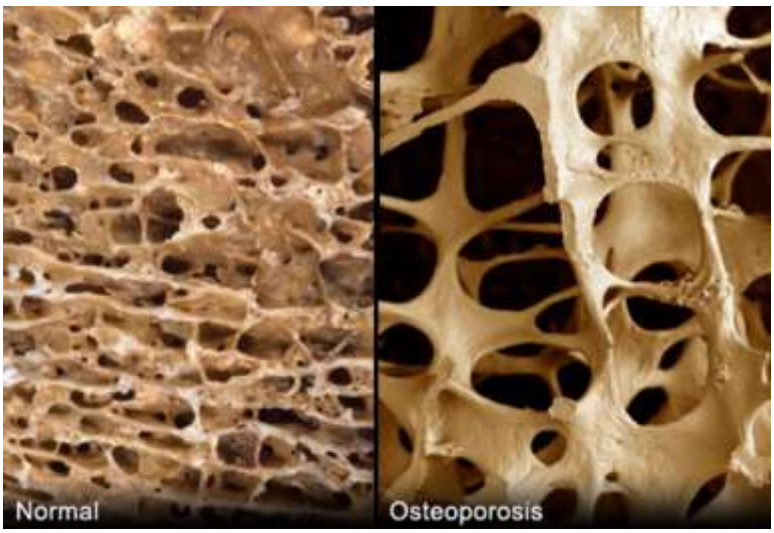

Figure 9. Images comparing the structure of normal healthy bone against osteoporotic bone.[79]

It is clearly evident that a Zn-deficiency can have many negative consequences within the bodies of humans, and many other animals. With that in mind, it is also important to understand how Zn actually works in the body, and how the introduction of Zn through degradable biomaterials might act to stimulate beneficial responses. In an attempt to learn how Zn affects bone metabolism, Yamaguchi *et al*. investigated it's role as an activator of bone metabolism in weanling rats.[80] The rats were given different doses

of zinc sulfate (either 5, 10, or 50 mg Zn/kg body weight) over a three day period, and the effects were evaluated daily. It was observed that in the rats given 5 and 10 mg Zn/kg doses, dose-dependent increases in the amount of Zn, DNA, collagen, and Ca were observed in the femoral diaphysis. A dose-dependent increase in alkaline phosphatase (ALP) activity was also observed. These findings are important because ALP activity directly correlates with the calcification of bone, collagen is one of the main structural proteins found in the bone matrix, and DNA quantity indicates the number of bone cells present (osteoblasts, osteoclasts, and osteocytes). Due to the increase of each of these entities responsible for the formation of new, healthy bone, it is evident that the addition of Zn to biodegradable materials could help to promote new bone formation. In addition, a study conducted by Aina *et al*. aimed to determine whether or not endothelial cells could adhere and proliferate on the surface of Zn-containing bioactive glasses.[81] This study compared three different glasses; one control glass (0% Zn), one glass containing 5 wt% Zn, and one glass containing 20 wt% Zn. It was discovered that *in vitro*, endothelial cells showed much higher affinity for adhering to the surface of the bioactive glass containing 5 wt% Zn than to the other two glasses, while the least amount of cells adhered to the glass containing 20 wt% Zn. This study also discovered that the spreading of endothelial cells was significantly increased on the surface of both Zn-containing glasses compared to the control. These findings are important because the purpose of bioactive glasses is to promote the growth of new, healthy bone over time. A vital piece of engineering materials which promote the generation of new bone, is designing a material which allows angiogenesis (vascularization) to occur, and allows for sufficient flow of blood and nutrients throughout the newly constructed bone.[82,83] Angiogenesis is particularly important in the construction of a mineralized tissue such as bone, as it is a prerequisite for proper osteogenesis.[84,85] The results of this study are also important because they lend some insight as to how the presence of Zn might affect the physical breakdown of bioactive glasses upon implantation. Since endothelial cells have been proven to be extremely sensitive to pH fluctuations, and this study found that endothelial cells adhere best to glass containing small amounts of Zn, and that these cells proliferate at a much higher rate on Zn-containing glasses, a contributing factor may be that the presence of Zn slows the dissolution rate of a bioactive glass. This is suggested because a

slower dissolution rate would mean a lower number of ions would be released from the glass, resulting in less fluctuation in pH levels.

Zn also expresses several other properties which make it a prospective element for inclusion into implantable biomaterials. On top of the pre-discussed effects that have been observed, bioactive glasses doped with Zn have also exhibited the ability to enhance the formation of an HCA layer on the surface of the glasses. This ability has been demonstrated in both biological fluids[86], and in SBF.[87,88] Studies have also been conducted to evaluate the effects of Zn on bone resorption, rather than focusing on bone formation. In a 1992 study by Yamaguchi *et al*. it was discovered that Zn has the ability to inhibit the resorption of bone *in vitro*.[89] This study also revealed that Zn inhibited the parathyroid hormone (PTH)-induced increase in glucose consumption and lactic acid production by the bone in medium, and that Zn inhibited the PTH-increased acid phosphatase activity of the bone. In addition, it was observed that Zn acted to inhibit the PTH-decreased ALP activity of the bone. All of these observations lead to the conclusion that Zn has the ability to directly inhibit bone resorption *in vitro*.

Since it was learned that Zn possessed the ability to inhibit the resorption of bone through effects on PTH, the next step was to identify any other mechanisms through which zinc might inhibit resorption, and to determine if it might have a direct effect on osteoclasts themselves. In a study by Kishi *et al*. using mouse bone marrow cells, it was observed that when the medium did not contain Zn, significant increases in the number of osteoclast-like cells occurred, while the presence of Zn in the medium inhibited the increase of osteoclast-like cells.[90] Another study also revealed that Zn was effective in inhibiting the formation of osteoclast-like, multi-nucleated cells from marrow cells at the earlier stage of the culture, but had no effect on the number of cells, or the lysosomal enzyme (β-glucuronidase) activity in the pre-formed osteoclasts from femoral-diaphyseal tissues. These results indicate that Zn is capable of inhibiting osteoclast-like cell formation, but it is incapable of inhibiting osteoclast function.

Zn has also been implicated in other roles within the bone, including the physical process of aging. The mechanisms behind the deterioration of bone cell function over time are not yet fully understood, but it has been demonstrated that Zn content in the cellular components of the femoral diaphysis is lower in elderly rats (30 weeks old), than

in weanling rats (3 weeks old).[91,92] Since Zn is known to play a role as an activator of bone formation in weanling rats, the decrease in Zn content with age may contribute to the disruption of normal bone metabolism. To demonstrate this theory, [^{3}H] leucine incorporation by rat bone tissues were compared. The amount of leucine incorporated into the residues of bone tissues from elderly rats was much less than the amount incorporated into the residues of weanling rat bone tissues. To determine if Zn could have an effect in this instance, zinc sulfate was administered to the elderly rats for three days, and after three days, the rate of leucine incorporation into the bones of the elderly rats was much improved, indicating that as aging occurs, the supply of Zn within the body may be important in preventing the deterioration of bone metabolism. All of these studies contribute to prove why Zn is an important element in the development and maintenance of healthy bones, and why it is a beneficial element to include in bioactive glasses.

2.5. Gallium (Ga)

2.5.1. Introduction

One trace element which is of particular interest to our research is the element gallium (Ga). Ga is a group IIIA metal that was first discovered by Paul-Emile Lecoq de Boisbaudran in 1875[93], and in its raw form, displays a silvery-white color, and is obtained as a byproduct from the extraction of aluminum and zinc ores.[94] Over the past thirty years, the unique properties of gallium have caused this element to be utilized more frequently in the field of medicine. Its radioactive form (^{67}Ga) has been proven to localize in malignant cells after injection[95], and this ability is what led to the development of the ^{67}Ga scan, which is commonly used post-treatment to detect residual or relapsed disease in patients stricken with Hodgkin's and non-Hodgkin's lymphomas.[96,97] In cases where ^{67}Ga is incorporated into lymphoma cells which have remained viable post-treatment, the amount of Ga present in the cells correlates to the rate at which the cells have proliferated, allowing the observer to determine the rate at which the tumors are growing within the patient.[98] The following is a review of the array of other abilities Ga has demonstrated within the field of medicine, along with their proposed mechanisms of action.

2.5.2. Disease Treatment

The absorption of radioactive ^{67}Ga by malignant cells (Figure 10) led to the research conducted by the National Cancer Institute (NCI), in which they investigated the ability, or lack thereof, of salts of group IIIa metals to inhibit the growth of malignant cells in mice and rats.[99] In this study, gallium nitrate ($Ga(NO_3)_3$) exhibited the ability to suppress the growth of subcutaneously implanted tumors, while also exhibiting the least toxicity of the compounds. Since these abilities of $Ga(NO_3)_3$ were discovered, many clinical trials have been conducted in an attempt to identify which forms of cancer this compound is most effective against. To this point, $Ga(NO_3)_3$ has been proven most effective in the treatment of non-Hodgkin's lymphoma and bladder cancer. Additionally, $Ga(NO_3)_3$ has been proven effective when administered as a single agent, as well as in combination with other antineoplastic (anti-cancer) drugs. In the case of non-Hodgkin's lymphoma, $Ga(NO_3)_3$ was proven effective as a single agent in both a trial in the 1980's [100], as well as in a 2004 trial [101], and in combination with other antineoplastic agents in three separate trials.[102-104] It has also exhibited antineoplastic properties against bladder cancer when used as both a single agent [105,106], and when used in combination with other anti-cancer agents.[107-109] Along with exhibiting effectiveness in the treatment of different forms of cancer, $Ga(NO_3)_3$ is able to combat these diseases without causing myelosuppression (bone marrow suppression), which is a trait that is rare amongst chemotherapeutics.[110] This unique property allows $Ga(NO_3)_3$ to be one of few drugs which can be administered to patients who have already been through extensive treatment and as a result, have a low amount of white blood cells. Other *in vitro* studies have also suggested that $Ga(NO_3)_3$ may not only be compatible with, but may be more effective, when used simultaneously with other antineoplastic agents such as hydroxyurea, interferon-α, and gemcitabine.[111-113]

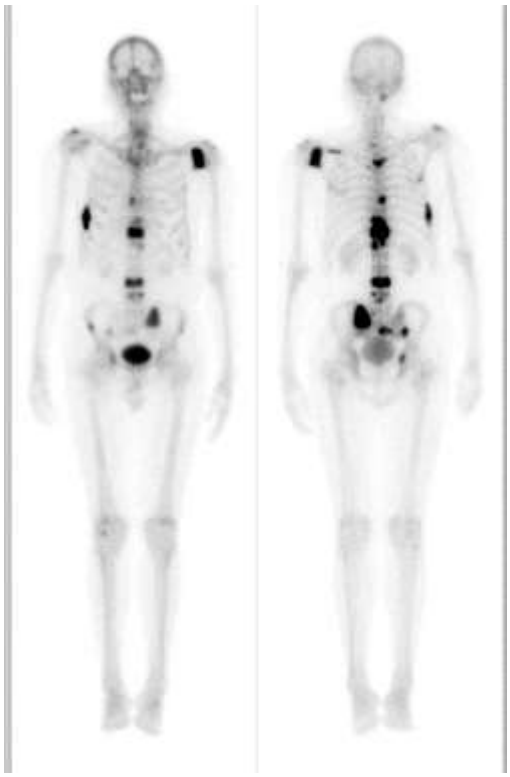

Figure 10. Bone scan using radioactive ^{67}Ga.[114]

In a 1983 study which was evaluating the antineoplastic properties of $Ga(NO_3)_3$, it was discovered that many patients who were receiving infusions of the drug were also experiencing decreasing levels of Ca in their bloodstreams.[100] This was an important discovery because hypercalcemia, which is characterized by elevated Ca levels in the blood, is a condition that is often contracted by cancer patients, with several different routes of contraction.[115] In some patients with malignant tumors, their tumors are capable of producing a protein that closely resembles PTH, and thus causes the release of excessive Ca from the patient's bones into the blood. Metastasis, or the spread of cancer, to a patient's bones, can also cause hypercalcemia. Cancer patients are also at elevated risk for developing hypercalcemia because their diseases may cause them to spend increased amounts of time sitting or lying down, which results in decreased load-bearing being performed by the bones, and can thus result in increased bone resorption and blood Ca levels. Since hypercalcemia is usually an indication of bone resorption, it is very important that the condition be corrected as soon as possible. This is why the discovery of the ability of $Ga(NO_3)_3$ to lower blood Ca levels was so intriguing, because it offers a

way to simultaneously treat different forms of cancer, while also preventing skeletal breakdown. In order to clinically evaluate the efficacy of $Ga(NO_3)_3$ against hypercalcemia, studies were conducted to compare the compound versus different bisphosphonate drugs, as well as calcitonin (which is a leading non-bisphosphonate drug), used to treat hypercalcemia. In one study, $Ga(NO_3)_3$ proved to be equally effective in controlling hypercalcemia when compared against the bisphosphonate drug pamidronate[116], while in another study, $Ga(NO_3)_3$ proved to be superior to the bisphosphonate drug etidronate.[117] Then, in a study against calcitonin, $Ga(NO_3)_3$ again proved superior in acutely controlling blood Ca.[118] Due to the effectiveness that was clinically exhibited during these studies, the $Ga(NO_3)_3$ drug Ganite™ was finally approved for management of cancer-related hypercalcemia by the Food and Drug Administration (FDA) in 2003.[119]

With $Ga(NO_3)_3$ already having proven effective against hypercalcemia, the question arose as to whether or not this compound might also contain the ability to inhibit bone turnover. In a study evaluating the effects of $Ga(NO_3)_3$ on bone turnover in patients with pre-existing bone metastases, decreased levels of urinary Ca excretion, hydroxyproline excretion, and ionized serum Ca and P were observed after seven days of treatment, indicating that $Ga(NO_3)_3$ reduces the biochemical markers associated with accelerated bone turnover.[120] A later study conducted by Warrell *et. al.* investigated the effects of administering $Ga(NO_3)_3$ in combination with standard anti-myeloma agents in patients with osteolytic disease (disease defined by accelerated resorption of bone matrix by osteoclasts), over a one year period[121], and the results indicated that when low doses of $Ga(NO_3)_3$ were added to the regular anti-myeloma drugs, the rate of bone turnover was dramatically reduced, suggesting that $Ga(NO_3)_3$ can be used under these circumstances to slow bone loss.

Another condition involving accelerated bone metabolism is Paget's disease of bone. Victims of this disease experience localized distortion in the rates at which old bone is broken down and new bone is constructed. This disease results in an increase in the rate of bone resorption, as well as an alteration in bone architecture and geometry as the osteoblasts cannot maintain the integrity of the bone when resorption rates are elevated.[122] Matkovic *et al.* evaluated the effects of $Ga(NO_3)_3$ on bone turnover in

patients with Paget's disease of bone[123], and after 5 days of being intravenously treated with $Ga(NO_3)_3$, patients exhibited significantly reduced serum Ca, P, and ALP levels, and urinary Ca and hydroxyproline excretion. Bockman *et al*. also evaluated the effects of $Ga(NO_3)_3$ against Paget's disease of bone[124], and discovered that the administration of $Ga(NO_3)_3$ resulted in a decrease in serum ALP, urinary hydroxyproline excretion, and N-telopeptide collagen cross-links excretion, indicating that lower quantities of bone were being dissolved by osteoclasts, and therefore the rate of bone resorption was slowed.

2.5.3. Antimicrobial Effects

Another factor which must be considered when designing implantable biomaterials is the risk of infection. Bioactive glasses are desirable materials not only because of their ability to leach ions which stimulate specific therapeutic responses, but also for their potential ability release ions which act as anti-microbial agents, helping to stave off infection within the body. Although many bioactive glasses specifically contain certain elements with proven anti-bacterial properties (e.g. Zn), a material becomes even more desirable if it contains more than one element which has the ability to help prevent infection. In addition to the various anti-cancer and bone-promoting properties Ga-containing compounds have expressed, they have also demonstrated their ability to act as anti-microbial agents. Olakanmi *et al.* investigated the effects of both $Ga(NO_3)_3$ and transferrin-Ga on the bacterial species *Mycobacterium tuberculosis* and *Mycobacterium avium*, discovering that these two Ga compounds acted to inhibit the iron (Fe)-dependent growth of the bacteria both extracellulary, and within human macrophages.[125] This was a logical result, as one of the proposed mechanisms behind the anti-neoplastic activity of Ga is interference with cellular acquisition of Fe. Kaneko *et al*. also investigated the effects of $Ga(NO_3)_3$ on *Pseudomonas aeruginosa* pneumonia in mice.[126] This investigation revealed that the Ga-compound inhibited the growth of *P. aeruginosa*, and also prevented the formation of biofilm. This study also revealed that $Ga(NO_3)_3$ again interfered with Fe uptake, resulting in the death of both planktonic and biofilm bacteria *in vitro*. In a 2009 study conducted by DeLeon *et al*., astonishing results were observed in a mouse model investigating the effects of the relatively new compound gallium maltolate ($Ga(C_6H_5O_3)_3$), against *P. aeruginosa*.[127] The results of this study were astonishing because in the control group, which received no $Ga(C_6H_5O_3)_3$, 100% mortality was

observed, while in the groups which received $Ga(C_6H_5O_3)_3$, 100% survival was observed. With all of these promising results demonstrating the ability of Ga-containing compounds to effectively halt the growth of *P. aeruginosa*, work is being done to try and utilize Ga against anti-biotic resistant *Pseudomonas* lung infections, which are often contracted by patients with cystic fibrosis. If it is found that Ga is indeed effective in this application, that will only add to the value of synthesizing bioactive glasses containing the element.

2.5.4. Pharmacological Activity

Despite all of the desirable medical properties that Ga has exhibited, the key to harnessing these properties and utilizing them in specific applications is to understand how this element interacts with other components within the body to elicit each unique response. An early study conducted in 1981 by Vallabhajosula *et al*., aimed to determine what causes ^{67}Ga to localize at the sites of malignant tumors.[128] In this study it was discovered that when injected into rabbits, radioactive ^{67}Ga citrate binds to the Fe transport protein transferrin, and will then circulate throughout the body. Since malignant cells such as lymphoma and bladder cancer cells are known to express large numbers of transferrin receptors[129,130], the preferential binding of ^{67}Ga to tranferrin upon injection resulted in higher concentrations of Ga at cancer cell sites. A separate study also demonstrated that *in vitro*, malignant cells uptake significantly larger amounts of ^{67}Ga when transferrin is added to the culture medium.[131] It has also been observed that small amounts of Ga can be incorporated into cells through mechanisms independent of transferrin transport[132,133], but most Ga is taken into cells *via* the transferrin receptor-facilitated pathway. The affinity of ^{67}Ga to bind to transferrin can be inferred when the similarities between Ga and ferric iron (Fe(III)) in terms of ionic radii (0.062nm and 0.064nm, respectively), and electronegativity (1.6 and 1.8, respectively), are considered. Despite the similarities between these two elements, non-radioactive Ga, which is utilized in drugs such as $Ga(NO_3)_3$, does not express the same affinity for binding to transferrin as radioactive ^{67}Ga. It has been shown that although non-radioactive Ga is capable of binding to both of the metal-binding sites on the transferrin molecule, it expresses an affinity 300 times less than ferric iron.[134] Despite the much lower affinity of non-radioactive Ga for binding to transferrin, only about one-third of circulating transferrin is occupied by Fe at any time anyway[93], so two-thirds of the transferrin present in the body

is free to be bound by Ga. The large amount of available circulating transferrin also poses a problem, as it has been shown that when patients were infused with 400-700 mg/m^2 of $Ga(NO_3)_3$ over a 30 minute period, 69% of it was excreted in the urine in the first 24 hours following the infusion, and 91% was excreted 48 hours after the infusion.[135] The same trend was observed at even higher doses. The large amount of available transferrin is great for the initial binding of Ga, but since the transferrin is circulating, it fully circulates much of the Ga completely out of the body at a rapid rate. This also poses toxicity issues as it is desirable to have larger amounts of Ga in a patient's system for longer periods of time, but in order to achieve this with brief periods of injection, higher concentrations of Ga-containing drugs must be administered. To address this problem, the current solution is to continuously infuse patients with drugs such as $Ga(NO_3)_3$ for extended periods of time (e.g. 7 days) with lower doses (e.g. 200 mg/m^2/day), rather than administering extremely high doses in brief infusions. This type of administration schedule allows the patient to achieve a steady-state plasma Ga level of about 1-2 µg/ml while receiving the infusions, and this level will slowly diminish once the infusions are completed.[135,136]

2.5.5. Mechanism of Action

Although it has been thoroughly demonstrated that Ga is primarily incorporated into malignant cells through the transferrin receptor-facilitated pathway, it is also critical that the mechanisms which actually allow Ga to combat these cells be understood. For comparison, the sequence of reactions that take place along the normal Fe-transferrin pathway are illustrated in Figure 11. After Ga has been introduced into the body, bound to transferrin, and transported to malignant cells, these cells will uptake the Ga-transferrin complexes through endocytosis.[137] The presence of these Ga-transferrin complexes then disrupts the metabolism of Fe in two different ways. First, the physical presence of Ga-transferrin complexes at the surface of a cell interferes with the cellular uptake of Fe, simply because many of the sites where the cell processes transferrin complexes are already occupied by Ga-containing complexes, resulting in less Fe being physically taken in by the cell.[138] The increased physical presence of these Ga-transferrin complexes also disrupts the metabolism of Fe by causing a disturbance in it's release from Fe-transferrin complexes. This disruption occurs in the period between when the Fe-containing

complexes are brought into the cell and when they are delivered to lysosomes for processing. During this period, the complexes are contained in endosomes, which act as a sort of cellular delivery package. Normally, these endosomes will easily recognize the Fe-transferrin complexes and will cause Fe to dissociate into the cytoplasm, but with the presence of Ga-transferrin complexes, less Fe content has been observed in the cytoplasm, indicating that less Fe is being dissociated from the Fe-transferrin complexes.[138] These two factors which disrupt Fe metabolism combine to inhibit the Fe-dependent function of the enzyme ribonucleotide reductase.[111] The presence of Ga within the cell decreases the presence of Fe, which ultimately means that there is less Fe to fill the R2 subunit of ribonucleotide reductase, and less activity of this enzyme will be observed.[139] Since this enzyme is essential for deoxyribonucleotide (DNA) synthesis, decreasing the Fe content within the cell, and thus decreasing the ribonucleotide reductase activity, causes the inhibition of DNA synthesis[140], and in the case of malignant cells, this is the main objective. It was also observed in a study conducted by Chitambar *et al*. that Ga also has the ability to directly inhibit the activity of ribonucleotide reductase in cell lysates.[141] This finding indicates that Ga inhibits the synthesis of DNA through methods that directly affect Fe transport within the cell, and methods which act directly on the enzyme.

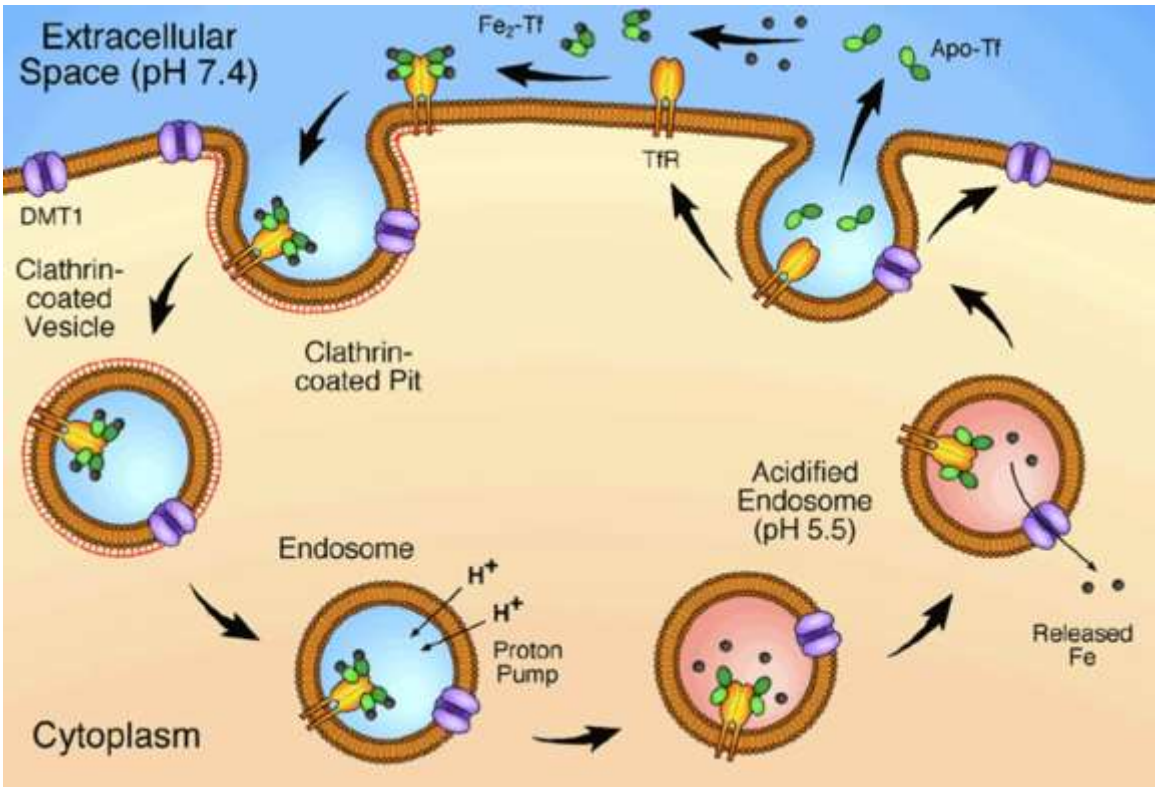

Figure 11. Mechanism of normal Fe-transferrin action.[142]

In studies observing the effects of Ga on lymphoma cells, it has been observed that Ga is also able to trigger cell death (apoptosis) in lymphoma cells, in addition to inhibiting DNA synthesis.[143] Using the compounds $Ga(NO_3)_3$ and $Ga(C_6H_5O_3)_3$, it was discovered that these compounds induce apoptosis in human lymphoma cells. It was then determined that the death of these cells was triggered by the cascade of reactions these compounds ignite in the mitochondria. The method by which these compounds are able to trigger apoptosis in the lymphoma cells is believed to be a four-step process, beginning with the activation of the protein Bax, which promotes apoptosis once activated. Upon activation, this protein undergoes a conformation shift and then attaches to the outer membrane of the mitochondria, ultimately resulting in the loss of membrane potential. This loss of membrane potential then stimulates the release of cytochrome C into the cytoplasm, which will then bind apoptotic protease activating factor.[144] The cytochrome C-containing complex will finally activate the protein caspase-3, which will carry out the physical execution of the lymphoma cell.[145,146] A second pathway has also been discovered which leads to the programmed cell death of human lymphoma cells. This

pathway is believed to begin when $Ga(NO_3)_3$ enters the cell and generates reactive oxygen species (ROS). The generation of ROS then triggers a cytoprotective response, which is eventually overwhelmed and results in the death of the cell.[146] Other mechanistic studies not involving human lymphoma cells have uncovered that the competition posed by the presence of Ga against magnesium (Mg) can result in the inhibition of Mg-dependent ATPase.[147] Additionally, it has been observed that the compound $GaCl_3$ possesses the ability to inhibit the polymerization of the protein tubulin, which may contribute to the antineoplastic activity expressed by Ga-containing compounds.[148]

The mechanism by which Ga interacts with bone metabolism has also been uncovered. It has been discovered that upon administration, Ga accumulates at two different sites in the bone, both in a dose-dependent manner. These two sites include the metaphysis of bone, which is the wide growth zone at the end of long bones[149], and the diaphysis of bone, which is the mid-section or the shaft of a long bone.[150] At these two sites, Ga accumulates at the interface between the collagen and the mineral components of the bone. Having Ga present at this interface alters the solubility of crystallized HCA, which ultimately allows the bone to resist resorption.[151] It has also been observed that the Ca content of bone significantly increases when treated with Ga, which also contributes to resistance against resorption. In addition, Ga has been shown to inhibit the activity of osteoclasts without killing them, demonstrating another pathway to prevent the resorption of bone.[151] Treatment with $Ga(NO_3)_3$ has also been shown to increase the expression of type 1 collagen and fibronectin in bone and fibroblast cells, demonstrating that Ga may act to not only resist the resorption of bone, but also to bolster its structure.[152] As previously stated, the ability to regulate serum Ca levels exhibited by Ga-compounds in cancer research and therapy has resulted in increased curiosity as to whether or not Ga might be useful in the treatment of disorders affecting bone metabolism without the presence of cancer. The main issue delaying the use of Ga to treat such conditions is the method by which Ga-containing compounds are currently administered, which is through continuous intravenous infusion. This type of administration is not feasible for the treatment of conditions such as osteoporosis, which is a long-term disease requiring constant, long-term treatment in order to slow the breakdown and maintain the strength of bones. Recently, a preliminary study conducted to evaluate the effects of an oral form of

Ga treatment provided encouraging results[153], but the lack of a concrete administration method is a part of what has inspired our use of Ga in bioactive glasses, in order to determine whether Ga might be effective in its ionic form upon dissolution from a glass matrix within the body.

3. Summary of Glasses Used in Current Study

In the current study, a glass series was synthesized with the formula $0.42SiO_2$-$0.10Na_2O$-$0.08CaO$-$(0.40–x)ZnO$-$(x)Ga_2O_3$, where (x = 0, 8, or 16 mol%), in order to include the previously detailed elements, while maintaining bioactivity. Si was incorporated to act as the primary glass network former, and to aid in the deposition of functional HCA surface layers upon submersion in physiological fluid. Na was included to act as the primary network modifier and to initiate the cascade of reactions which allows for the formation of a chemical bond between bone and implant upon implantation. Ca was included to not only aid in the deposition of HCA layers with functional Ca:P ratios, but also because of its demonstrated bone-promoting properties via glutamate-signaling pathways in osteoblasts. The inclusion of Zn was justified by its long list of benefits, including its anti-bacterial and anti-resorption properties, along with bone-promoting properties such as the upregulation of ALP activity and collagen synthesis. Finally, Ga was added as a constituent to this glass series in order to evaluate whether Ga^{3+} released from a glass network could provide some of the bone-promoting, anti-bacterial, and anti-cancerous properties exhibited by its pharmaceutical forms. Prior work[154], demonstrated that this glass series is soluble in aqueous media, and that the properties exhibited by these glasses can be tailored through the manipulation of the initial batch composition, suggesting bioactive properties, and thus justifying further study. Throughout this study, the bioactive, anti-bacterial, and anti-cancerous properties of this glass series were analyzed, and the results were extremely encouraging. As a result, work was also undertaken to develop a delivery mechanism by which these glasses could be delivered, and the therapeutic benefit could be localized and sustained at the site of the bone void. To achieve this goal, two different polymers were functionalized and cross-linked to form hydrogels, throughout which particles of these glasses were seeded to obtain glass-hydrogel composites. These composites were then thoroughly analyzed to

gather information pertaining to their molecular structures, and to evaluate their *in vitro* compatibility with an array of different cells.

Polymer Hydrogels

1. Hydrogel Properties

As previously stated, the primary focus of this research moving forward will be the development and characterization of hydrogels, which will be tailored to provide a structural scaffold and delivery system, upon which our Ga-containing bioactive glasses can be incorporated, that facilitates leaching of the beneficial ions from the glasses into the surrounding environment. In order to properly develop hydrogels for this application, we must first understand their inherent structures and properties. First developed by Wichterle and Lim for use as soft contact lenses[155], hydrogels can be defined as cross-linked networks of hydrophilic polymers, which contain large amounts of water (usually in the range of 30-95 wt%).[156] The presence of water drastically effects the properties of these materials and in the case of impregnating them with bioactive glasses and using them as implantable materials, higher water content can lead to increased rate of dissolution of the glass particles as the particles will be surrounded by fluid not only in the implanted environment, but within the material's structure. Increased water content can also promote diffusion through the material of not only substances such as oxygen and proteins from the environment, but also diffusion of the ions being released from the glass particles into the environment.[156] Increased water content also translates to a softer material, allowing for easier molding during implantation, and faster integration with tissues post-implantation.[156]

The cross-linking of these polymer networks can be achieved either chemically or physically, however, there are positive and negative consequences associated with both methods. In hydrogels where the polymer cross-linking is performed by a chemical process, as is performed in the current study, the resulting gel that forms is comprised of either an ionically or a covalently cross-linked network. These types of gels can be created through processes such as combining a polyelectrolyte with a multi-valent ion of opposite charge, combining polyelectrolytes of opposite charge, or by using a cross-linking agent to cross-link water-soluble polymers.[157] Chemical cross-linking leads to a

slightly more regular structure than physical cross-linking, which can result in increased mechanical strength, but also a decrease in biodegradability. In hydrogels where the polymer cross-linking is achieved through a physical process, the resulting gel that forms is held together by the entanglement of polymer chains, and/or secondary forces.[158] Physically cross-linked polymers will form a more amorphous structure than their chemically cross-linked counterparts, which can result in increased biodegradability at the expense of mechanical strength. Illustrations of both forms of cross-linking can be seen below in Figure 12. Regardless of the method used to induce cross-linking, cross-linked hydrogels will reach an equilibrium swelling point upon submersion in an aqueous solution. This equilibrium swelling point is mainly dependent on the cross-link density present within the network, which can be estimated as the molecular weight between links.[159]

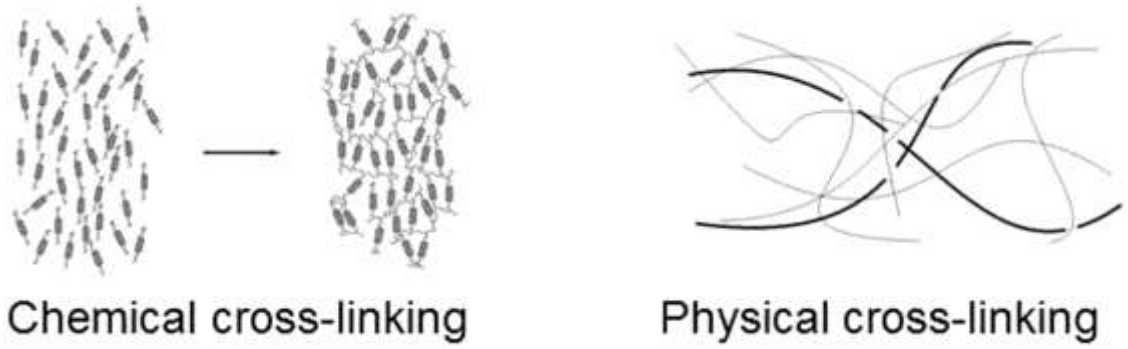

Figure 12. Illustrations of both chemical and physical cross-linking within polymer hydrogels.[160]

In addition to there being different methods for cross-linking polymer networks, there are also many different macro-molecular structures that can be formed. The three main structures observed in hydrogels are cross-linked networks of linear homopolymers (chains consisting of identical monomer units), networks of linear copolymers (chains consisting of multiple monomers), and graft copolymers (main chains and side chains are composed of different monomers).[157] Since hydrogels can exhibit several different structures, they can also exhibit several different physical forms such as solid molds (e.g. contact lenses), pressed powders (e.g. capsules for oral ingestion), coatings, membranes, and even liquids which can form gels upon the application or deprivation of heat. The

desired cross-linking method, macro-molecular structure, and ultimate physical form of a hydrogel are all dictated by the intended application, which is why one must understand all three aspects of these materials in order to properly tailor their hydrogel to adequately perform in a specific setting.

As briefly discussed earlier, the water content of a hydrogel impregnated with glass particles can determine the permeability of nutrients into the gel, and ionic dissolution products out of the gel. When a dry hydrogel is created, and water is then added, the first water molecules to interact will become the "primary bound water". These water molecules enter the polymer matrix and hydrate the most polar, hydrophilic groups present.[157] As hydration of these polar groups proceeds, the overall network begins to swell, resulting in the exposure of hydrophobic groups to the ingressing water molecules. These hydrophobic groups will lightly bind water molecules, resulting in what is known as "secondary bound water".[157] The combination of the "primary" and "secondary" water molecules is called the "total bound water" and is an important characteristic when characterizing hydrogels. Beyond this point, the network can still absorb more water. The amount of additional water that can be endured by the gel is determined by the degree of opposition between the osmotic driving force of the polymer chains to achieve infinite dilution, and the inherent cross-link density of the polymer network. When these two forces are equal, the hydrogel will have reached its equilibrium swelling point. All of the water that is contained within the network that is not "bound" water is called "free water", and this "free water" is believed to occupy the spaces between chains and any pores that may be present throughout the structure. The total amount of water present in a hydrogel is what will determine the absorption and diffusion of solutes throughout the network.

2. Hydrogels Used in Current Study

Once the structures of hydrogels are understood, it is then important to investigate the different raw ingredients that can potentially be used. Hydrogels can be made from either natural or synthetic polymers, but again, there are positive and negative consequences associated with both forms. Natural polymers, such as collagen and fibrin, are biocompatible, biodegradable, and are readily solubilized in physiological fluid. However, there are also several problems associated with natural polymers including potential immunogenicity, disease transmission, and difficulty in processing, since they are derived from a biological source. These natural polymers are also mechanically weak and can experience rapid degradation upon implantation, which can be detrimental in some scaffold applications.[161] Synthetic polymers, such as polylactic acid (PLA) and polyethylene glycol (PEG) possess less potential for immunogenicity and disease transmission, while also providing the ability to tailor the chemical and mechanical properties of the gel. However, synthetic polymers do have the potential to induce acute and/or chronic inflammatory responses, and to possibly cause localized pH decreases due to degraded by-products.[161]

In this study, hydrogels will be formed by mixing two naturally-sourced polymers, carboxymethyl cellulose, sodium salt (CMC) and dextran (Dex), which will be synthesized, functionalized, lyophilized, dissolved in phosphate buffered saline solution (PBS), and then simultaneously plunged through a dual-chambered syringe in order to initiate polymerization via hydrazone bond formation. Images of these gels after swelling and lyophilization are displayed in Figure 13. These two polysaccharides were chosen to be the basis of these hydrogels because of their biocompatibility and slow degradation rates within the body, as exhibited by Hudson *et al*.[162]

Figure 13. Swollen and lyophilized forms of hydrogels used in the current study.

As these polysaccharides degrade slowly within the body, the hydrogels are expected to deliver the beneficial ions leaching out of the seeded glass particles into the local environment for significant durations of time (up to 30 days). As these gels also have been proven to polymerize within a matter of seconds, and to conform to the shapes of molds[23], their high degree of physical moldability is another key reason as to why these two polymers have been selected to form hydrogel scaffolds for *in situ* delivery of the Ga-containing bioactive glasses.

3. Polymers Used in Current Study

3.1. Carboxymethyl Cellulose (CMC)

Carbohydrates are the most abundant organic compounds on Earth, comprising ¾ of the dry weight of all plant matter.[163] The carbohydrate cellulose, which is the world's largest renewable resource, is a polydisperse polymer with an average degree of polymerization (DP) on the order of 3,500-36,000.[163] Native cellulose is the principle component of cotton, hemp, flax, and wood, and its molecules exist in thread-like strands called "fibrils". Although these fibrils are relatively linear, they are not water-soluble due to the presence of strong intermolecular hydrogen bonding. As can be seen in Figure 14, which displays the native cellulose structure with the constituent carbon molecules labeled, these fibril are made up of many D-glucose units joined by β(1→4) linkages.

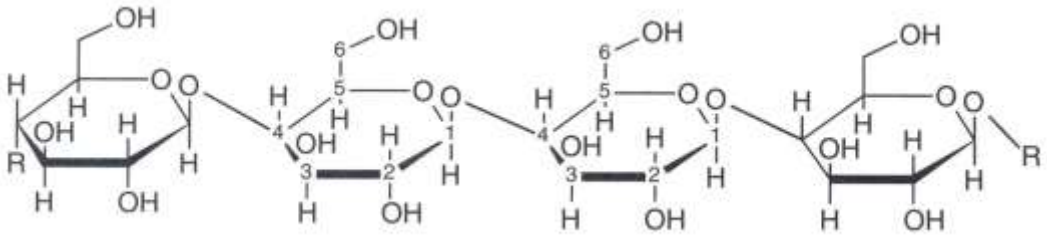

Figure 14. Cellulose structure with the carbons of the glucoside repeat units labeled.[163]

As can be seen in Figure 14, these linear fibrils align with the hydroxyl groups held on the outside of the chain, which provides for close contact and hydrogen bond formation between neighboring chains. The hydrogen bonding between chains results in the formation of rigid, insoluble fibers, which is why this material is found in the cell

walls of plants. Although cellulose is often used in its native form as fibers for textile and paper, the dissolving of the native material requires strong solvents such as inorganic acids, ammonium hydroxide, and lithium chloride to break the hydrogen bonds. In order to ease the manipulation of this material without using strong solvents, cellulose can be reacted with different compounds to produce water-soluble forms. In the current work, the chosen water-soluble form is called sodium carboxymethyl cellulose, and it is formed through the reaction of sodium chloroacetate with basic cellulose solutions, which is described below, and can be seen in Fig 15.

$$\text{Cellulose-OH, NaOH} + \text{Cl-CH}_2\text{COONa} \rightarrow \text{Cellulose-O-CH}_2\text{-COONa}$$

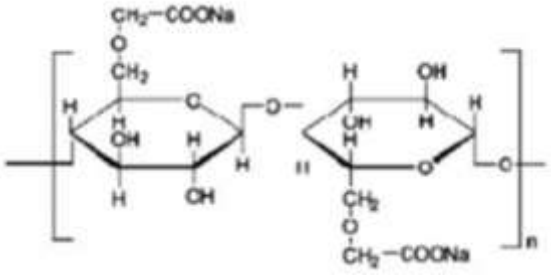

Figure 15. Structure of the cellulose derivative sodium carboxymethyl cellulose.[164]

Although cellulose can be converted to derviative forms such as sodium-CMC which allow for less hazardous handling, it is important to note that these materials are still comprised of β-linkages, which cannot be broken down by enzymes in the human body. These linkages can be broken down by stomach acid over time, but not nearly as readily as α-linkages, so in order to prevent negative reactions towards degradation products, one should aim to use CMC chains with a lower DP when designing implantable biomaterials.

In the current study, CMC was functionalized with hydrazine groups (H_2NNH_2), to form CMC-hydrazide (CMC-ADH), following the method published by Bulpitt and Aeschlimann[165], and the results can be seen in Figure 16. Hydrazines were coupled to the carboxyl group of the water-soluble derivative sodium CMC using adipic hydrazide and *N*-hydroxysulfosuccinimide (Sulfo-NHS), and the water-soluble carbodiimide used to perform the coupling was 1-ethyl-3-[3-dimethylaminopropyl] carbodiimide (EDC). In an attempt to limit the variety of amines added to the CMC chains, the pH of the solution

was maintained at 6.8 from the time Sulfo-NHS was added, to the completion of the reaction when dialysis was performed.

Lyophilized CMC-ADH

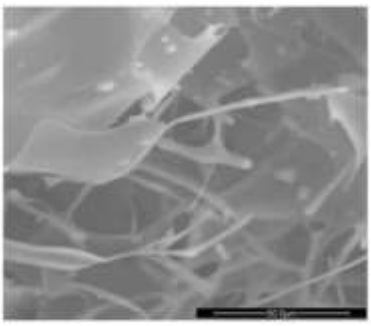

Lyophilized CMC-ADH (SEM)

Figure 16. Image and SEM micrograph of functionalized CMC-ADH obtained in the current study.

3.2. Dextran (Dex)

Another polysaccharide which is formed by the linking of D-glucose units is called dextran. Dextrans can be defined as high-MW, branched, extracellular polysaccharides, which are synthesized by bacteria through the breakdown of sucrose.[163] Dextran-producing bacteria can be found in many places, with one of the most prevalent being inside the human mouth, where they feed on sucrose-containing food trapped between teeth. The high-MW of dextran contributes to the build-up of dental plaque and can clog the filters and pipes beneath sinks, however, this same property can also be capitalized upon, allowing for the utilization of dextran as blood-plasma substitutes (MW $\approx 10^6$ Da), and molecular sieves (MW $\approx 10^9$ Da).[163] As the glucose molecule possesses a number of reactive sites, there are several different dextran structures which can occur, and these can be seen in Figure 17.

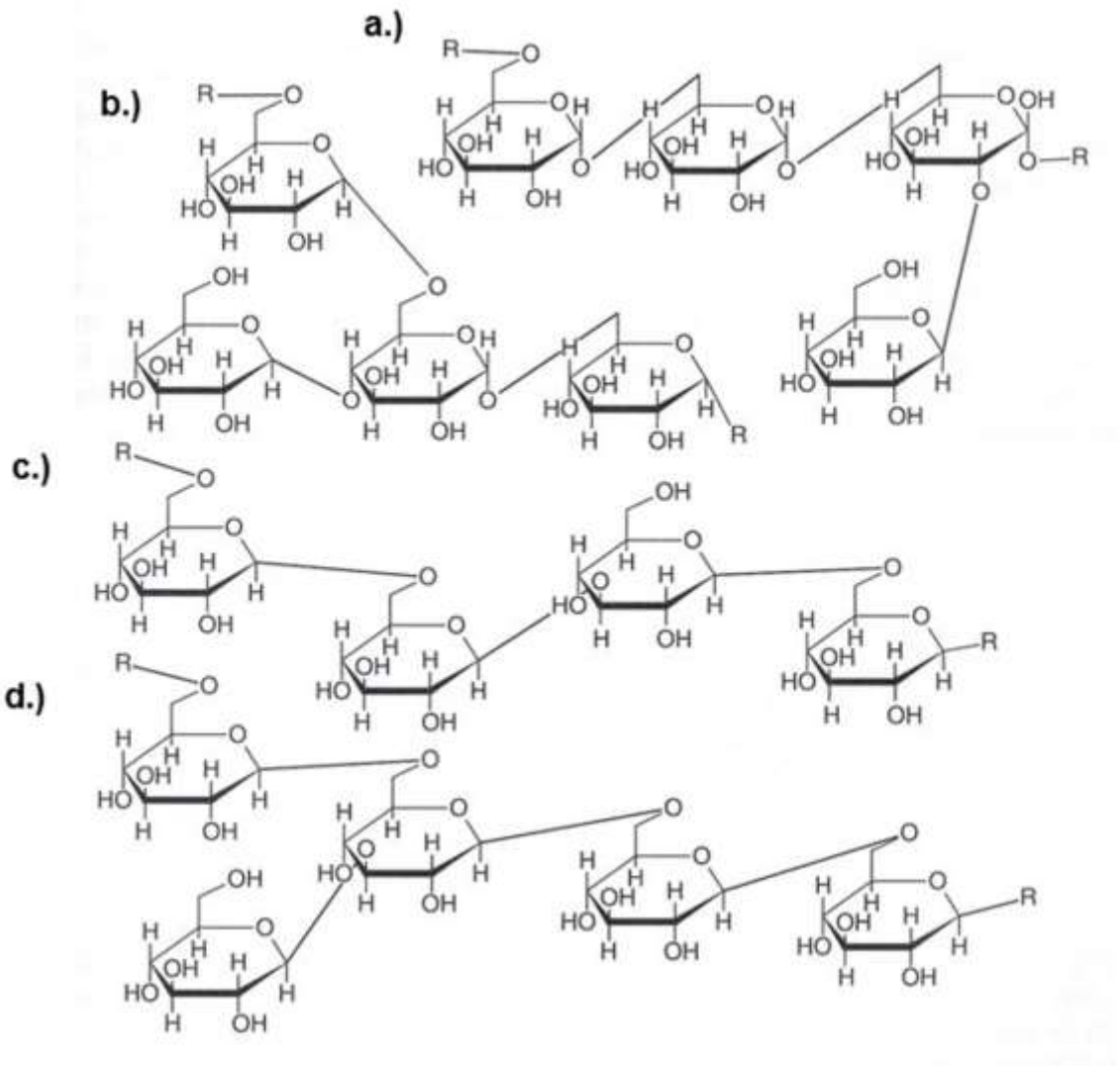

Figure 17. Structures of different possible dextran arrangements. Glucose units exhibit: a.) α(1→2) branch (top right), b.) α(1→4) branch (top left), c.) α(1→6) and α(1→3) linear linkages (middle), and d.) α(1→3) branch (bottom).[163]

As can be seen in Figure 17, dextran is a polysaccharide consisting of D-glucose chains with α(1→6) linkages, and the most common structures contain branches stemming from α(1→3) linkages.[166] This figure displays 4 possible dextran structures, with the top left containing an α(1→4) branch, the top right containing an α(1→2) branch, the middle containing a linear chain with both α(1→6) and α(1→3) linkages, and the bottom structure illustrating a linear glucose chain of α(1→6) linkages with an α(1→3) branch. It is important to note that dextrans contain all α-linkages, which are capable of being lysed by enzymes in humans, allowing for the degradation of these

chains to energy-providing glucose units.[163] This property of dextran renders it an excellent candidate as an implantable biomaterial, as its degradation products (which are excreted by our own natural processes), would not only be harmless to the host (so long as these degradation products were not of extremely high-MW), but beneficial, as they would simply be converted to food (glucose). Additionally, dextran possesses abundant pendant hydroxyl functional groups, which makes it highly amenable to chemical modification.[167]

In the current study, dextran was modified through periodate oxidation using the method published by Bruneel and Schacht[168], in order to obtain dextran-aldehyde (Dex-CHO). This oxidation leads to the opening of the glucose unit, and introduces aldehyde groups. In the case of α(1→6)-linked anhydroglucoside units, as are found in dextran, total oxidation is a two-step process, which first generates an α-hydroxy aldehyde group, which can then be subsequently oxidized further to obtain formic acid and a dialdehyde group (Figure 18). The resulting polymer which was obtained in the current study can be seen in Figure 19.

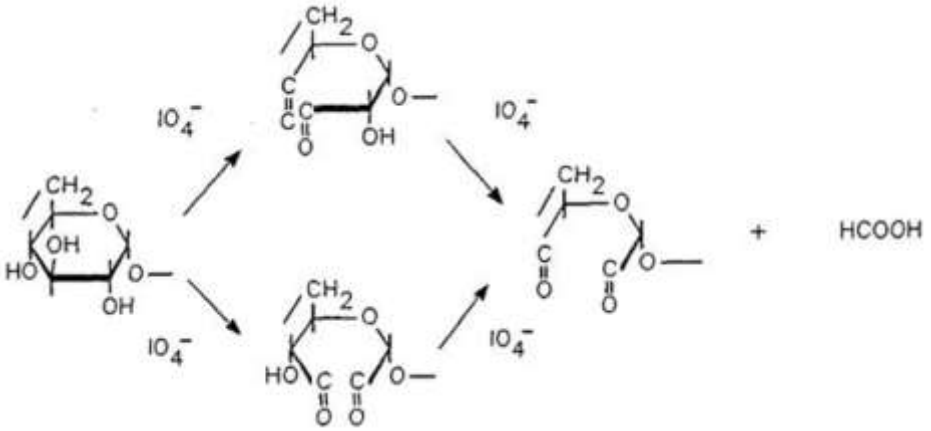

Figure 18. Oxidation of an α(1→6)-linked anhydroglucoside unit (dextran).[168]

Figure 19. Image and SEM micrograph of functionalized Dex-CHO obtained in the current study.

3.3. Method of Cross-Linking

The methods of functionalization of CMC and Dex in this study were selected because the amino compounds (e.g. hydrazine groups) added onto the CMC chains can be coupled with the polyaldehydes formed by Dex through periodate oxidation to form Schiff base structures.[168] This reaction can be seen in Figure 20, which displays the hydrazone group that is formed as a result of the combination of these two functional groups. These hydrazone bonds act as the cross-links in these hydrogels and have been shown to be durable *in vivo*[162], with degradation of these bonds only being expected to occur due to eventual hydrolytic cleavage and the action of inflammatory cells.

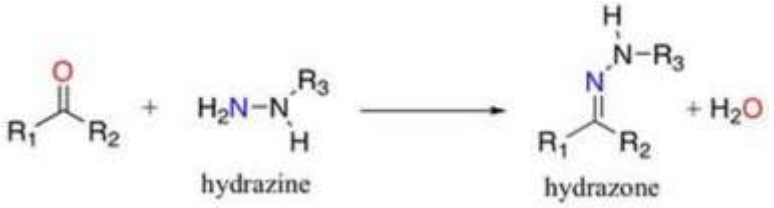

Figure 20. Formation of a hydrazone bond from an aldehyde and a hydrazine group.[169]

4. Reported Properties of CMC/Dex Hydrogels and Composites

The main focal points of the current study were to fully evaluate the bioactivity of the Ga-containing glass series, and to successfully impregnate polymer hydrogels with these glasses in order to create composite materials which could theoretically be cross-linked *in situ* into critical-sized bone defects, and induce osteostimulation while also

potentially providing anti-bacterial, anti-fungal, and anti-cancerous effects. A hydrogel matrix based on the cross-linking of functionalized forms of CMC and Dex was selected for this study, as prior work conducted by Hudson *et al*. had characterized the possible degrees of functionalization to obtain for Dex based on $NaIO_4$ addition, the ideal concentrations of functionalized polymer to use when cross-linking, and the anti-fungal efficacy of these gels when combined with the anti-fungal agent amphotericin B (AmB).[162] The prior study had synthesized Dex-CHO using different amounts of $NaIO_4$ addition to obtain degrees of functionalization ranging from 33-75%, and found that uniform and durable hydrogels were obtained using each functionalized Dex. However, to eliminate variables in the study, Dex-CHO that was obtained when 64 mol% $NaIO_4$ ($[IO_4^-]$/[glucose] x 100) was added was used for all data collection, which resulted in Dex with a 48% degree of functionalization. It was also discovered that the molecular weight of dextran was significantly reduced by the oxidation reaction, and that more highly oxidized polymers exhibited the lowest molecular weights. Additionally, the degree of dextran oxidation achieved was much lower than predicted from the mol% of periodate added, which is thought to possibly be due to the formation of a stable six-membered hemiacetal which may act to protect the aldehydes from further reaction.[168] The prior study did however, not vary the degree of functionalization of CMC, and 51% functionalized CMC was used in all trials. It was then determined that to obtain the most homogeneous and durable gel discs (retaining their shape for 3 weeks when suspended in PBS), 2.5% wt/volume CMC-ADH and 6% wt/volume Dex-CHO were to be used, with increased concentration of the highly viscous CMC-ADH resulting in poor mixing, and increased Dex-CHO concentration resulting in no increase in mechanical properties.[162] Work was also carried out to determine the anti-fungal efficacy of gel composites containing AmB against *C. albicans*. It was found that both composites which physically entrapped AmB during cross-linking, and composites in which AmB was conjugated to Dex-CHO prior to cross-linking, exhibited significant anti-fungal abilities when in direct contact with *C. albicans*, while only composites with conjugated AmB were shown to release anti-fungal extracts.[162] Finally, this study showed that these gels do not induce negative effects *in vivo*, and that they have the ability to remain at the site of injection for the duration of therapy.

5. Rationale for Use in Current Study

Currently, to combat invasive fungal infections, therapies are required which act through prolonged administration (two weeks or more) of anti-mycotic agents, and are then followed by therapy with an oral agent, which in the case of candidal osteomyelitis, can last up to a year.[170] While receiving intravenous therapy, patients are not only exposed to the hardships and risks of maintaining constant intravascular access over a period of multiple weeks, but they are also at risk for the systemic side effects that can be introduced by some anti-mycotics, such as nephrotoxicity for AmB.[162] Also, as previously discussed, many cancer pharmaceuticals require either prolonged intravenous administration or heavy dosing, both of which can result in serious complications. Additionally, bioactive glasses have the potential to provide many benefits as bone void-filling materials, such as the ability to form a chemical bond between bone and implant, and the ability to release therapeutic ions into a localized environment, however, the currently available delivery mechanisms leave much to be desired. Ideally, composite materials like those synthesized in the current study, would be able to provide multiple therapies to a local area, including osteostimulative, anti-bacterial, anti-fungal, and anti-cancerous properties, all from a single injection, for durations comparable to those used in systemic therapies, and at concentrations that would be extremely difficult to obtain through the use of systemic therapy. It has been shown that composite materials containing these CMC/Dex gels cross-link *in situ* and remain at the injection site for extended periods of time, exhibiting anti-fungal properties without inducing immune responses from healthy tissues, which is why it has been hypothesized that composites combining these gels with the Ga-containing glass series will be able to retain their shapes for multiple weeks, and exhibit anti-bacterial, anti-fungal, and potentially, anti-cancerous properties, without inducing toxic effects in healthy tissue.

6. Expected Results in Current Study

The current study was broken into four stages of work, and this work was conducted in a manner which continuously built upon what had been previously discovered, in order to garner an understanding of these materials in terms their physical properties, their interactions with cell cultures, bacteria, and fungi, and culminated with

an in-depth investigation into their molcular structures. In the first stage, the long-term solubility of the glass series was analyzed, and the cytocompatibility of the liquid extracts produced were then evaluated against healthy fibroblasts and osteoblasts. Next, glass-hydrogel composites were synthesized, with 3 different levels of glass-loading, and the physical properties of these materials were analyzed, as well as their solubility and cytocompatibility with fibroblasts and osteoblasts, over a period of 30 days. After obtaining solubility and cytocompatibility information for both the glasses and the glass-hydrogel composites, the anti-bacterial and anti-fungal potential of these materials were then evaluated against the Gram (+ve) bacteria *Staphylococcus aureus*, the Gram (-ve) bacteria *Escherichia coli*, and the fungus *Candida albicans*. Finally, insight into the structures of the glass-hydrogel composites was gained through the use of thermal analysis and ^{13}C cross-polarization magic angle spinning nuclear magnetic resonance (^{13}C CP/MAS-NMR), and the anti-cancerous potential of these materials was gauged. Based on the prior work conducted using this glass series[154], we expected that these glasses would exhibit long-term solubility, and that these dissolution products would not inhibit the viability of healthy fibroblasts nor osteoblasts. We also expected to be able to successfully functionalize CMC and Dex to obtain CMC-ADH and Dex-CHO, and to successfully cross-link these polymers in the presence of glass particles to obtain glass-hydrogel composites. Based on prior work[162], we then expected these composites to retain their shapes for several weeks while still releasing glass dissolution products into solution, and we expected these released ions to also prove to be compatible with healthy fibroblast and osteoblast cells. Additionally, we anticipated that both the glasses by themselves, and in combination with the hydrogels, would express anti-bacterial abilities towards the Gram -ve *E. coli*, as these bacteria possess thinner barriers to the outside environment than Gram +ve bacteria such as *S. aureus*[171], and that they would potentially express some efficacy towards inhibiting the growth of *C. albicans*. Heading into the 4th and final stage of the work, we expected to confirm that we had indeed been able to functionalize CMC and Dex, that we had synthesized glass-hydrogel composites that were held together by hydrazone cross-links, and we expected to find that Ga-containing liquid extracts from the glasses and glass-gel composites would express some inhibitive effects towards the viability of cancerous osteosarcoma cells, and potentially towards

cancerous myeloma cells as well. Throughout this study we obtained many of the expected results, however, we also found in several instances, that the experimental outcomes were much different than anticipated.

Part I: Relating Ion Release and pH to *in vitro* Cell Viability for Gallium-Inclusive Bioactive Glasses

Keenan T.J., Placek L.M., McGinnity T.L., Towler M.R., Hall M.M., and Wren A.W., "Relating Ion Release and pH to *in vitro* Cell Viability for Gallium-Inclusive Bioactive Glasses", *Journal of Materials Science*, 51(2), p. 1107-1120 (2016).

The first part of this study focused solely on the characterization and cytocompatibility analysis of the Ga-containing glass series. This section discusses the results pertaining to the glass series in terms of:

- Particle size analysis
- Thermal analysis
- HA-deposition during incubation in simulated body fluid
- Scanning electron microscopy and energy-dispersive x-ray spectroscopy
- Surface area analysis
- Long-term solubility in ultrapure water
- pH evaluation
- Cell viability analysis (L-929 Fibroblasts, MC3T3-E1 Osteoblasts)

For this portion of the study, a bioactive glass series in which Ga was substituted for Zn was investigated to determine whether the ionic form of Ga (Ga^{3+}), can elicit effects similar to the pharmaceutical $Ga(NO_3)_3$. After incubation at 37ºC for one year, the glass (*TGa-1*) containing the smaller Ga-addition (8 mol%) released the most Na^+ (1420 mg/L), Si^{4+} (221 mg/L), and Ga^{3+} (1295 mg/L), while the glass (*TGa-2*) containing the larger Ga-addition (16 mol%), exhibited release levels between *TGa-1*, and the 0 mol% Ga (*Control*) glass. The pH of all 3 glass extracts steadily increased over time, with maximums observed after 365 days for *Control* (10.0), *TGa-1* (12.2), and *TGa-2* (9.7). Cell viability analysis suggested that Ga^{3+}-release over long time periods produced toxic effects in L-929 fibroblasts, with less than 3% viability for both *TGa-1* and *TGa-2* extracts after 90, 180, and 365 days, however, no significant decrease in MC3T3-E1 osteoblast viability was observed for *TGa-1* extracts after any time period, despite the higher ion release and pH values, and a significant decrease to 51.4% viability was only

observed for *TGa-2* extracts after 365 days. These results suggest that tailoring the release of Ga from BG is not only possible, but also beneficial to the host, thus rendering such glasses potentially useful in bone void-filling applications.

IA. Introduction

Bioactive glasses (BGs) are materials which have been formulated for applications in dental and orthopedic surgery and can be used to aid in the repair or restoration of mineralized tissues which have sustained injury as a result of either disease or traumatic injury. Upon implantation, partial dissolution of the BG surface occurs, as ion exchange is conducted between the glass surface and the surrounding aqueous medium, ultimately resulting in the formation of a chemical bond between the implanted material and the surrounding tissue.[172] The most well-known BG, Bioglass® 45S5, was developed by Hench *et al.* in 1969. With a composition of 45%SiO_2-24.4%Na_2O-24.4%CaO-6%P_2O_5 (wt%), a thin apatite layer forms at the glass-tissue interface upon implantation into a living host, which then facilitates a strong chemical bond between the implant and bone tissue.[4] From these findings, engineers began to design implantable materials with the intent to bond and interact with host tissues, rather than remaining separate and inert upon implantation.[23]

In addition to forming strong interfacial bonds between the implant and the host tissue, ionic dissolution products from BGs can elicit other beneficial effects. For instance, it has been observed that the release of silicon and calcium from Bioglass® 45S5 results in a dramatic increase in osteostimulation, which is characterized by an increase in both alkaline phosphatase activity and DNA production in osteoblasts, translating to increased proliferation and differentiation.[173] BGs can be formulated to include different elements which, upon dissolution from the glass network in their ionic forms, can elicit specific therapeutic effects. One of the most common additional elements to be incorporated in BGs is zinc (Zn), which can increase osteostimulation.[174] The increase in collagen and calcium content that accompanies osteostimulation increases the compressive and flexural strengths of the bone, resulting in increased mechanical properties.[175] Zn is also included in BGs because it exhibits toxicity towards pathogenic bacteria such as *Staphylococcus aureus* (Gram +ve), and *Escherichia coli* (Gram -ve), which cause opportunistic infections at the site of implantation.[176]

Although Zn is included in our glass series, the element of most interest in this study is gallium (Ga). Ga has been incrementally substituted for Zn in these glasses (8 and 16 mol%), for several reasons. Although there have been some recent studies

conducted on the structural role of Ga in different BG compositions, and the effects its inclusion may have on *in vitro* interactions with simulated body fluid (SBF)[177-179], decades of research have been dedicated to investigating Ga in its pharmaceutical form, gallium nitrate ($Ga(NO_3)_3$). This compound has exhibited the ability to suppress the growth of subcutaneously implanted tumors in mice and rats, while also exhibiting low toxicity compared to other anti-cancer compounds.[99] Gallium nitrate has displayed effectiveness against an array of cancer types, most notably against non-Hodgkin's lymphoma[100-104], and bladder cancer.[105,106,108,180] In addition to exhibiting effectiveness in the treatment of different forms of cancer, gallium nitrate has also been shown to combat these diseases without causing myelosuppression (bone marrow suppression)[110], which is a trait that most chemotherapy drugs cannot claim. It has also been shown to decrease levels of calcium in the bloodstream of patients undergoing cancer therapy[118,181,182], and to reduce the biochemical markers associated with accelerated bone turnover.[120]

Although the effects of Ga^{3+} have not been studied nearly as thoroughly as the pharmaceutical form ($Ga(NO_3)_3$), the potential ability to harness some of the same therapeutic abilities through release of Ga from a BG network justifies this investigation. Here, a glass with a starting composition of $CaO\text{-}Na_2O\text{-}ZnO\text{-}SiO_2$ was employed. Calcium (Ca^{2+}) and sodium (Na^{+}) act as network modifiers within this glass system, and promote glass dissolution and ion exchange, while silicon (Si^{4+}) acts as the network former. Zinc (Zn^{2+}) can act as a network intermediate, assuming either a network-forming or network-modifying role.[178] However, the principal purpose of this study is to evaluate the effect that gallium (Ga^{3+}) has on the structure, long-term solubility, and *in vitro* cytocompatibility of this glass system. Ga^{3+} is a glass network intermediate[178,183], which has prompted studies in which Ga^{3+} has been investigated as a substitute for aluminum (Al^{3+}) in glassy materials[184], and is the reason why it has been substituted for Zn^{2+} in prior work conducted by the authors.[183] However, its effect on the long-term solubility of this system has not yet been determined. This study aims to investigate the influence of Ga_2O_3 addition on BG solubility over extended time periods (up to 1 year), and to determine if this influence translates to effects on the *in vitro* cell viability of L-929 Fibroblasts and MC3T3-E1 Osteoblasts.

IB. Materials & Methods

1. Glass Synthesis

Three glasses were formulated for this study: Two Ga-containing glasses (*TGa-1, TGa-2*) and a Ga-free CaO-Na_2O-ZnO-SiO_2 glass *(Control)*. The Ga-containing glasses *(TGa-1, TGa-2)* contain incremental concentrations of Ga_2O_3 at the expense of ZnO (Table 1). The powdered mixes of analytical grade reagents (Fisher Sci., PA, USA) were mixed using silica beads, and then oven dried (100ºC, 1 h) and fired (1500ºC, 1 h) in platinum crucibles and shock quenched into water. The resulting frits were dried, ground using a Gy-Ro Mill (Glen Creston Ltd, South West London, UK) in 10 second intervals at 3400 rpm, and sieved to retrieve glass powders with a maximum particle size of 90μm.

Table 1. Glass Compositions (mol. fr.)

	Control	***TGa-1***	***TGa-2***
SiO_2	0.42	0.42	0.42
Ga_2O_3	0.00	0.08	0.16
ZnO	0.40	0.32	0.24
Na_2O	0.10	0.10	0.10
CaO	0.08	0.08	0.08

1.1. Preparation of Cell Culture/Ion Release Extracts

50g of each glass (*Control, TGa-1 and TGa-2*, where *n=3*) was sterilized using γ-irradiation at 25kGray (Isotron ltd, Mayo, Ireland) prior to incubation. Ultrapure water obtained using a Milli-Q water purification system (EMD Millipore, MA, USA) was selected as the solvent to prepare extracts. A surface area of 1 m^2 of each sample (n = 3), was aseptically immersed in 10 mL of the ultrapure water and agitated for periods of 1, 7, 14, 30, 90, 180, and 365 days at 37°C. Each of the subsequent extracts were prepared for ion release analysis by adding 1 ml aliquots (n = 3) of each extract to 9 ml of ultrapure water, to create a 1:10 dilution. 10 µl aliquots (n = 3) of each extract (except for 14 day extracts), were later used for cell viability analysis.

1.2. Preparation of Glass Plates for SBF Testing

Analytical grade reagents (Fisher Sci., PA, USA) were batched according to Table 1, and mixed using silica beads in order to obtain powdered mixes. These mixes were then oven dried (100°C, 1 h) and fired (1500°C, 1 h) in platinum crucibles. Glass castings were then produced by pouring the molten glass into graphite molds. After cooling for 1 h, the glasses were removed from the molds and annealed at their respective glass transition temperatures (T_g). The glass casts were then shaped into plates with approximate dimensions of 15x3x3 mm. These dimensions were achieved by first cutting with a diamond blade on an Isomet 5000 Linear Precision Saw (1500 rpm, 0.4 mm/min), and then by grinding with 60 µm silicon carbide grinding paper (Buehler, IL, USA) on a Phoenix 4000 grinding machine.

2. Glass Characterization

2.1. Particle Size Analysis

Particle size analysis was performed using a Beckman Coulter Multi-Sizer 4 Particle Size Analyzer (BeckmanCoulter, CA, USA). Glass powder samples were suspended in ultrapure water and evaluated in the range of 0.4 µm – 20.0 µm, with a run time of 60 s. Relevant volume statistics were calculated and reported for each glass.

2.2. Thermal Analysis

The glass transition temperature (T_g) of each glass was measured using an SDT Q600 Simultaneous DSC-TGA (TA Instruments, DE, USA). The samples were heated at a rate of 10˚C/min between 30˚C and 1300˚C in an air atmosphere with alumina in a matched platinum crucible as a reference. .

2.3. Simulated Body Fluid (SBF) Study

SBF was produced in accordance with the procedure outlined by Kokubo *et al*[185]. The composition of SBF is outlined in Table 2. The reagents were dissolved in order, from reagent 1–9, in 500 ml of ultrapure water using a magnetic stirrer. The solution was maintained at 36.5 ˚C. 1 M-HCl was titrated to adjust the pH of the SBF to 7.4. Ultrapure

water was then used to adjust the volume of the solution up to 1L. Glass plates (*n = 1*) were each immersed in 10 ml of SBF, and were subsequently stored for 1, 7 and 14 days in an incubator, at 37˚C.

Table 2. SBF Recipe

Order	Reagent	Amount Added
1	NaCl	7.996 g
2	$NaHCO_3$	0.35 g
3	KCl	0.224 g
4	$K_2HPO_4.3H_2O$	0.228 g
5	$MgCl_2.6H_20$	0.305 g
6	1M-HCl	40 ml
7	$CaCl_2$	0.278 g
8	Na_2SO_4	0.071 g
9	$NH_2C(CH_2OH)_3$	6.057 g

2.4. Scanning Electron Microscopy (SEM) and Energy Dispersive X-ray Spectroscopy (EDAX)

A Quanta 200F Environmental Scanning Electron Microscope was used to image the samples under a vacuum at a pressure of 0.90 torr. The electron beam was used at an accelerating voltage of 20 kV and a spot size of 4.0. Energy dispersive x-ray spectroscopy was carried out using an FEI EDAX system equipped with a silicon-drift detector.

2.5. Accelerated Surface Area and Porosity (ASAP)

The surface area of each glass was determined using the Accelerated Surface Area and Porosimetry (ASAP) 2010 System Analyzer (Micrometrics Instrument Corp., GA, USA). Approximately 60 mg of each glass was used with a mixture of nitrogen and helium gases, to calculate the specific surface areas through the Brunauer-Emmett-Teller (BET) method.

2.6. Ion Release Profiles

Powder samples were weighed out to contain 1 m^2 of glass per incubation sample (n=3), and were then submerged in ultrapure water for periods of 1, 7, 14, 30, 90, 180, and 365 days. After the incubation times were complete, the aqueous solution from each sample was removed and filtered using Amicon® Ultra-4 Centrifugal Filters (Merck KGaA, Darmstadt, Germany). Dilutions of each extract were then prepared (1:10), and ion release analysis was performed. Solutions were analyzed for Na, Ca, Si, Zn, and Ga content.

The ion release profile of each glass was measured using Inductively Coupled Plasma – Optical Emission Spectroscopy (ICP-OES) on a Perkin-Elmer Optima 8000 (Perkin Elmer, MA, USA). ICP-OES calibration standards for Ca, Si, Na, Zn and Ga ions were prepared from stock solutions on a gravimetric basis. Three target calibration standards were prepared for each ion, and ultrapure water was used as a control.

2.7. pH Testing

The pH of each extract solution was measured using an Accumet® Excel XL 15 pH meter (Fisher Scientific, NH, USA). 3 ml aliquots of each sample (n=3) were removed from the 10 ml extract solutions and placed into separate sterile 15 ml centrifuge tubes for pH analysis in order to avoid contamination of extract solutions prior to cell viability analysis.

3. Cell Viability Analysis

The established cell lines L-929 (American Type Culture collection CCL 1 fibroblast, NCTC clone 929), and MC3T3-E1 Osteoblasts (ATCC CRL-2593), were used in this study. L-929 fibroblasts were cultured, as required by ISO10993 part 5 [186], in HyClone® Medium 199/EBSS (Thermo Scientific, MA, USA), which included Earl's balanced salts and L-glutamine, and was supplemented with 10 vol% fetal bovine serum (Thermo Scientific, MA, USA). MC3T3-E1 osteoblasts were cultured in HyClone® MEM Alpha Modification (1X) media (Thermo Scientific, MA, USA), which included L-glutamine, ribonucleosides, and deoxyribonucleosides, and was supplemented with 10 vol% fetal bovine serum (Thermo Scientific, MA, USA). Cells were maintained on a

regular feeding regime in a cell culture incubator at 37˚C, with a 5% CO_2/95% air atmosphere. Cells were then seeded into 96 well plates at a density of 10,000 cells per well and incubated for 24 hours prior to the addition of extracts. The cytotoxicity of glass extracts were evaluated using the Methyl Tetrazolium (MTT) assay. 10 µl aliquots of undiluted extract were then added into wells containing cells in culture medium (100 µl), and incubated for an additional 24 hours. 10 µl of the MTT assay was then added to each well and incubated for an additional 4 hours. After 4 hours, the cultures were removed from the incubator, and the resultant formazan crystals were dissolved by first removing all of the aqueous media from each well, and then adding 100 µl of MTT Solubilization Solution (10% Triton x-100 in Acidic Isopropanol. (0.1 n HCI)). Once the crystals were fully dissolved, the absorbance was measured at a wavelength of 570 nm using a µQuant Plate Reader (Bio-Tek Insturments, Inc., VT, USA). 10 µl aliquots of ultrapure water were used as control additions, and cells were assumed to have metabolic activities of 100%. Glass extracts in media without cells were also tested, and were found not to interfere with the MTT assay.

4. Statistical Analysis

Particle size data for BG particles are presented as means ± standard deviations, and represents 3 trials per glass. Ion release, pH, and cell assay data are also presented as means ± standard deviations, and represents data from 3 individual extract replicates per glass, per incubation interval. One-way analysis of variance (ANOVA) was used to compare both ion release, and cytocompatibility of the BG extracts in relation to 1) incubation time, and 2) Ga-content. Comparison of relevant means was performed using the post hoc Bonferroni test. Differences between groups were deemed significant when $p < 0.05$.

IC. Results

1. Glass Characterization

1.1. Particle Size Analysis

Particle size analysis was conducted for each glass powder sample, and the results are presented in Figure 21. Mean particle size was similar for each glass at 11.1 µm, 10.3 µm, and 10.2 µm for *Control*, *TGa-1*, and *TGa-2*, respectively.

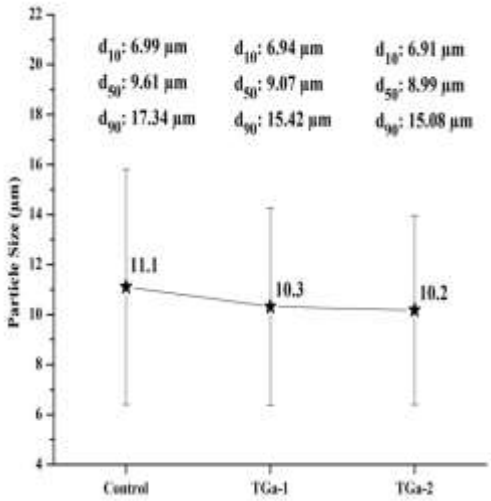

Figure 21. Particle sizes of Ga-glass series.

1.2. Thermal Analysis

DTA results are presented in Figure 22, and show that the glass containing the highest Ga concentration (*TGa-2)* exhibited the highest T_g of 614°C, along with the highest crystallization temperature (T_c) at 832°C. The glass with lower Ga-content (*TGa-1*) exhibited a slightly lower T_g (597°C) and T_c (774°C) and the Ga-free glass (*Control*) exhibited the lowest T_g (586°C) and T_c (732°C). *Control* glass also clearly exhibited a second crystallization temperature at 879ºC, along with a melting temperature (T_m) of 977ºC, which was higher than both *TGa-1* (947ºC) and *TGa-2* (938ºC).

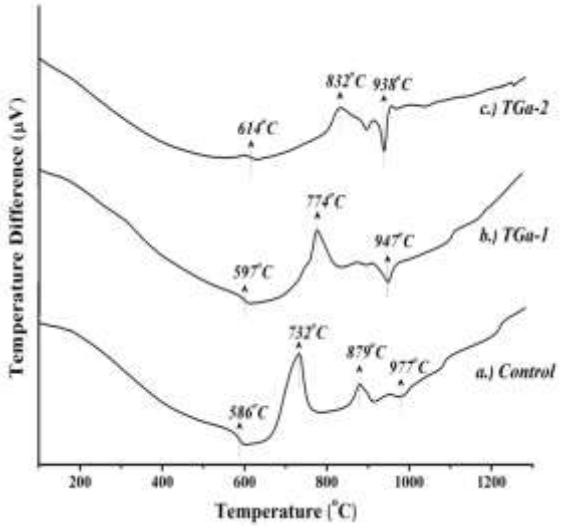

Figure 22. Differential thermal analysis of Ga-glass series.

1.3. SEM to visualize Ca/P depositions on Glass Surfaces

SEM micrographs of the *Control*, *TGa-1*, and *TGa-2* glasses after 30 days of incubation in SBF at 37°C, along with the corresponding EDAX spectra for the observed surface depositions, are presented in Figure 23. Depositions on the surface of the *Control* glass exhibit similar morphology and appear to be apatite-like depositions[187,188], which was further suggested by the presence of Ca, P, and O in the EDAX spectra. However, there appears to be depositions of two different basic morphologies on the surfaces of both the *TGa-1*, and *TGa-2* glasses. EDAX analysis revealed that both the larger, agglomerated depositions, and the smaller, dendritic depositions on the glass surfaces contained Ca, P, and O, although quantitative information revealed there were large differences in the Ca:P ratios of the different depositions

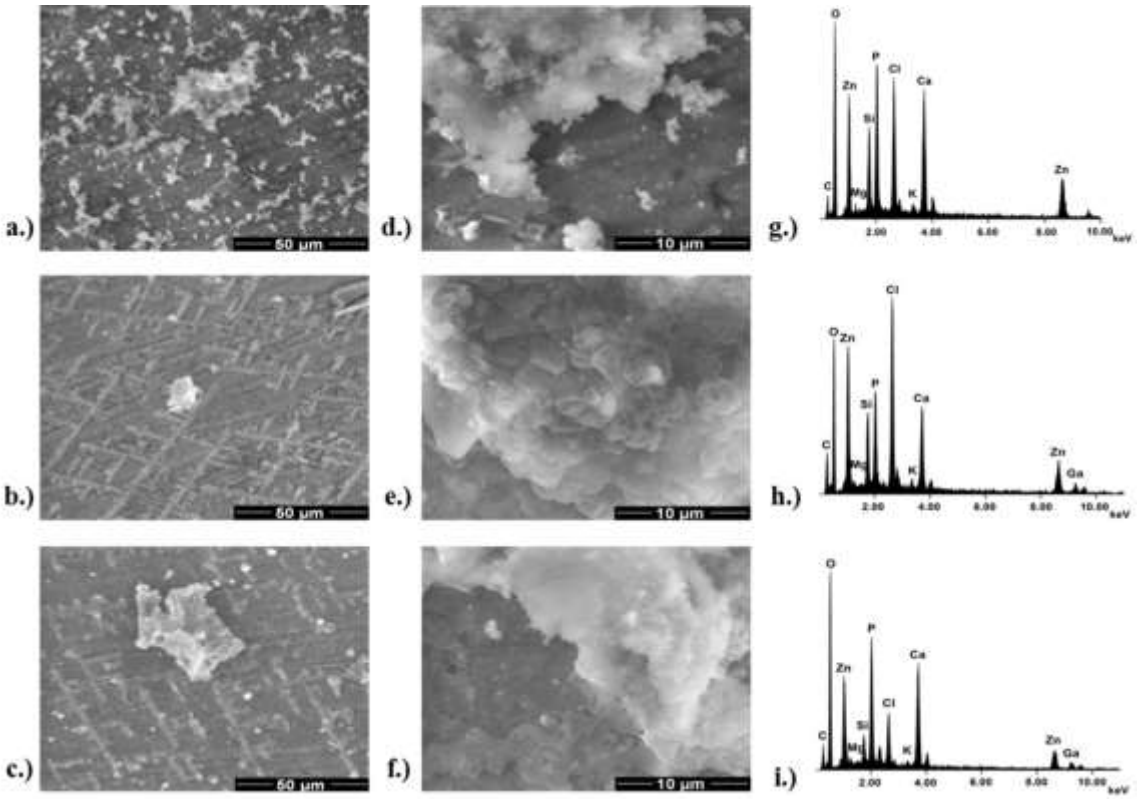

Figure 23. SEM micrographs and EDAX spectra for depositions on surfaces of a,d,g.) Control , b,e,h.) TGa-1, and c,f,i.) TGa-2 glass surfaces after 30 days.

1.4. Surface Area Determination

Prior to incubating glass powder samples in order to obtain extracts to be used in ICP-OES, pH, and cell viability analysis, the amount of surface area available for each sample was normalized using gas adsorption in combination with the BET method. Powder samples exhibited an average surface area of 2.28 m^2/g, 1.55 m^2/g, and 1.79 m^2/g for the *Control*, *TGa-1*, and *TGa-2* glasses, respectively. Each glass was then weighed out to obtain 1 m^2 of powder per incubation sample. The surface area of each glass, as well as the corresponding amount of glass used in each sample can be seen in Table 3. Glass additions were calculated to be 0.439g, 0.645g, and 0.559g for the *Control*, *TGa-1*, and *TGa-2* glasses, respectively.

Table 3. Surface Area and Weight Added per Incubation Sample for Ga-Glass Series

	Surface Area (m^2/g)	Wt. / Incubation Sample (g)
Control	2.28	0.439
TGa-1	1.55	0.645
TGa-2	1.79	0.559

1.5. Elemental Analysis of Ions Released From Glasses

The Na-release of each glass over the different time periods is presented in Figure 24a, and displays similar trends for all three sample types. Na-release was observed, but remained relatively constant for the first 30 days of incubation for all glass types, and then an increase in Na-release occurred for all sample types after 90 days. *Control* glass released the least amount of Na over the year-long incubation period, with a release of 22.1 mg/L observed after 30 days, and a maximum release of 179.4 mg/L after 365 days. *TGa-1* glass released a small amount of Na over the shorter incubation periods, releasing 16.6 mg/L after 30 days, but released much more Na after 90, 180, and 365 days than the other two glasses, with a maximum of 1419.7 mg/L after 365 days. *TGa-2* glass released 20.9 mg/L of Na after 30 days, and then fell between the other 2 glasses over the longer time periods, releasing a maximum of 565.9 mg/L after 180 days, and exhibiting a very slight decrease to 556.4 mg/L after 365 days.

The Si-release profiles for each glass can be seen in Figure 24b, which exhibits similar trends for all 3 glass types. *Control* glass released the least Si over each time period, at 11.5 mg/L after 14 days, then decreasing to just 1 mg/L after 30 days. This same trend was observed after long-term incubation, as a maximum of 135.3 mg/L was released after 180 days, which then decreased to 107.1 mg/L after 365 days. Similar trends were seen in the *TGa-1* glass, with short- and long-term maxima of 23.2 mg/L and 296.2 mg/L after 14 and 180 days, respectively, and with short- and long-term minima of 9.8 mg/L and 221.4 mg/L after 30 and 365 days, respectively. Again, *TGa-2* exhibited the same trends, with short- and long-term maxima of 66 mg/L and 193.3 mg/L after 14 and 180 days, respectively, and with short- and long-term minima of 30.2 mg/L and 126.6

mg/L after 30 and 365 days, respectively. It is noteworthy that there was no significant difference in Si-release after 365 days between *Control* and *TGa-2* extracts.

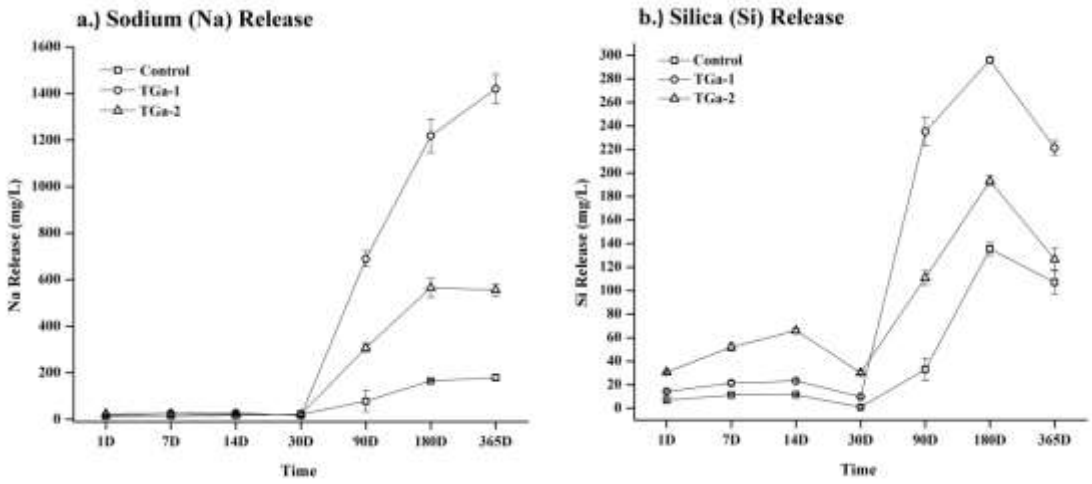

Figure 24. a.) Na- and b.) Si-release profiles for Ga-glass series.

Ca-release profiles are presented in Figure 25a, with all three glasses releasing much less Ca than either Na or Si. Although trends are much less clearly observed for Ca-release, it can be seen that for incubation periods of up to 30 days, *TGa-2* released more than both *Control* and *TGa-1*, and all of the glasses exhibited similar short-term trends to what was observed in the Si-release profiles, with maxima after 14 days, and then slight decreases after 30 days. There was no significant difference in Ca-release between the three glasses after 90 days, and there were again long-term maxima observed after 180 days for the two Ga-containing glasses, which then decreased after 365 days. Also, although *TGa-2* released significantly more Ca (8.3 mg/L) than both the *Control* (1.9 mg/L, p=0.012) and *TGa-1* (2.3 mg/L, p=0.016) after 365 days, the amount of Ca released from each glass was not statistically different from their respective amounts in solution after just 30 days.

Zn-release information is presented in Figure 25b, displaying low release totals for all 3 glasses. After 30 days, the *Control*, *TGa-1* and *TGa-2* glasses had each only released 0.3 mg/L of Zn. The amount of Zn released exhibited a significant change after 180 days when compared to 30 day solutions for all 3 glasses, with *Control*, *TGa-1*, and *TGa-2* releasing 4.9 mg/L, 6.5 mg/L, and 5.9 mg/L, respectively. As with Si and Ca, a significant decrease in Zn-release was observed for each glass after 365 days.

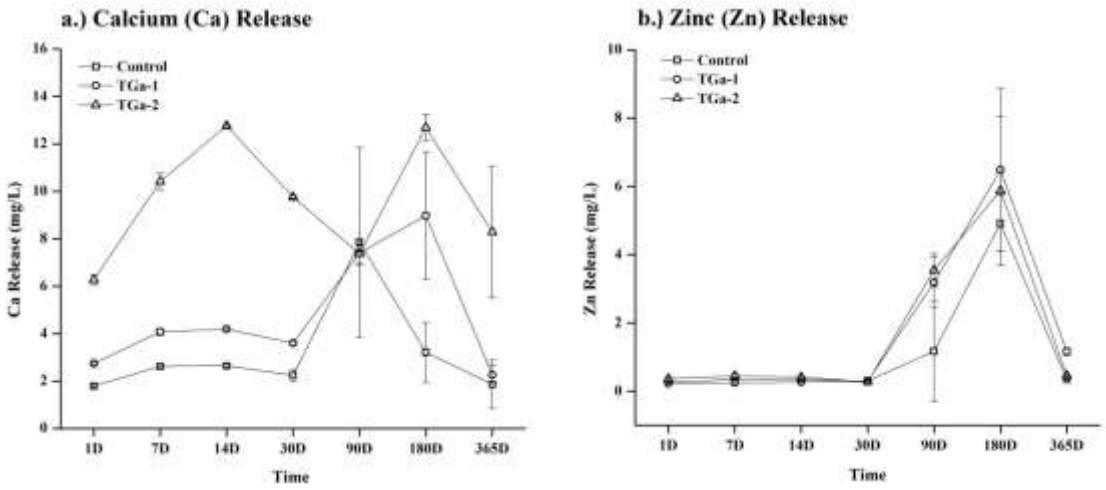

Figure 25. a.) Ca- and b.) Zn-release profiles for Ga-glass series.

Ga-release profiles are presented in Figure 26. As seen in the Si- and Ca-release profiles, maxima in the short-term incubation period occurred after 14 days, with *TGa-1* and *TGa-2* releasing 19.6 mg/L and 123.9 mg/L, respectively. Then, after 30 days, the amount of Ga in solution decreased to 3.4 mg/L and 19.8 mg/L for *TGa-1* and *TGa-2*, respectively. Beyond 30 days, both glasses exhibited substantial increases in Ga-release, and there was not a significant difference observed between the two until the final 365 day period, when *TGa-1* had released 1295.3 mg/L, and *TGa-2* had released 1006.3 mg/L.

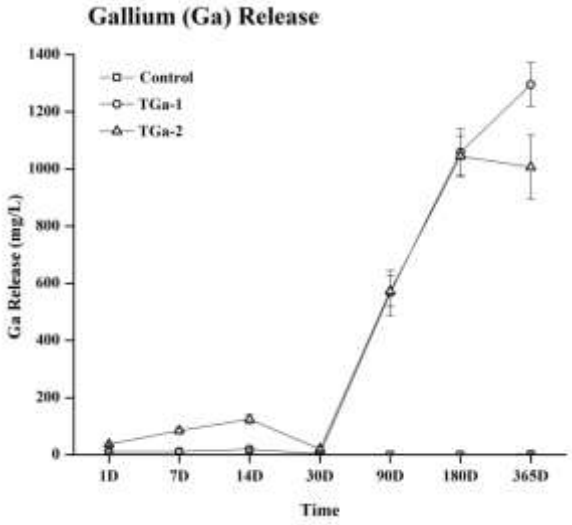

Figure 26. Ga-release profiles for Ga-glass series.

1.6. pH of BG Extracts

pH data for all 3 glasses are presented in Figure 27, and shows pH fluctuations which are very similar to the observed Si-, and Na-release profiles. As with Si- and Na-releases, all 3 glasses exhibited very similar pH levels after 30 days, with *Control*, *TGa-1*, and *TGa-2* expressing pH's of 7.2, 7.4, and 7.4, respectively. Also in line with the trend observed in the Si-release profiles, *Control* and *TGa-2* expressed similar pH levels after 365 days of 10.0 and 9.7, respectively, while *TGa-1* possessed a higher pH of 12.2.

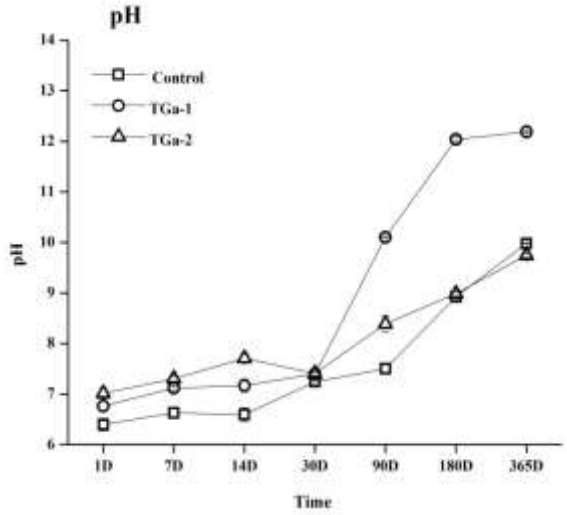

Figure 27. pH of extracts from Ga-glass series.

2. Cell Viability Analysis

2.1. L-929 Fibroblast Viability

Cell viability analysis was conducted using the extracts which were obtained from incubating glass powder samples in ultrapure water. Figure 28a presents L-929 fibroblast viability data for extracts obtained after 1, 7, and 30 day incubation periods, and shows that viability was not effected by any of the 3 glasses after 1 and 7 days, but was nearly equally reduced by all 3 glasses after 30 days, with *Control*, *TGa-1*, and *TGa-2* glasses expressing average viabilities of 68.4%, 77.6%, and 79.2%, respectively. Figure 28b presents the results of cell viability analysis after 90, 180, and 365 day incubation periods, and shows that the *Control* glass extracts only slightly reduced viability (90.6%, 90.7%, and 96%, respectively), compared to the extract-free control cells over all 3 time

periods, while both *TGa-1* and *TGa-2* exhibited significant decreases in viability. *TGa-1* extracts obtained after 90, 180, and 365 days decreased viability to 2%, 0.9%, and 1.1%, respectively, while the *TGa-2* extracts produced similar viability levels of 3%, 1.3%, and 0.8%, respectively.

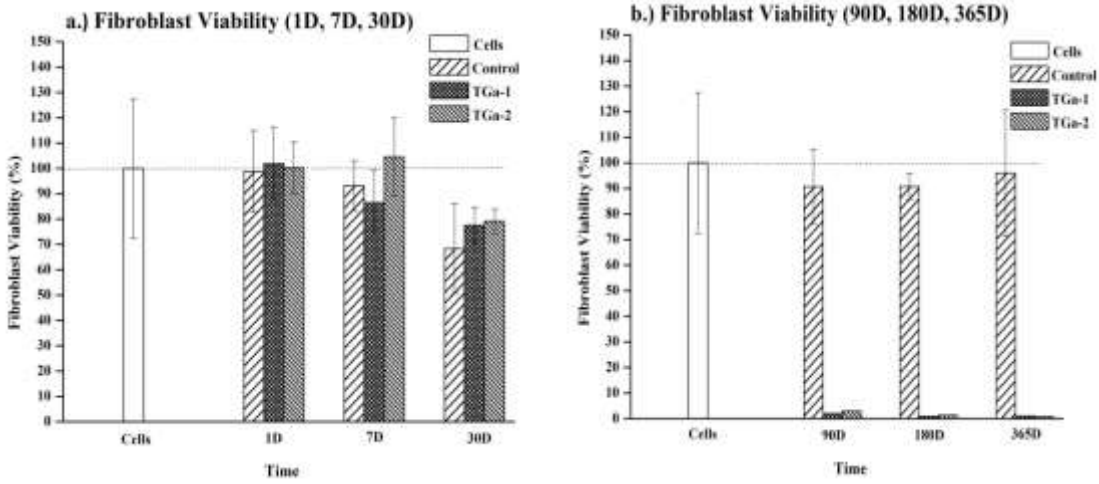

Figure 28. L-929 fibroblast viability for extracts of Ga-glass series obtained after a.) 1, 7, and 30 days, and b.) 90, 180, and 365 days.

2.2. MC3T3-E1 Osteoblast Viability

MC3T3-E1 osteoblast viability data for extracts obtained from all 3 glasses after 1, 7, and 30 days are displayed in Figure 29a, and shows that osteoblast viability exhibits some small changes over these time periods. However, statistical analysis proved that none of these fluctuations were significant at a 95% confidence level with respect to incubation time or Ga-content. Extracts removed after 1 day of incubation resulted in a slight decrease for *Control* (89.6% viability), while increases of nearly equivalent magnitudes were observed for *TGa-1* and *TGa-2* as they expressed viabilities of 117.1% and 120.2%, respectively. However, after 7 days, *Control* and *TGa-1* extracts expressed nearly identical viabilities of 114.1% and 115.8%, respectively, while *TGa-2* extracts caused a decrease to 86.7% viability. The trend once again changed after 30 days, as extracts of *TGa-1* and *TGa-2* produced viabilities of 121% and 132.4%, respectively, while *Control* extracts resulted in an average viability of 93.4%. Figure 29b presents MC3T3-E1 viability data for extracts obtained from the 3 glasses after 90, 180, and 365 days, and exhibits more consistent trends than were observed over the shorter time

periods. In this data, a general decrease in viability with respect to time was observed for all 3 extract types. After 365 days, the presence of *Control* and *TGa-1* extracts exhibited insignificant decreases to 71.6% and 64% viability, respectively, while *TGa-2* extracts exhibited a significant decrease to 51.4% (p=0.01) viability. The only significant viability decreases within data sets for the same extract types, were observed for *TGa-2* extracts between 1 and 365 days (p=0.047), and between 30 and 365 days (p=0.009).

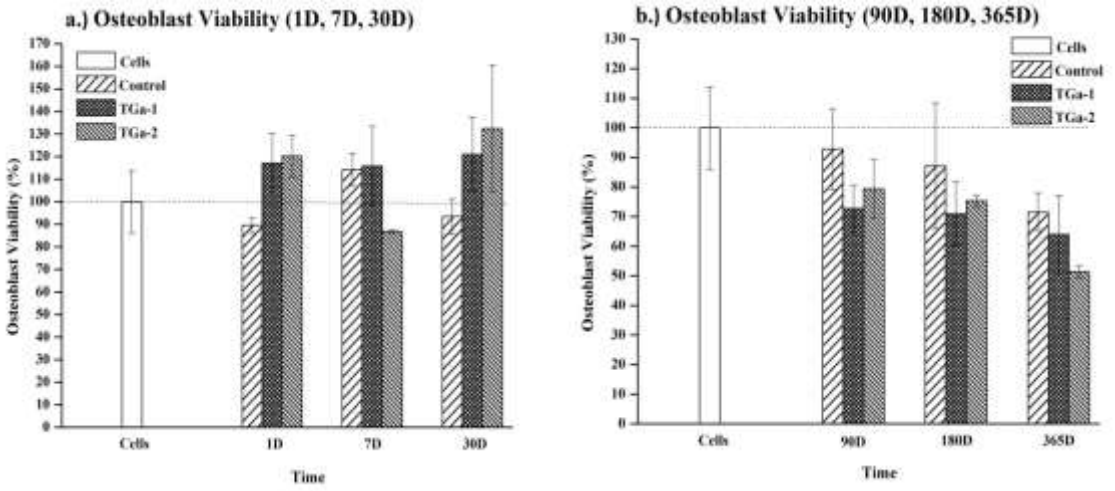

Figure 29. MC3T3-E1 osteoblast viability for extracts of Ga-glass series obtained after a.) 1, 7, and 30 days, and b.) 90, 180, and 365 days.

ID. Discussion

1. Glass Characterization

In a study published in 1980 by Gross *et al.*, it was observed that the additions of multi-valent cations such as aluminum (Al) and titanium (Ti) to glass compositions based on 45S5 Bioglass® resulted in the inhibition of rapid bonding to bone tissue in animal models, due to decreased solubility of the implants.[189] However, if the intention of an implant is to deliver a payload of therapeutic ionic dissolution products over an extended period of time, then perhaps there is a tailorable limit of multi-valent cations which can be added to a batch composition to allow for both bone-bonding, and long-term ionic dissolution. A core goal of this study is to demonstrate an ability to control the stability of the glass structure and its relationship with glass dissolution, while also exhibiting the ability of the Ga-containing glasses to release potentially therapeutic ions, including Si, Ca, Zn, and Ga. We also aim to demonstrate that these glasses will allow calcium phosphate to deposit on their surfaces, in order to demonstrate the possibility of using these glasses as implant materials, and potentially harness some of the anti-cancerous and bone-promoting properties that the Ga ion may possess.

DTA was conducted in order to determine if the incorporation of Ga into the glass network would influence T_g. Increasing Ga-content caused an increase in T_g and T_c, suggesting that the addition of Ga into these glasses creates a more stable structure with a reduced tendency towards crystallization, implying that Ga is acting primarily as a glass network former. This concurs with structural characterization work previously conducted on this glass series[183], which utilized ^{29}Si-MAS-NMR to show that increased Ga-content resulted in a larger presence of higher-ordered Q-species, suggesting that increased Ga-content results in a more connected glass structure, comprised of a higher fraction of bridging oxygens (BO) between Si ions.

SBF studies are a preliminary *in vitro* method used to simulate the immersion of a sample into physiological fluid, in order to evaluate whether or not the multi-step cascade of events will be triggered, and result in the deposition of calcium phosphate on the sample surface.[185] The SEM images and EDAX spectra show that although depositions containing Ca, P and O did not deposit with as much uniformity across Ga-containing glass surfaces as they did across the *Control* glass, they did deposit. In addition,

evaluation of quantitative information obtained through EDAX revealed that *TGa-1* was the only glass upon which depositions with Ca:P ratios similar to stoichiometric hydroxyapatite (HA) were seen. Depositions on the surface of the *Control* glass possessed a Ca:P ratio of 1.10 (based on wt% detected), while the smaller, dendritic depositions present on the surface of *TGa-1* possessed a Ca:P ratio of 1.74, which is much closer to the Ca:P ratio of 1.67 possessed by stoichiometric HA. The dendritic depositions seen on the surface of *TGa-2* possessed a Ca:P ratio of 1.00. In addition, the larger, brighter depositions seen on the surfaces of both *TGa-1* and *TGa-2* possessed respective Ca:P ratios of 1.29 and 1.08. This information suggests that the increased presence of Ga from 8 mol% to 16 mol% reduced solubility and caused irregular depositions to form on the glass surfaces, and that based on the Ca:P ratios of surface depositions, *TGa-1* is a stronger candidate than *TGa-2* to allow stoichiometric HA to deposit on its surface, and function as a bioactive scaffold.

A vital characteristic of a BG is the ability of the surface to react with an aqueous environment through ion exchange. In order to study *in vitro* ion release, ICP-OES was employed, and revealed several unexpected trends. A previous study conducted by Ahmed *et al.* demonstrated that as the ratio of glass network-former (P_2O_5) to glass network-modifier (Na_2O) in glass fibers increased, T_g increased, while solubility in distilled water decreased.[190] Prior studies such as these, along with our current DTA results, lead us to hypothesize that increased glass network stability would lead to lower ionic dissolution upon submersion in aqueous solution. However, for each of the 5 elements analyzed, the lowest release totals were actually observed from the Ga-free *Control* glass, assuming that precipitation of ions out of solution did not occur at different rates between samples. Although the Na- and Zn-releases were nearly equal between *Control* and *TGa-2* after 30 days, significantly more Si was released from the 16 mol% Ga-containing *TGa-2* than *Control*, with *TGa-1* releasing a quantity between the two. These results directly contradict our predictions, as it was expected that increased Ga-content would correlate with increased stability, but these ion release results show that as Ga-content increases, more of the primary glass network-forming constituent (Si), is released, suggesting that increased Ga-content translates to faster dissolution of the glass over a period of 30 days. However, the long-term trials (90, 180, 365 days) show that the

8 mol% Ga-containing *TGa-1* glass exhibits greater release of each constituent (other than Ca), than *TGa-2*. This trend leads us to suspect that a threshold exists, pertaining to the amount of Ga that can be included in such a BG formulation before ion release begins to be inhibited, and Ga^{3+} begins to act less like a modifying glass network intermediate, and more like the intermediate Zn^{2+} which it was substituted for, over long time periods. In 1996, Hill published "An alternate view of the degradation of bioglass", in which he proposed that the mechanism of bioglass degradation presented by Dr. Larry Hench was not particularly predicitve of the reactivity of bioglasses as a function of their composition.[191] Hill theorized that silicate glasses can be considered as inorganic polymers of oxygen crosslinked by Si atoms, and that the properties of these glasses may be predicted using the crosslink density of the glass network. Using these principles, he suggested that decreased crosslink density would result in lowered T_g, thus resulting in increased reactivity and solubility, and that the transition from a less reactive three-dimensional network to a more reactive linear polymer occurs at a network connectivity (NC) of 2. However, he also suggested that glasses with a NC just above 2 could still remain highly reactive, and that small changes in composition can greatly affect reactivity and biological properties. Prior characterization work on this glass series predicted the NC values of each glass assuming Ga acted as both a network former and modifier[183], and utilizing compositional data obtained from XPS analysis, suggested that the respective connectivities of *Control*, *TGa-1*, and *TGa-2* were 1.51, 2.16, and 2.82 if Ga acted purely as a former, and 1.51, 1.51, and 1.71 if Ga acted purely as a modifier. Considering the prior ^{29}Si MAS-NMR data, as well as the currently presented DTA data, it is suggested that Ga performed primarily in a glass network forming role in this series, which according to the NC calculations, would indicate that *TGa-1* possesses a NC slightly above 2, while *TGa-2* possesses a NC much closer to 3. Although this aids in the explanation of the larger long-term ion release from *TGa-1* compared to *TGa-2*, it does not explain their increased reactivity in comparison to *Control*, or the increased solubility of *TGa-2* compared to *TGa-1* over the first 30 days. Hill also theorized that if alumina is included in a bioactive silicate glass, the Al^{3+} ion will take on a tetrahedral coordination surrounded by four oxygens, and in the absence of phosphorus, its charge deficiency will be compensated in the first instance by an Na^+ ion, and in the second instance by half of a

Ca^{2+} ion.[191] If we assume that Ga^{3+} will perform similarly to Al^{3+} in this series of glass structures, then we can assume that GaO_4^- tetrahedra will exist, with Na^+ ions acting as the primary charge compensators, and Ca^{2+} in a secondary compensation role. The ICP-OES results in this study show that despite the increase in T_g observed with increased Ga-content, the largest amounts of Na^+, Si^{4+}, and Ga^{3+} are released over the course of 365 days from *TGa-1*, followed by *TGa-2*, and then *Control*. This finding suggests that although the introduction of Ga^{3+} increases NC, the GaO_4^- tetrahedra require a charge compensator, and as Na^+ ions from the glass surface interact with H_3O^+ ions in solution, the primary charge compensating ions are removed from the glass, exposing charged network-forming tetrahedra, which may explain the observed increased in solubility. Also, since all 3 glasses were batched to contain the same amounts of Na_2O and CaO (10 and 8 mol%, respectively), and *TGa-1* contains 8 mol% Ga_2O_3, while *TGa-2* contains 16 mol%, it is suggested that a greater fraction of the total number of GaO_4^- tetrahedra present are charge compensated by monovalent Na^+ ions in *TGa-1* than in *TGa-2*, which is why the increased Na^+ release from *TGa-1* in comparison to the other two glasses translates to more disruption of the network, and larger release of Si^{4+} and Ga^{3+}. Additionally, inhomogeneity of the glass particles is one possible explanation for the increased solubility of *TGa-2* compared to *TGa-1* over the first 30 days of incubation. It may be possible that GaO_4^- tetrahedra with Na^+ ions as charge compensators arranged more readily near the surface of *TGa-2* particles than *TGa-1*, and tetrahedra with Ca^{2+} or Zn^{2+} ions as charge compensators were more prevalent in the bulk, resulting in increased degradation initially, and slower degradation over longer time periods, as the less mobile divalent cations[191] came into contact with solution. This suggestion will also be further investigated by the authors using EDAX line scans across cross-sections of the different glasses to determine if there are compositional inhomogeneities present between the bulk and surfaces of the particles. These results are most encouraging, as it suggests that we may be able to manipulate a Ga-containing BG composition to tailor the charge compensation occuring within the glass network, and ultimately control the rate of dissolution over long time periods.

Another key finding in the ICP-OES results was that both of the Ga-containing glasses successfully released Ga from the glass network into solution, over all of the time

periods, ranging from 11.3 mg/L (*TGa-1*) and 36.4 mg/L (*TGa-2*) after 1 day, to 1295.3 mg/L (*TGa-1*) and 1006.4 mg/L (*TGa-2*) after 365 days. This was an important observation, as the main purpose of including Ga in this glass series is to facilitate its release from the network to allow for interaction with cells within the local environment. With regards to the decrease in release at 365 days after release maxima at 180 days observed several times in these studies, one explanation could be that since these glass powder samples were only incubated in 10 ml of ultrapure water without exchange for such long time periods, perhaps saturation limits were exceeded and ions which had been released from the glass structure precipitated back onto the particle surfaces. Decreases were also observed in the release profiles after 14 days of incubation, and minima were obtained at 30 days before increasing again, indicating a prior period where precipitation of ions out of solution and onto the particle surfaces occurred. Similar behavior has been observed before by Oliveira *et al.*[192], when a series of SiO_2-P_2O_5-CaO-MgO BGs exhibited the ability to develop dual silica-calcium phosphate layer when incubated in SBF. This group also demonstrated that glasses richer in MgO develop a thicker silica gel layer on their surface, and that this can play a decisive role in layer detachment through the gel. The decrease observed in the presented release profiles after 14 days, the increase until 180 days, and then a second decrease to 365 days suggests that ions precipitated out of solution to form gel layers on the particle surfaces between 14-30 days of incubation, portions of these gel layers then dissolved or detached between 30-90 days, and further degradation of the glasses occurred until between 180-365 days, when ions again precipitated out of solution onto the particle surfaces, thickening the silica gel layers. To further investigate these claims, future work will be conducted to observe cross-sections of the glass particles after different incubation periods using SEM and EDAX to determine if surface layers are present, to determine the compositions of these layers, and compare the EDAX results to ICP-OES information. In addition to ICP-OES, pH studies were conducted in order to aid in the understanding of this observed trend, however, the consistent increase in Na-release for all 3 glasses, and the large Ga-release totals of the two Ga-containing glasses may have made it difficult to observe the effects of the relatively small decreases in Si, Ca, and Zn-content in solution.

It is important to monitor pH in addition to ion release, as deviations from physiological pH levels can have detrimental effects on host tissue. The pH results after 30 days displayed expected trends, as relatively low levels of each element was detected in the 3 glasses during ICP-OES studies, which we expected would lead to similar pH levels for all 3 extracts. The pH results after 365 days mostly produced the predicted tendencies, as it was expected that *TGa-1* extracts would possess the highest pH levels, due to the elevated release levels observed during ICP-OES analysis. However, it was also predicted that *TGa-2* extracts would possess a higher pH than *Control* extracts after 365 days, since the ICP-OES results indicated that *TGa-2* released significantly more Na^+ than *Control,* and since it released a large amount of Ga^{3+}, while *Control* released none, but pH testing actually revealed that after 365 days, *TGa-2* extracts exhibited a pH of 9.7, while the average pH of *Control* extracts was 10.0. This result suggests that Na-release from *TGa-2* (which was significantly lower than *TGa-1*), had less influence on pH than in *TGa-1* extracts, and Ga-release had no effect on pH, which resulted in the slight acidity introduced by Si-release exhibting more influence on the pH of extract solutions. Overall, all three glasses used in this study exceeded expectations, as prior work conducted by Cerruti *et al.*[193] demonstrated that upon submersion in DI water, Bioglass® 45S5 powder raises the solution pH to ~10.5 after only 2 days, while only one of the glasses in the current study (*TGa-1*) exceeds a pH of 10, and that did not occur until after 180 days of submersion. While these results are encouraging, due to the length of time required to elicit large pH increases from glass samples shaking at 37°C, they do not directly translate to clinical relevancy as the solutions were not changed at any point throughout incubation, which does not accurately replicate physiological conditions.

2. Cell Viability Evaluation

Due to the similarity in effects produced by all 3 glasses on fibroblast viability over the first 30 days, and the difference in effects produced by the non-Ga-containing *Control* glass extracts and the extracts of the two Ga-containing glasses *TGa-1* and *TGa-2* after 90, 180, and 365 days, it seems plausible that Ga is the element responsible for the dramatic decrease in viability. This suggestion is supported by the ICP-OES data. Na-release profiles show similar release levels for all 3 glasses up to 30 days, and then an

increase in Na-release from *TGa-1* and *TGa-2*. However, *TGa-1* released significantly more Na than *TGa-2* after 90, 180, and 365 days, which would suggest that unless Na-release from both glasses had surpassed toxic levels for L-929 fibroblasts after 90 days, then extracts from *TGa-2* should exhibit higher viability levels than those from *TGa-1* over these time periods, which they do not. A similar trend was observed in the Si-release profiles, however, Si-release levels for the *Control* glass was very similar to *TGa-2* after 365 days, so if Si was the main element contributing to changes in L-929 fibroblast viability, then extracts from these two glasses should produce similar viabilities after 365 days, which they do not. Since the only element contained in *TGa-1* and *TGa-2* that is not contained in the *Control* glass is Ga, and the ICP-OES results did not show a dramatic increase in Ga-release from the Ga-containing glasses until after 90 days, we can conclude that the main culprit in decreasing L-929 fibroblast viability is the presence of elevated levels of Ga in solution. This conclusion is similar to that of a study by Schedle *et al.*[194], which found that ^{3}H-thymidine incorporation by L-929 fibroblasts was completely inhibited in the presence of at least 0.1 mmol/L Ga^{3+}, however, fibroblasts in the current study were able to sustain higher concentrations of Ga^{3+} before exhibiting cytotoxic effects.

Unlike the results obtained from the L-929 fibroblast studies, MC-3T3-E1 viability analysis does not directly correlate with any of the ion release profiles, and instead appears to be more efficiently explained using the results obtained from pH testing. It has been previously shown that osteoblasts are sensitive to changes in extracellular pH, as these changes may alter the potential across the cell membrane, resulting in the inhibition of ion exchange systems and the subsequent build-up of intracellular H^{+}, which can lead to protein denaturation.[195,196] Kaysinger *et al.* studied the effects of pH levels of 7.0 to 7.8 on human osteoblasts, and determined that osteoblasts exhibited cellular activity at all pHs, although plateaus in the data suggested that their preferred pH was 7.2.[197] This finding helps to interpret the MC-3T3-E1 viability data obtained in the current study, as the viabilities produced by the *TGa-1* and *TGa-2* extracts do not display an observable decrease until after 90 days, when their respective pH values were 10.1 and 8.4, which are both well above 7.2. In addition, the extracts of all 3 glasses exhibit their lowest viabilities of all the incubation times after 365 days, which is when

each extract type expressed its highest pH. As with the pH results, the cell viability data for MC-3T3-E1 osteoblasts exceeded expectations, as these assays were conducted in a static environment rather than a dynamic environment, which they would be exposed to in a host, and despite this disadvantage, there was only one significant decrease observed over all of the time periods for the 3 glasses (*TGa-2* 365 day extracts, compared to 1 and 30 day extracts).

IE. Conclusion

During this first part of the study, we were able to successfully:

- Characterize the size of the glass particles
- Examine the thermal behavior of the glass series
- Examine deposits containing Ca and P that accumulated on glass surfaces after incubation in SBF for 30 days
- Characterize the ion release profiles of liquid extracts from the glass series after incubation for up to 365 days
- Characterize the pH of liquid extracts from the glass series after incubation for up to 365 days
- Relate ion release and pH information to information provided by cell viability analysis using L-929 fibroblasts and MC3T3-E1 osteoblasts

Ion release studies were conducted, and produced unexpected results, as both of the Ga-containing glasses released significantly more Na^{+} and Si^{4+} than the *Control* glass after at least 90 days, in addition to releasing large amounts of Ga^{3+}, suggesting that Ga was acting in more of an intermediate role. Increased pH was also observed for extracts from these glasses when compared to extracts from the *Control*. Cell viability data suggested that the large amounts of Ga^{3+} released by *TGa-1* and *TGa-2* after at least 90 days induced toxic effects on the L-929 fibroblasts. However, this data also suggested that these extracts did not negatively affect the viability of MC3T3-E1 osteoblasts, leading to the conclusion that Ga-containing BGs have potential for bone void-filling applications.

The ability of this glass series to release ions, accumulate Ca/P-containing deposits on the surfaces, the compatibility of the liquid extracts with both L-929 fibroblasts and MC3T3-E1 osteoblasts for up to 30 days, and the compatibility with the osteoblasts for extended time periods, all combined to suggest that these glasses have potential in bone void-filling applications. The next phase of this study focused on synthesizing polymer hydrogels, throughout which, particles of this glass series could be embedded, in order to create bioactive glass-hydrogel composites, which could be injected into bone void sites *in situ*, and potentially provide several different therapies.

Part II: Synthesis, Characterization, and *in vitro* Cytocompatibility of Ga-Bioactive Glass/Polymeric Hydrogel Composites

Keenan T.J., Placek L.M., Keenan N.L., Hall M.M., and Wren A.W., "Synthesis, Characterization, and *in vitro* Cytocompatibility of Ga-Bioactive Glass/Polymeric Hydrogel Composites" *Journal of Biomaterials Applications* (Under Peer Review).

The second part of this study focused on functionalizing the polymers CMC and Dex to obtain CMC-ADH and Dex-CHO, and then cross-linking these functionalized polymers to obtain hydrogels. Particles of the Ga-glass series were then loaded into these hydrogels in three different amounts (0.05, 0.10, and 0.25 m^2/batch), to obtain glass-hydrogel composites, and the remainder of this portion of the study concentrated on the characterization and cytocompatibility analysis of these composites. This section discusses the results pertaining to the glass-hydrogel composites in regards to:

- Composite weight fractions
- Swelling characteristics
- Scanning electron microscopy and energy-dispersive x-ray spectroscopy
- Solubility in aqueous solution
- Cell viability analysis (L-929 fibroblasts, MC3T3-E1 osteoblasts)

During the second part of this study, the Ga-glass series was incorporated into CMC-Dex hydrogels at three different loadings (0.05, 0.10, and 0.25 m^2), and SEM and EDAX were used to confirm that the glass particles were distributed throughout the hydrogels, while swelling studies showed that glass presence can increase the amount of fluid that can be absorbed by the hydrogels after 7 days of immersion in PBS by up to 180%. Several trends were observed in the ICP-OES data, with the most important being the release of Ga^{3+} from both Ga-containing glasses at all three loadings, with a maximum of 4.7 mg/L released after 30 days of incubation in PBS. Cell viability analysis suggested that most composite extracts did not decrease either fibroblast, nor osteoblast viability. These results indicate that it is possible to embed Ga-containing bioactive glass particles into CMC-Dex hydrogels, and upon submersion in aqueous media, release ions from the glass particles that may elicit therapeutic effects.

IIA. Introduction

Bone is a complex, dynamic, composite tissue, which possesses the ability to consistently regenerate and remodel. However, defects can occur due to trauma, infection (osteomyelitis), or tumor resection, which are too large for the body's cells to repair on their own.[198] Bone grafting procedures are commonly elected as the treatment of choice, and although there are several varieties of biological grafts available, including autografts, allografts, and xenografts, each has potentially devastating limitations, such as the need for a second surgery site which increases a patient's risk of infection and pain[199], or a risk of tissue rejection by host cells.[200] As an alternative, synthetic bone graft substitutes can potentially function as a sufficient void-filling material, while avoiding the afore mentioned complications.

Of particular interest in bone regeneration applications are a class of materials known as bioactive glasses (BG). First formulated by Hench *et al*.[201], these glasses characteristically possess a low glass network-former content, and a high glass network-modifier content, which allows for a cascade of surface reactions, and ultimately, the dissolution of the glass, upon implantation into the body. The dissolution of these glasses is desirable, as the eroding network releases ions which promote bone-growth properties[202], as well as other therapeutic effects, which can include anti-bacterial[203,204] and potentially, anti-cancerous properties. In the current study, a BG series ($0.42SiO_2$-$0.10Na_2O$-$0.08CaO$-$(0.40 - x)ZnO$-$(x)Ga_2O_3$) was utilized , in which ZnO was substituted with up to 16 mol% Ga_2O_3. This composition was selected to allow for dissolution of the glasses upon submersion in aqueous media, and because each constituent has been shown to play a role in either bone metabolism, or the establishment of an interfacial bond between implant and bone. Silicon (Si), which acts as the primary glass network-former in this series, is an element which is essential in the formation and calcification of bone tissue[205,206], with aqueous Si having proven the ability to induce the precipitation of hydroxyapatite.[207] Sodium (Na), which acts as the primary glass network-modifier, exchanges with H_3O^+ ions in solution[208], initiating a cascade of surface reactions which ultimately leads to the formation of a chemical bond between implant and host tissue. Calcium (Ca) was added for its ability to increase the expression of insulin-like growth factors, which are responsible for osteoblast proliferation[209], while zinc (Zn) was

included for its ability to increase osteostimulation[174], and for its toxicity towards opportunistic bacteria.[176] Gallium (Ga) was incorporated in an attempt to harness some of the bone-promoting[120,123,124], anti-bacterial[125,126], and anti-cancerous[99-101,106,180] properties exhibited by the pharmaceutical gallium nitrate ($Ga(NO_3)_3$), from the ionic form (Ga^{3+}), upon dissolution from a glass network. Prior characterization work[210] suggested that Ga assumes a network-intermediate role in this series, while also demonstrating the ability of these glasses to release ions upon submersion in deionized (DI) water, as well as long-term (365 days) cytocompatibility of liquid extracts with MC3T3-E1 osteoblasts *in vitro*. However, despite the promising characteristics displayed by this BG series, physical implantation or delivery into a bone-void is a considerable challenge. While materials such as glass-ceramic scaffolds[210-212] and glass-ionomer/polyalkenoate cements[213-216] have been extensively studied for skeletal restoration applications, each can still pose limitations, such as the need for pre-implantation shaping, delayed setting times[217], and damaging exothermic reactions.[218] One group of materials garnering interest for BG-delivery, which can avoid such complications while still potentially acting as a bone-promoting scaffold, is known as polymeric hydrogels.

Hydrogels can be defined as cross-linked networks of hydrophilic polymers, which contain large amounts of water (in excess of 30 wt%).[219] The presence of water influences the rate of hydrogel degradation, and in the case of impregnating them with a BG, higher water content can lead to an increased rate of dissolution of the glass particles, as the particles will be surrounded by fluid not only in the implanted environment, but also within the polymeric hydrogel scaffold. Increased water content can also promote diffusion of oxygen and proteins from the environment through the material, and of ions from the glass particle surfaces into the local environment, while also translating to a softer material, allowing for easier molding during implantation, and faster integration with tissues post-implantation.[219]

To date, many different composites have been studied using a wide range of materials, with each possessing different positive and negative attributes. Proteins, such as collagen, have been seeded with mesenchymal stem cells (MSCs) and have been shown to promote both bone and cartilage formation. However, due to the rapid degradation of the collagen scaffold, the mechanical properties of the generated tissue

were significantly lower than normal tissue.[220] Polysaccharides, such as hyaluronic acid (HA), have been used as a matrix for tissue engineering applications[221], however, the hydrophilic, polyanionic surfaces of HA materials do not thermodynamically favor cell attachment or tissue generation.[222] Cellulose is another polysaccharide which has been studied for tissue engineering applications, with hydroxyapatite/cellulose composites exhibiting enhanced osteoconductivity.[223] Composites containing the polysaccharide dextran (Dex) have also been studied, with Dex gels seeded with bone morphogenic protein (BMP)-loaded polyethylene glycol (PEG) microspheres exhibiting that the BMP release kinetics could be controlled by varying the preparation parameters of the scaffold.[224]

This study aims to synthesize composites consisting of degradable carboxymethyl cellulose (CMC)/Dex hydrogels, which rapidly cross-link *in situ* via hydrazone bond formation (Hudson *et al.*[162]), impregnated with various loadings of Ga-BG particles, and to characterize their potential as bone graft substitutes for critical size defects caused by tumor resection or osteomyelitis. Traditional methods for hydrogel characterization have been employed, including scanning electron microscopy (SEM), as well as the determination of water content and time-dependent swelling characteristics. In addition, ion release and cell viability information was gathered using composite extracts obtained over a 30 day incubation period, to determine if glass composition or content within the composites translates to controllable levels of dissolution and cell survival.

IIB. Materials & Methods

1. Glass Synthesis

Three glasses were formulated for this study: 2 Ga-containing glasses (*TGa-1, TGa-2*) and 1 Ga-free CaO-Na_2O-ZnO-SiO_2 glass *(Control)*. The Ga-containing glasses *(TGa-1, TGa-2)* contain incremental substitutions of Ga_2O_3 at the expense of ZnO (Table 1). The powdered mixes of analytical grade reagents (Fisher Sci., PA, USA) were mixed using silica beads, and then oven dried (100ºC, 1 h) and melted (1500ºC, 1 h) in platinum crucibles and shock quenched into water. The resulting frits were dried, ground and sieved to retrieve glass powders with a maximum particle size of 10 μm.

2. Polymer Synthesis

2.1. Materials

Carboxymethyl cellulose, sodium salt (CMC), adipic acid dihydrazide (AAD), N-hydroxysulfosuccinimide, sodium salt (Sulfo-NHS), dextran (150,000 M.W.) (Dex), and dimethyl sulfoxide (DMSO) were obtained from Acros Organics (NJ, USA). N-(3-dimethyl laminopropyl)-N'-ethylcarbodiimide hydrochloride (EDC), sodium (meta) periodate ($NaIO_4$), ethylene glycol (EG), 0.1M sodium hydroxide (NaOH), and 0.1M hydrochloric acid (HCl) were obtained from Thermo Fisher Scientific (MA, USA).

2.2. Modification of CMC

CMC was functionalized with hydrazine groups to obtain CMC-hydrazide (CMC-ADH), using the method published by Bulpitt *et al.*[225] 1g of CMC was dissolved in 200 ml DI water with a stir bar in a round bottom flask above a magnetic stirrer. 3g AAD was then added to the spinning flask and left for 1 hour. During this time, 2 separate 8 ml mixtures (4 ml DMSO, 4 ml DI water) were prepared in separate 15 ml centrifuge tubes. 220 mg EDC was then added to one tube, while 248 mg Sulfo-NHS was added to the other. These mixtures were then left to dissolve for the remainder of the hour. The Sulfo-NHS and EDC mixtures were then added to the flask and left to dissolve for 4 hours. The pH of the solution was measured 3 times per hour over the 4 hour period, and either 0.1M NaOH or 0.1M HCl were added dropwise to maintain a pH of 6.8. After 4 hours, the

solution was dialyzed against DI water using a 3500 MWCO membrane, and the resulting solution was frozen at -80°C for 24 hours, and then lyophilized.

2.3. Modification of Dex

Dex was oxidized to Dex-aldehyde (Dex-CHO) using the method published by Bruneel *et al.*[168] 3g of dextran was dissolved in 300 ml DI water with a stir bar in a round bottom flask above a magnetic stirrer and left for 2 hours. During this time, 2.208 g $NaIO_4$ was dissolved in 10 ml DI water in a 15 ml centrifuge tube, and this mixture was added to the spinning flask at the end of the 2 hours, and left for an additional 2 hours. 1.6 ml EG was then added to the spinning flask and left for 1 hr. The solution was then dialyzed against DI water using a 3500 MWCO membrane, and the resulting solution was frozen at -80°C for 24 hours, and then lyophilized.

3. Hydrogel Synthesis

To produce hydrogels, 75 mg CMC-ADH and 180 mg of Dex-CHO were each dissolved in separate 15 ml centrifuge tubes containing 3 ml of phosphate-buffered saline solution (PBS) overnight. The dissolved polymers were then each individually added to one chamber of a dual-chambered 1 ml syringe, with one needle (21 gauge) at the tip. The 2 solutions were then simultaneously plunged through the dual-chambered syringe into rubber molds (6 mmϕ x 4 mm) between 2 glass slides, and allowed to set for 60 seconds. Gelation occurred within 2-3 seconds. Glass-free hydrogels were synthesized as controls (*Blank*).

4. Glass-Hydrogel Composite Synthesis

Using the same process, weighed amounts of each of the 3 glasses (Table 4) were added to the CMC-ADH/PBS mixture after dissolving overnight. Glass particles were dispersed throughout the mixture by vortexing at 3000 rpm for 30 seconds.

Table 4. Glass-Loading (g)

	Control	*TGa-1*	*TGa-2*
Gel + 0.05 m^2 Glass	0.041	0.044	0.047
Gel + 0.10 m^2 Glass	0.082	0.088	0.094
Gel + 0.25 m^2 Glass	0.205	0.220	0.235

The resulting mixtures, along with Dex-CHO, were then each individually added to one chamber of the syringe, and both chamberes were simultaneously plunged into the molds. The dual-chambered syringe, along with a composite gel after removal from the mold, can be seen in Figure 30.

Figure 30. a.) Dual-chambered syringe and b.) Glass-gel composite after removal from mold.

5. Glass Characterization

5.1. Particle Size Analysis

See Section IB

5.2. Surface Area Analysis

See Section IB

6. Hydrogel/Glass-Hydrogel Composite Characterization

6.1. Composite Weight Fraction

The relative weight percentage (wt%) of each component of the composite materials was evaluated, and the polymer, glass, and water contents were calculated. Samples (n=8) were gelled at room temperature, weighed using an electronic balance,

and then frozen at -80ºC. These samples were then lyophilized and re-weighed, and the relative component weight fractions (water, polymer, glass) were calculated.

6.2. Determination of Swelling Characteristics

The swelling ratio was calculated for the *Blank* hydrogel (*n*=10) and the BG-composite hydrogels (*n*=10) by determining the change in weight (ΔWt) of newly prepared, hydrated gels, as a function of immersion time in PBS. The material weight was measured from 1-7 days.

6.3. SEM & EDAX

See Section IB

6.4. Ion Release Profiles

Blank hydrogels (*n*=3) and BG-hydrogel composites (*n*=3) were submerged in 1 ml of static PBS at 37ºC for periods of 1, 7, and 30 days. After the incubation times were complete, the aqueous solution from each sample was removed and filtered using Amicon® Ultra-4 Centrifugal Filters (Merck KGaA, Darmstadt, Germany). Volumetric dilutions of each extract were then prepared (1:100), and ICP-OES was performed. Solutions were analyzed for Na, Ca, Si, Zn, and Ga content. The ion release profile of each glass was measured using Inductively Coupled Plasma – Optical Emission Spectroscopy (ICP-OES) on a Perkin-Elmer Optima 8000 (Perkin Elmer, MA, USA). ICP-OES calibration standards for Na, Ca, Si, Zn and Ga ions were prepared from stock solutions on a volumetric basis. Three target calibration standards were prepared for each ion, and dilute PBS (1:100) was used as a control.

6.5. Cell Viability Analysis

The established cell lines L-929 (American Type Culture collection CCL 1 fibroblast, NCTC clone 929) and MC3T3-E1 Osteoblasts (ATCC®-CRL-2593™) were used in this study. L-929 fibroblasts were cultured, as required by ISO10993 part 5 [226], in HyClone® Medium 199/EBSS (Thermo Scientific, MA, USA), which included Earl's balanced salts and L-glutamine, and was supplemented with 10 vol% fetal bovine serum

(FBS) (Thermo Scientific, MA, USA). MC3T3-E1 osteoblasts were cultured in HyClone® MEM Alpha Modification (1X) media (Thermo Scientific, MA, USA), which included L-glutamine, ribonucleosides, and deoxyribonucleosides, and was supplemented with 10 vol% FBS. Cells were maintained on a regular feeding regime in a cell culture incubator at 37˚C, with a 5% CO2/95% air atmosphere. Cells were then seeded into 96 well plates at a density of 10,000 cells per well and incubated for 24 hours prior to the addition of extracts. The cytotoxicity of hydrogel and BG-hydrogel composite extracts were evaluated using the Methyl Tetrazolium (MTT) assay. 10 µl aliquots of undiluted extract were then added into wells containing cells in culture medium (100 µl), and incubated for an additional 24 hours. 10 µl of the MTT assay was then added to each well and incubated for an additional 4 hours. After 4 hours, the cultures were removed from the incubator, and the resultant formazan crystals were dissolved by first removing all of the aqueous media from each well, and then adding 100 µl of MTT Solubilization Solution (10% Triton x-100 in Acidic Isopropanol. (0.1 n HCI)). Once the crystals were fully dissolved, the absorbance was measured at a wavelength of 570 nm using a µQuant Plate Reader (Bio-Tek Insturments, Inc., VT, USA). 10 µl aliquots of PBS were used as control additions, and control cells were assumed to have metabolic activities of 100%. Hydrogel and BG-hydrogel composite extracts in media without cells were also tested, and were found not to interfere with the MTT assay.

7. Statistical Analysis

Particle size and surface area data for BG particles are presented as means ± standard deviations, and represents 3 trials per glass. Weight fraction and swelling data are presented as means ± standard deviations, and represents data from 10 replicates per sample. Ion release and cell viability data are also presented as means ±standard deviations, and represents data from 3 individual extract replicates per hydrogel/BG-hydrogel composite, per incubation interval. One-way analysis of variance (ANOVA) was used to compare both ion release, and cytocompatibility of the BG extracts in relation to 1) incubation time, and 2) Ga-content. Comparison of relevant means was performed using the post hoc Bonferroni test. Differences between groups were deemed significant when $p < 0.05$.

IIC. Results

1. Glass Characterization

1.1. Particle Size Analysis

Particle size analysis was conducted for each glass powder sample, and the results are presented in Table 5. Mean particle size was similar for each glass at 3.8 µm, 3.4 µm, and 3.6 µm for *Control*, *TGa-1*, and *TGa-2*, respectively.

Table 5. Particle Size (µm) Distribution of *Control*, *TGa-1*, and *TGa-2* Glasses

	Mean	S.D.	d10	d50	d90
Control	3.8	0.1	3.1	3.9	4.3
TGa-1	3.4	0.2	2.1	3.7	4.3
TGa-2	3.6	0.4	2.6	3.7	4.3

1.2. Surface Area Analysis

The surface area of each glass powder was also calculated, using gas adsorption in combination with the BET method, and these results are presented in Table 6. Mean surface area was similar for each powder at 1.23 m^2/g, 1.14 m^2/g, and 1.06 m^2/g for *Control*, *TGa-1*, and *TGa-2*, respectively.

Table 6. Surface Area (m^2/g) of *Control, TGa-1,* and *TGa-2* Glasses

	Mean	S.D.
Control	1.23	0.13
TGa-1	1.14	0.15
TGa-2	1.06	0.23

2. Hydrogel & BG-Hydrogel Composite Characterization

2.1. Weight Fraction Determination

Characterization of the composite materials began with determining the weight fraction of each component, and this information is presented in Table 7. The control *Blank* hydrogel was found to consist of 94.3% water, with 5.7% polymer, while the subsequent additions of glass to create glass-hydrogel composites resulted in these materials possessing lower fractions of both water and polymer compared to the *Blank*.

Table 7. Weight Fractions of *Blank* Hydrogel and Glass-Hydrogel Composites

		0.05 m²			0.10 m²			0.25 m²		
	Blank	***Control***	***TGa-1***	***TGa-2***	***Control***	***TGa-1***	***TGa-2***	***Control***	***TGa-1***	***TGa-2***
Water (%)	94.3	93.8	94.0	94.4	93.6	92.8	93.2	92.0	91.7	91.4
Polymer (%)	5.7	5.3	5.1	4.7	4.9	5.4	5.0	4.4	4.5	4.5
Glass (%)		0.9	0.9	0.9	1.5	1.8	1.8	3.6	3.8	4.1

2.2. Swelling Characteristics

Swelling behaviors were characterized by synthesizing *Blank* hydrogels, as well as glass-hydrogel composites, and then immersing them in PBS for up to 7 days, in order to observe any weight changes due to fluid absorption, and this data is presented in Figure 31. *Blank* hydrogels experienced no significant change after 7 days of immersion. For composites which had 0.05 m^2 glass added, significant swelling was observed for all 3 glass types after 7 days, with weight increases of 64.1%, 54.6%, and 37.4% for *Control*, *TGa-1*, and *TGa-2* glass composites, respectively. For composites which had 0.10 m^2 glass added, swelling behavior was almost identical for *TGa-1* and *TGa-2* composites as in the lower-loading samples (58% and 37%, respectively), while the *Control* glass composites experienced a significant increase in weight, swelling 179% after 7 days. Composites which contained 0.25 m^2 glass again exhibited similar trends, with *Control*, *TGa-1*, and *TGa-2* glass composites swelling 86.1%, 63.8%, and 38.9% after 7 days, respectively.

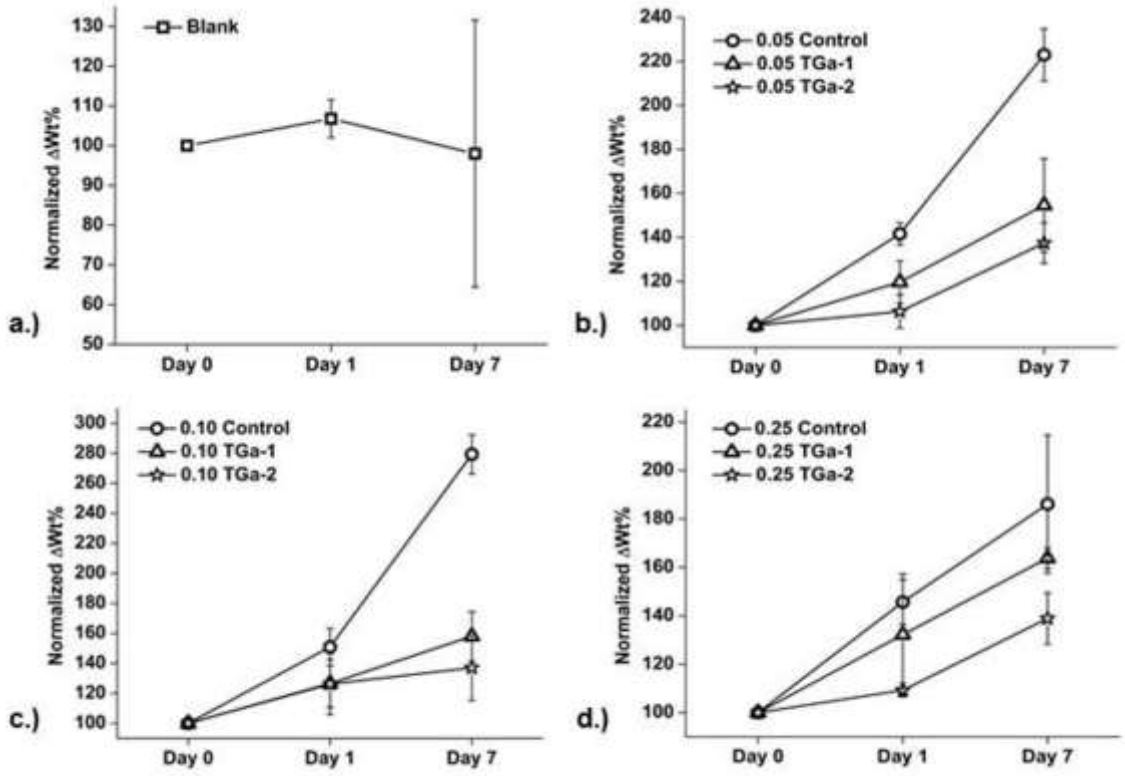

Figure 31. Weight changes due to swelling upon immersion in PBS for a.) *Blank* hydrogels, and hydrogel composites containing b.) 0.05 m^2, c.) 0.10 m^2, and d.) 0.25 m^2 glass.

2.3. SBF Studies

SEM micrographs of cross-sections obtained post-lyophilization, along with corresponding EDAX spectra for a *Blank* hydrogel, as well as composites containing 0.10 m^2 *Control*, *TGa-1*, and *TGa-2* glasses, are presented in Figure 32. The EDAX spectrum confirms that the *Blank* hydrogel does not contain any glass, while glass particles can be seen embedded within the polymer matrix of each of the composites. The corresponding EDAX spectrum for the *Control* glass composite confirms that there is no Ga present, while the EDAX spectra generated for the *TGa-1* and *TGa-2* composites confirm the presence of Ga.

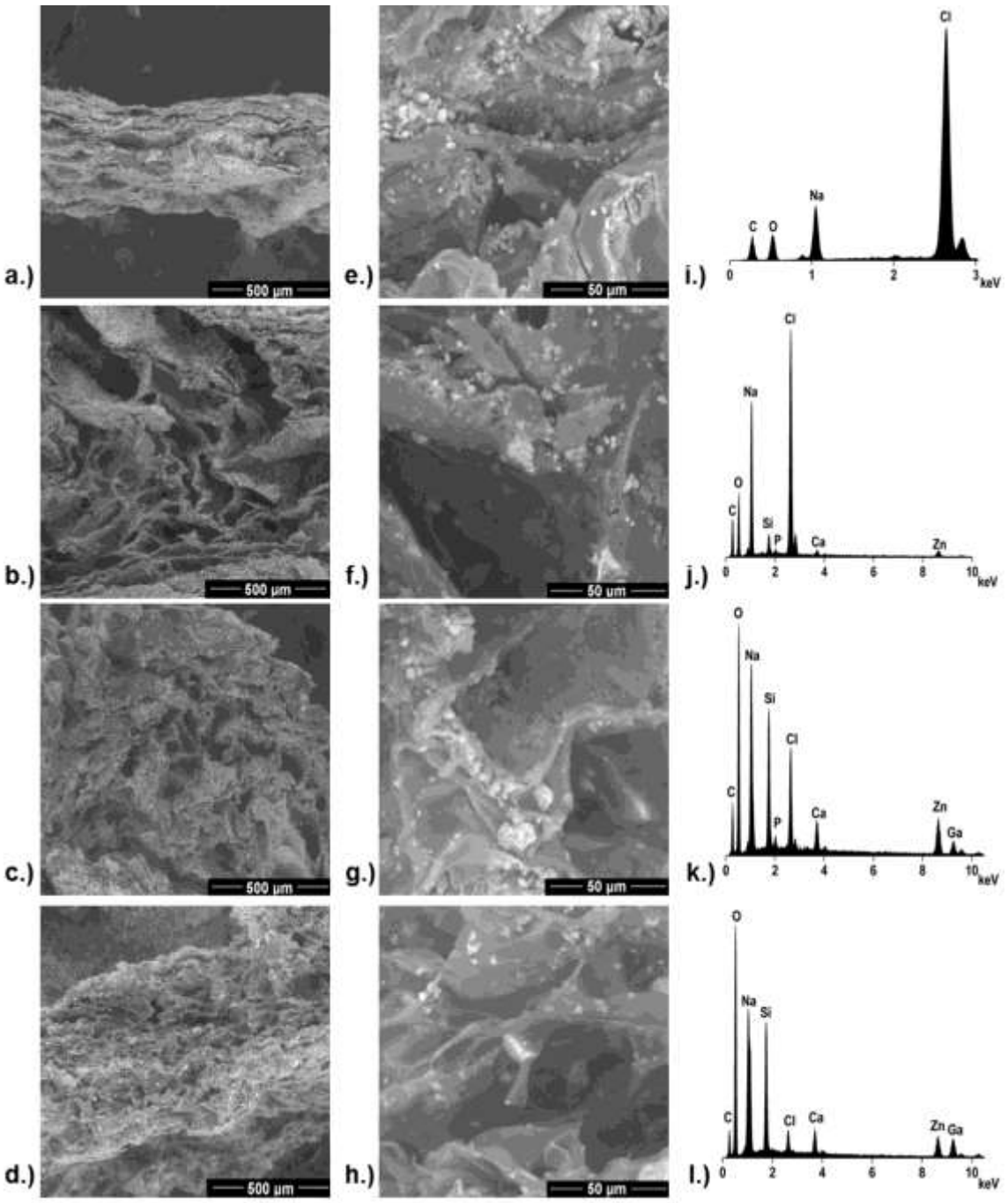

Figure 32. SEM micrographs and corresponding EDAX spectra for a,e,i.) *Blank* hydrogel, b,f,j.) 0.10 m^2 *Control* composite, c,g,k.) 0.10 m^2 *TGa-1* composite, and d,h,l.) 0.10 m^2 *TGa-2* composite.

2.4. Ion Release Studies

Profiles of Si^{4+} release for *Blank* hydrogels, as well as hydrogel composites containing 0.05, 0.10, and 0.25 m^2 glass over 30 days is presented in Figure 33. Figure 33a shows that relatively small amounts of Si^{4+} were detected in *Blank* extracts, with 3.8, 3.6, and 5 mg/L being observed after 1, 7, and 30 days, respectively. It can be seen in Figure 33b that for composites loaded with 0.05 m^2 glass, all 3 types exhibited significant increases in Si^{4+} release from 1 to 30 days, with *Control* releasing 94-157 mg/L, *TGa-1* releasing 80-157 mg/L, and *TGa-2* releasing 24-40 mg/L after 1 and 30 days, respectively. Figure 33c displays Si^{4+} release for hydrogels loaded with 0.10 m^2 glass, with *Control* releasing 157-197 mg/L, *TGa-1* releasing 84-162 mg/L, and *TGa-2* releasing 104-96 mg/L over the period of 1-30 days. In Figure 33d, Si^{4+} release profiles can be found for composites containing 0.25 m^2 glass, which show that for *Control*, Si^{4+} release reduced from 156-129 mg/L, while release from *TGa-1* and *TGa-2* increased from 93-98 mg/L and 60-91 mg/L, respectively, over the period of 1-30 days.

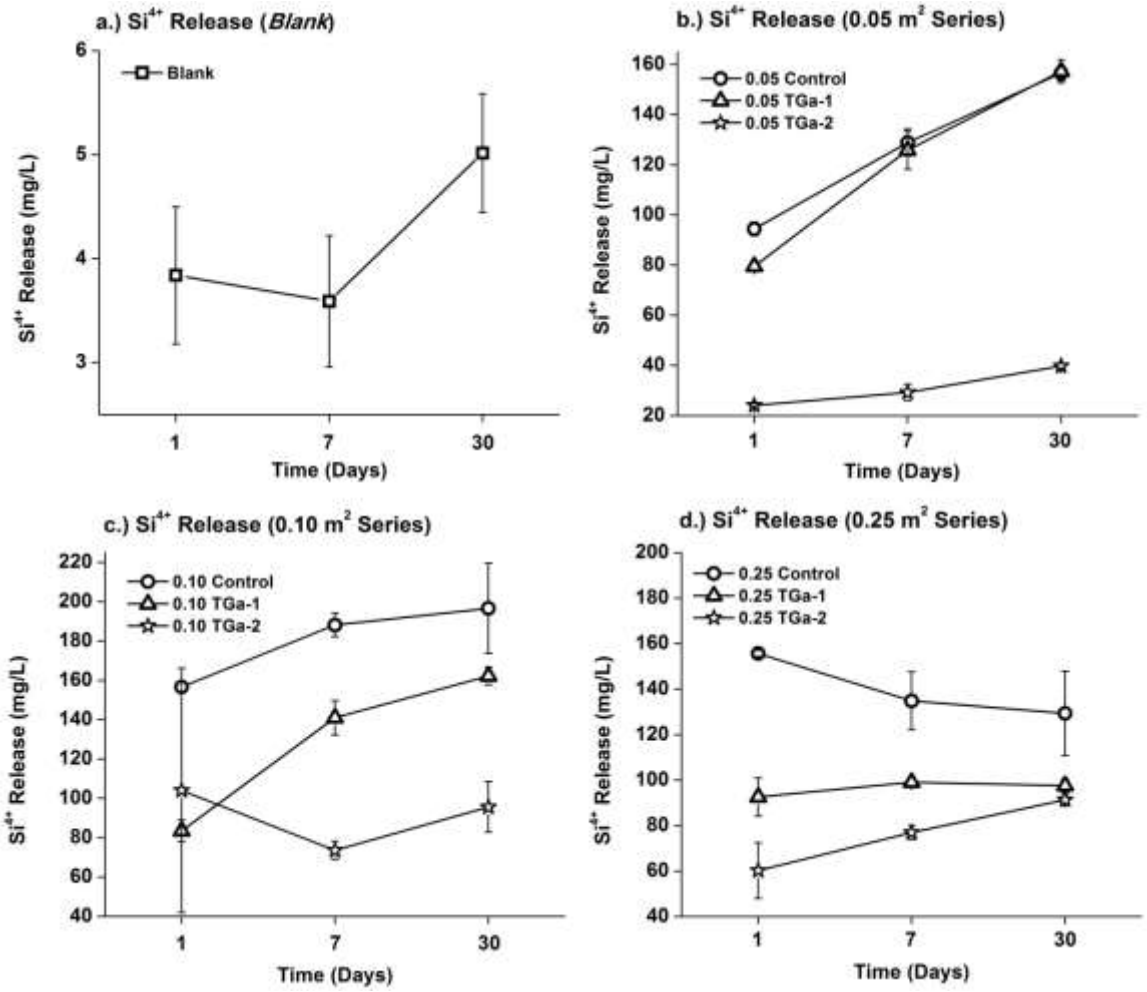

Figure 33. Si^{4+} release profiles for a.) *Blank* hydrogels, and hydrogel composites containing b.) 0.05 m^2, c.) 0.10 m^2, and d.) 0.25 m^2 glass.

The release of Ca^{2+} from composites containing 0.25 m^2 of glass over 30 days is presented in Figure 34. No significant release of Ca^{2+} was observed for either the *Blank* hydrogels, or composites containing 0.05 or 0.10 m^2 glass. For the composites containing 0.25 m^2 glass, a significant increase in Ca^{2+} release was observed for all 3 composite types after 30 days of immersion, compared to 1 day. Composites containing *TGa-1* and *TGa-2* glasses exhibited nearly identical Ca^{2+} release over each time period, with the *TGa-1* composites releasing 4, 6, and 9 mg/L, and the *TGa-2* composites releasing 5, 6, and 9 mg/L, after 1, 7, and 30 days, respectively. Composites containing *Control* glass exhibited higher Ca^{2+} release over the longer time periods, releasing 3, 12, and 20 mg/L after 1, 7, and 30 days, respectively.

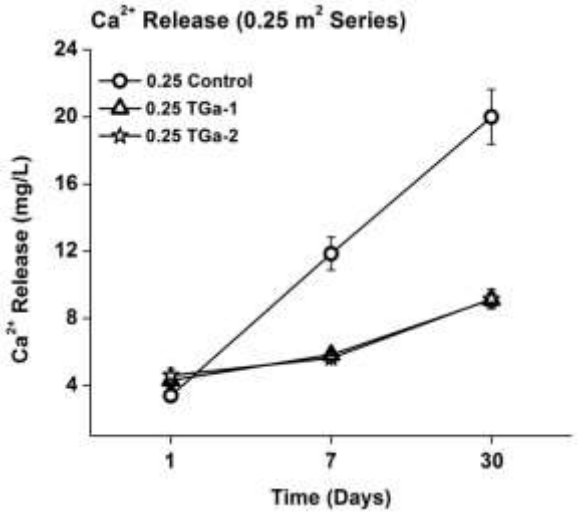

Figure 34. Ca^{2+} release profiles for hydrogel composites containing 0.25 m^2 glass.

Zn^{2+} release is presented in Figure 35, with release profiles for composites containing 0.05, 0.10, and 0.25 m^2 glass being shown in Figures 35a, 35b, and 35c, respectively. For hydrogels loaded with 0.05 m^2 glass, *Control* exhibited no significant release after any time period, while *TGa-1* released 7 mg/L after 30 days, and *TGa-2* released 2 and 7 mg/L after 7 and 30 days, respectively. Larger quantities of Zn^{2+} were released from composites containing 0.10 m^2 glass, with *Control* releasing 3 and 13 mg/L, *TGa-1* releasing 2 and 16 mg/L, and *TGa-2* releasing 4 and 7 mg/L after 7 and 30 days, respectively. Zn^{2+} release totals for hydrogels containing 0.25 m^2 glass were more similar to the 0.05 m^2 profiles, with neither *Control* nor *TGa-1* exhibiting release after any time period, while *TGa-2* released 6 mg/L after 30 days.

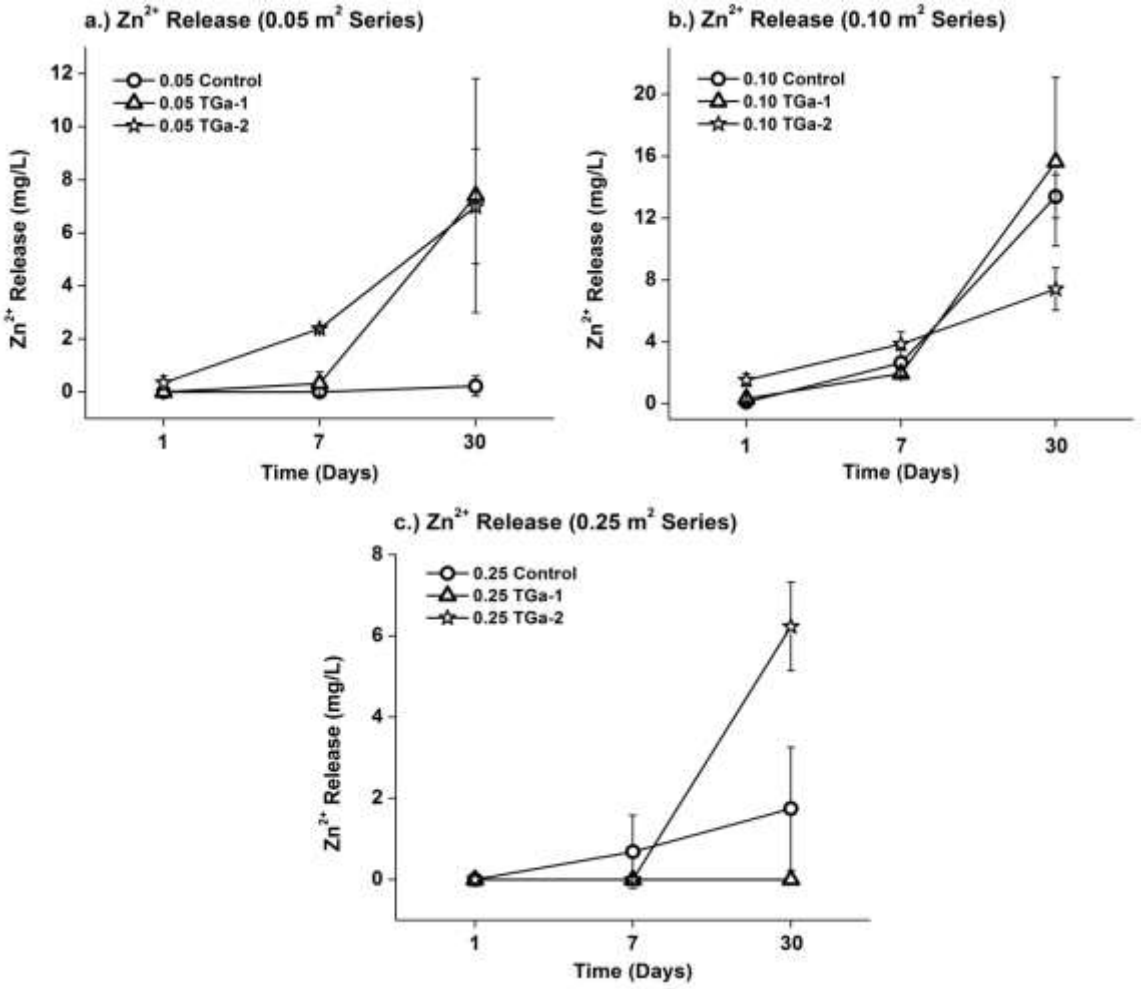

Figure 35. Zn^{2+} release profiles for hydrogel composites containing a.) 0.05 m^2, b.) 0.10 m^2, and c.) 0.25 m^2 glass.

The Ga^{3+} release profiles for hydrogel composites containing 0.05, 0.10, and 0.25 m^2 glass are presented in Figure 36. As expected, no Ga^{3+} release was observed for any of the *Control* composites, as this glass did not contain Ga. Figure 36a presents Ga^{3+} release data for hydrogels impregnated with 0.05 m^2 glass, and shows that both *TGa-1* and *TGa-2* composites exhibited significant increases from 1 to 30 days, with *TGa-1* releasing 1 and 4 mg/L, and *TGa-2* releasing 1 and 2 mg/L after 1 and 30 days, respectively. The release of Ga^{3+} from hydrogels loaded with 0.10 m^2 glass is shown in Figure 36b. Release from *TGa-2* does not exhibit any signifcant changes over the time periods, releasing 2 mg/L after 1, 7, and 30 days, respectively, while *TGa-1* exhibits a significant increase from 1 to 30 days, releasing 1 and 5 mg/L after 1 and 30 days, respectively. In Figure 36c it can be seen that for composites containing 0.25 m^2 glass, there is no significant

difference between Ga^{3+} release from *TGa-1* and *TGa-2* composites after 30 days, with the two materials releasing 3 and 4 mg/L, respectively.

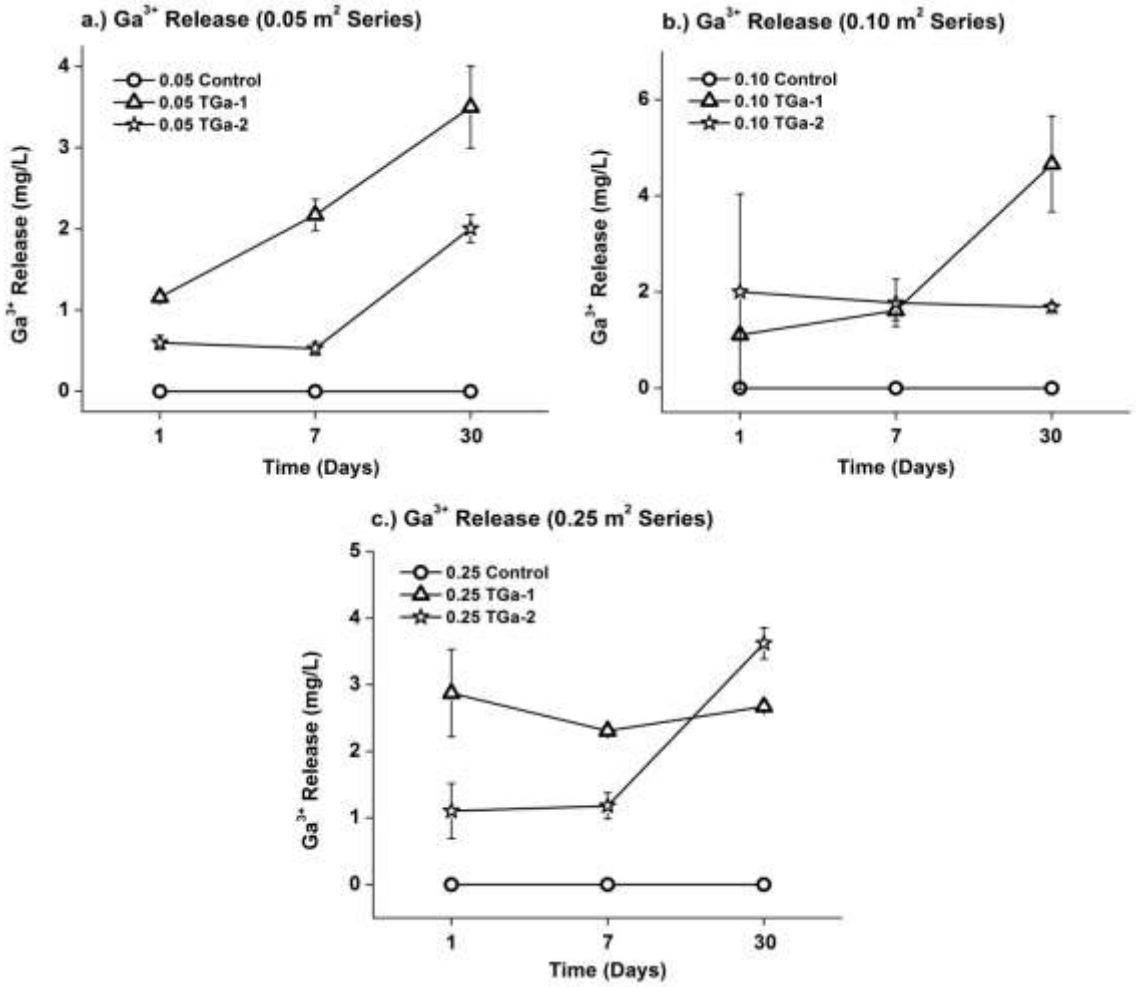

Figure 36. Ga^{3+} release profiles for hydrogel composites containing a.) 0.05 m^2, b.) 0.10 m^2, and c.) 0.25 m^2 glass.

3. Cell Viability Analysis

Cell viability analysis was conducted using the extracts which were obtained from incubating the *Blank* hydrogels and hydrogel-glass composites in PBS. Figure 37 presents L-929 fibroblast viability data for extracts obtained after incubation for 1, 7, and 30 days, and illustrates that neither glass addition, Ga-content, nor incubation time induce statistically significant changes in viability. Additionally, no significant changes in viability were observed over the 3 time periods within sample sets.

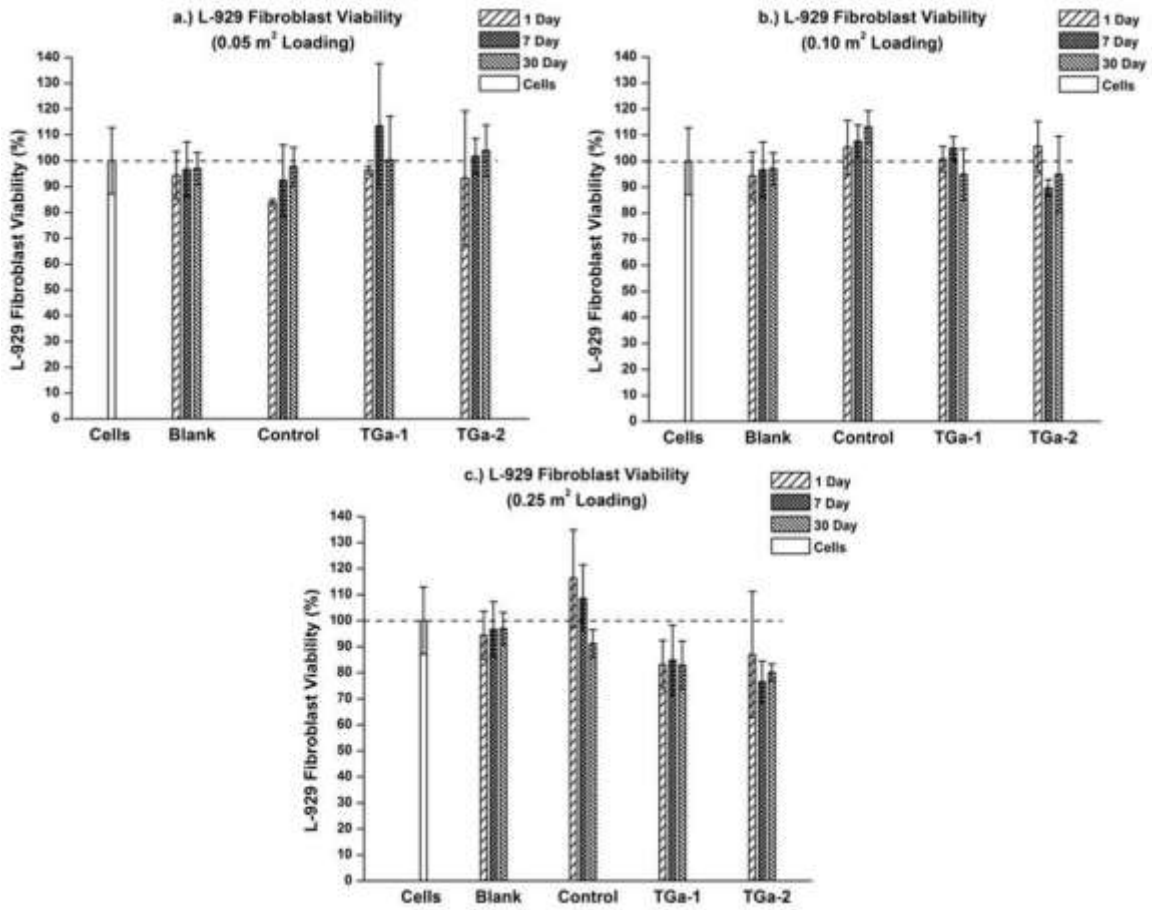

Figure 37. L-929 fibroblast viability for extracts obtained from *Blank* hydrogels, and glass-hydrogel composites after 1, 7, and 30 days.

MC3T3-E1 osteoblast viability data for extracts obtained from the *Blank* hydrogels, and the glass-hydrogel composites after 1, 7, and 30 days is displayed in Figure 38, and illustrates that neither glass addition, Ga-content, nor incubation time negatively affect the cells. The only statistically significant change observed was a decrease in viability of osteoblasts exposed to extracts obtained from hydrogels containing 0.05 m^2 *Control* glass, when a decrease occurred between 1 and 30 day extracts (p=0.02), although these 30 day extracts still produced a viability of 102.7%.

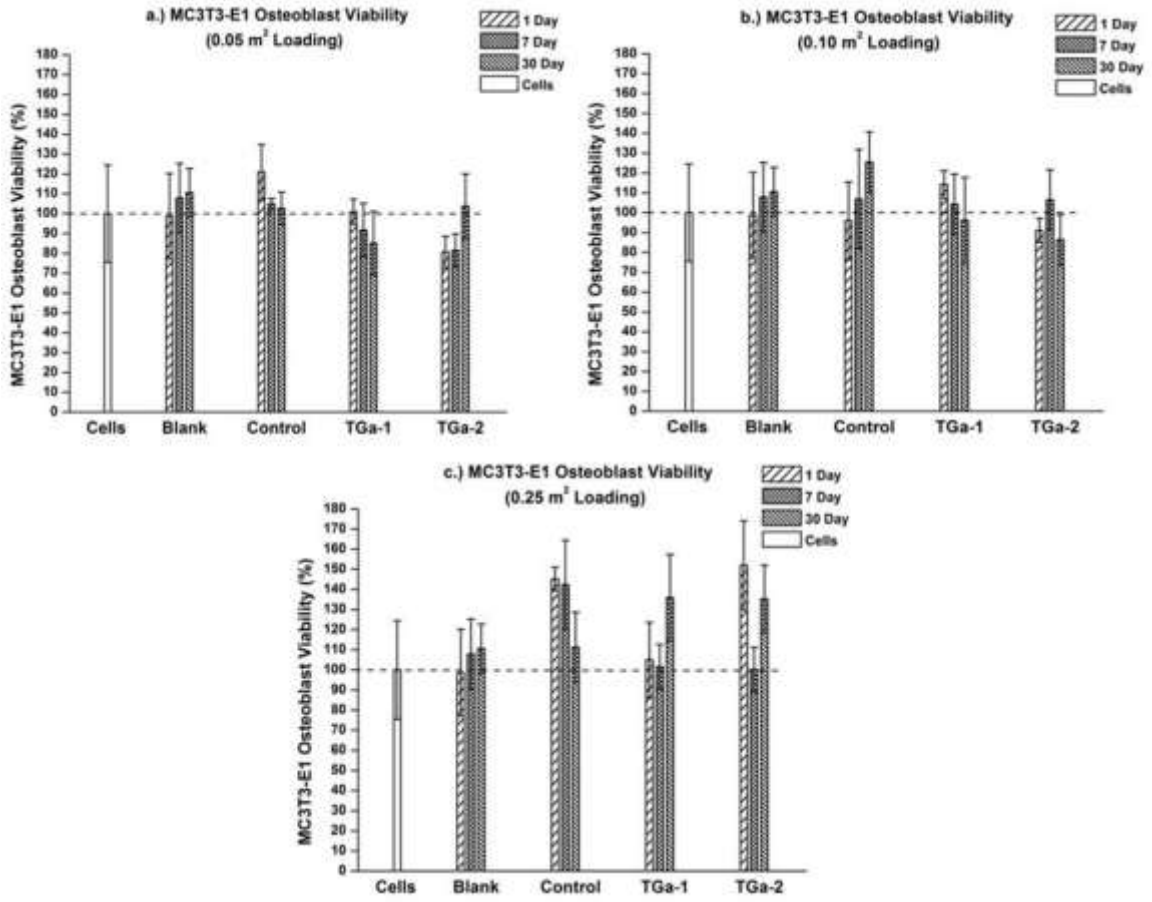

Figure 38. MC3T3-E1 osteoblast viability for extracts obtained from *Blank* hydrogels, and glass-hydrogel composites after 1, 7, and 30 days.

IID. Discussion

This study was conducted in order to determine whether CMC-Dex hydrogels could be used as a delivery vehicle for Ga-containing bioactive glass particles, to allow for *in situ* release of therapeutic ions. PSA confirmed that all glass particles presented a similar size distribution, while ASAP was used in conjunction with the BET method to confirm that all glass particles presented a similar surface area distribution. This information regarding surface area was also used to normalize and control the amount of each type of glass that was loaded into the composites.

Although BGs exhibit the ability to form chemical bonds to bone, and release ions which can induce many different therapeutic effects, ranging from increased osteoblast activity to bactericidal effects, these materials still require a delivery mechansim to be used in bone void replacement. One possible delivery system is polymer hydrogels, whose interconnected porous structure resembles the extracellular matrix, which can act as a scaffold upon which therapeutic materials may be seeded.[227] As previously stated, the porosity of these materials can allow for diffusion into the scaffold by components of the physiological fluid, including oxygen and proteins, and diffusion of therapeutic drugs and ions out of the scaffold and into the local environment. Increased water content within the gels also translates to a softer material, allowing for easier molding during implantation, and faster integration with tissues post-implantation. After considering each of these beneficial factors, CMC/Dex hydrogels were selected as our BG-delivery vehicle, due to their biocompatibility and slow degradation rates within the body, as exhibited by Hudson *et al*.[162] The water present within hydrogels affects their properties as it acts as an initiator for dissolution, and in the case of impregnating with BGs, higher water content can lead to increased rate of dissolution of the glass particles, as the particles will be surrounded by fluid not only in the implanted environment, but also within the composite structure.

To determine water content within the different composites, the weight fractions of each component were calculated, and it was observed that the *Blank* hydrogels consisted of 5.7% polymer and 94.3% water, and that while glass addition slightly affected water content, hydrogels impregnated with the highest loading of 0.25 m^2 glass still consisted of 92%, 91.7%, and 91.4% water for *Control*, *TGa-1*, and *TGa-2*

composites, respectively. Swelling characteristics were then observed over a 7 day period, as hydrogels can imbibe and retain large amounts of fluid while maintaining structural integrity. Swelling characteristics were studied to provide insight into the connectivity of the polymeric networks, as the total amount of water that can be endured by a hydrogel is determined by the degree of opposition between the osmotic driving force of the polymer chains to achieve infinite dilution, and the cross-link density of the polymer network.[157] The ability of these gels to swell, in addition to their ability to cross-link within seconds, emphasizes their candidacy as bone void-filling materials, as these properties would allow them to completely fill irregular defects. After 7 days there was no significant change in the weight of the *Blank* hydrogels, while the addition of glass at each level of loading resulted in significant increases in composite weight after 7 days. For all three glass-loading levels, composites containing *Control* glass exhibited the largest weight increases after 7 days, although there was no statistical difference between glasses for gels containing 0.25 m^2 glass. Also, for all three glass-loadings, there was no statistical difference observed between composites containing *TGa-1* glass, and those containing *TGa-2* glass, after 1 or 7 days. With a swelling range of 0-180 wt% for the gels and gel composites after 7 days, these materials absorb much less water at a much slower rate than other hydrogel candidates for drug delivery, such as hydrogels consisting of polyethylene glycol (PEG) polymerized with hydroxy acid and acrylate, which have been shown to swell up to 600 wt% after just 5 hours in HEPES-buffered saline.[228] However, a slower rate of swelling may translate to slower degradation of the polymer network, which is a desired trait when developing materials for sustained delivery of therapeutics. The presence and distribution of pores throughout the *Blank* gels, along with the distribution of glass particles throughout the composite materials, was studied using SEM and EDAX. SEM micrographs exhibited that the diameter of pores in the *Blank* gels, and in the glass-hydrogel composites, were on the order of 50-100 μm, and EDAX spectra confirmed that the different glass particles were embedded within the polymer matrix.

Ion release studies were conducted in order to determine if ions could leach from the embedded glass surfaces, through the polymer network, and diffuse into solution, over a period of 30 days. Each of the glass constituents were found to solubilize in

aqueous media, although trends varied as a function of both glass-addition and Ga-content. Na^+ release was not presented because large errors were present throughout the data, due to the high Na-content of the PBS media into which samples were immersed. For Si^{4+}, composites containing *Control* glass released the largest quantities at all three loadings, although there was no statistical difference between 0.05 m^2 *Control* and *TGa-1* composite extracts after 1, 7, or 30 days. Composites containing *TGa-1* glass released significantly more Si^{4+} than *TGa-2* composites after 7 days for all loadings, and significantly more after 30 days for 0.05 m^2 and 0.10 m^2 loadings. However, although *Control* and *TGa-1* composites released significantly less Si^{4+} after 30 days when 0.25 m^2 was embedded in the hydrogels (129 mg/L (p=0.000) and 98 mg/L (p=0.000), respectively) compared to 0.10 m^2 (197 mg/L and 162 mg/L, respectively), there was not a significant decrease observed in *TGa-2* composite extracts. In addition, nearly all three glass types released significantly more Si^{4+} after 30 days compared to 1 day for all three loadings, with the exception of 0.25 m^2 *Control*, 0.25 m^2 *TGa-1*, and 0.10 m^2 *TGa-2* composites. These findings contradict prior work, which found that increased Ga-content resulted in increased Si^{4+} release. In addition, this study exhibited higher Si^{4+} release after 30 days of incubation than prior work. However, prior work studied ion release of these glasses in ultrapure water, rather than in PBS, and since PBS possesses a higher pH (~7.4) which is further from the isoelectric point of SiO_2[229] than ultrapure water (pH≈5.4), the larger charge difference may have resulted in increased polarization of Si-containing surface groups on the glass particles, leading to increased Si^{4+} release. Much lower release quantities were observed for Ca^{2+}, and significant release was only recorded for composites containing 0.25 m^2 glass. *Control* composites released the largest concentration of Ca^{2+} (20 mg/L) after 30 days, which was significantly higher than both *TGa-1* (9 mg/L (p=0.000)) and *TGa-2* (9 mg/L (p=0.000)) composites. This release is important, as Maeno *et al.* observed that concentrations of Ca^{2+} below 10 mmol (400 mg/L) are suitable for osteoblast proliferation and differentitaion.[230] Zn^{2+} release concentrations were similar to those observed for Ca^{2+}, although the largest Zn^{2+} concentrations were released from composites containing 0.10 m^2 glass, rather than 0.25 m^2. As with the Si^{4+} profiles, extracts from hydrogels impregnated with 0.25 m^2 *Control* and *TGa-1* glasses exhibited significant decreases in Zn^{2+} release after 30 days of

immersion compared to the 0.10 m^2 composites (p=0.000 and p=0.000, respectively), while no significant change was observed between any of the different composites containing *TGa-2* glass. However, low Zn^{2+} release may be a desirable characteristic, as previous work has found that concentrations above 2 mg/L can cause damage in human osteoblasts via oxidative stress.[231] The profiles generated by Ga^{3+} release follow the previously established trends, with *TGa-1* composites releasing significantly more Ga^{3+} than *TGa-2* composites after 30 days for gels containing 0.05 m^2 and 0.10 m^2 glass, while there was no significant difference between release from those containing 0.25 m^2 glass. For each ionic species other than Ca^{2+}, the highest corresponding releases were observed for composites containing 0.10 m^2 glass rather than 0.25 m^2, which suggests that there is a physical limit to the amount of glass that can be added to CMC-Dex gels to obtain increased ion release. It was also observed that more Si^{4+}, Ca^{2+}, and Zn^{2+} was released after 30 days from composites containing 0.25 m^2 of glass or less than from 1 m^2 of glass in ultrapure water in prior work, suggesting that the inclusion of glass particles in a hydrated polymer network allows for more surface area to be exposed to aqueous media, thus leading to increased ion release. Additionally, the glass particles used in this study were found to possess particle sizes of 3-4 μm, while prior work utilized particles with diameters of 10-11 μm, which may have also contributed to increased ion release. These ion release profiles suggest that the release of specific ionic species by glass-hydrogel composites can be tailored by selecting the appropriate glass composition and glass-loading level, depending on which ionic species is of interest.

Cell viability analysis was conducted, assaying liquid extracts of *Blank* hydrogels and glass-hydrogel composites against L-929 mouse fibroblasts. After 30 days of incubation, no significant changes in viability were observed. Cell viability studies were also conducted using MC3T3-E1 human osteoblasts, and no inhibitory effects were expressed by the *Blank* hydrogels, or any of the glas-hydrogel composites, over any of the time periods. These results are in accordance with prior work by the authors, which obtained extracts from 1 m^2 *Control*, *TGa-1*, and *TGa-2* glasses, and showed that extracts obtained after 30 days did not reduce MC3T3-E1 osteoblast viability. In addition, although no significant increases were observed, the highest average osteoblast viabilities after 30 days were recorded for composites containing 0.25 m^2 *TGa-1* (136%) and *TGa-2*

(135%), which correlates with the ICP data, as these are the only composites containing Ga-glasses which exhibited Ca^{2+} release, which has been shown to promote osteoblast differentiation and proliferation in low concentrations.[230]

IIE. Conclusion

Throughout this second phase of the study, we successfully:

- Functionalized the polymers CMC and Dex to obtain CMC-ADH and Dex-CHO
- Cross-linked the functionalized polymers to create hydrogels
- Combined particles of the Ga-glass series with the polymer hydrogels to create viscous composite materials
- Calculated the weight fractions of the different components within the *Blank* hydrogels, and within the various glass-gel composites
- Determined the swelling characteristics of all of the gels
- Confirmed the distribution of glass particles, and the presence of pores, throughout the composite materials
- Characterized the release of glass dissolution products from the composites
- Determined that dissolution products from composites exhibited no inhibitory effects on either L-929 fibroblasts, or MC3T3-E1 osteoblasts

The second part of this study confirmed the distribution of glass particles throughout the polymeric network of CMC-Dex hydrogels, and showed that glass presence within the gels can increase the amount of fluid absorbed upon immersion in aqueous media. Ion release studies revealed that the highest release for the majority of the constituent ions after 30 days was observed at the intermediate glass-loading level of 0.10 m^2 for composites containing *Control* and *TGa-1* glasses, however, Ca^{2+} was only eluted from composites containing 0.25 m^2 glass. Cell viability data suggested that extracts from these composites do not induce cytotoxic effects in L-929 fibroblasts or MC3T3-E1 osteoblasts after 30 days, and revealed that rather than inducing negative effects, composites containing 0.25 m^2 *TGa-1* and *TGa-2* produce maximum average viabilities after 30 days. This portion of the study has shown that BG particles can be distributed throughout a polymer hydrogel, and that ions can be leached from the surface of these particles, and diffuse through the gel and into the local environment, in non-toxic concentrations, leading to the conclusion that composites consisting of CMC-Dex

hydrogels and Ga-containing BGs have potential as bone void-filling materials, which can swell to fill irregular sites, and subsequently release beneficial ions into the local environment.

After successfully synthesizing composites consisting of CMC-Dex hydrogels and the Ga-glass series, and determining that the intended therapeutic ions do leach out of the composite strucuture at no detriment to either L-929 fibroblasts or MC3T3-E1 osteoblasts, and considering that one of the intended applications of these materials is to act as a filler for bone voids caused by osteomyelitis, it was concluded that the next logical step was evaluate the *in vitro* anti-bacterial and anti-fungal efficacy of these materials, using both broth dilution and agar diffusion trials.

Part III: Anti-Bacterial and Anti-Fungal Potential of Ga-Bioactive Glass and Ga-Bioactive Glass/Polymer Hydrogel Composites

Keenan T.J., Placek L.M., Hall M.M., and Wren A.W., "Anti-bacterial and Anti-Fungal Potential of Ga-Bioactive Glass and Ga-Bioactive Glass/Polymeric Hydrogel Composites" *Journal of Biomedical Materials Research Part B: Applied Biomaterials* (Under Peer Review).

The main focus of the third phase of this study was evaluating the anti-bacterial and anti-fungal potential of both the glass series by itself, and in combination with the hydrogels in the form of composites. This portion of the study details the following results:

- Ion release profiles of the glass series incubated in PBS, rather than ultrapure water
- Liquid broth analysis using both glass and composite extracts against *E. coli*, *S. aureus*, and *C. albicans*
- Agar diffusion analysis using composites cross-linked *in situ* in agar against *E. coli*, *S. aureus*, and *C. albicans*

Liquid broth analysis was conducted using liquid extracts, which for glass samples were obtained after incubation for up to 30 days in both ultrapure water and phosphate buffered saline (PBS), while glass-hydrogel extracts were obtained solely in PBS. Glass extracts (incubated in water) decreased only *C. albicans* viability, while those obtained in PBS decreased the viability of both *E. coli* and *C. albicans*. Glass-hydrogel extracts exhibited slight inhibition of *E. coli* and *C. albicans*. None of the liquid extracts effectively decreased *S. aureus* viability. However, glass-hydrogel composites produced inhibition zones in all three microbial cultures, with the greatest efficacy against *C. albicans*. The results of this segment of the study suggest these materials have potential as bone void-filling materials which display anti-fungal, and possibly, anti-bacterial properties.

IIIA. Introduction

Bioactive glasses (BGs) are materials which can be used to aid in the repair of bone tissue which has been damaged by either disease or traumatic injury. The most widely known BG, called Bioglass® 45S5, was developed by Hench *et al.* and contains a composition of 45%SiO_2-24.4%Na_2O-24.4%CaO-6%P_2O_5 (wt%), which forms a thin apatite layer at the glass-tissue interface upon implantation, facilitating the formation of a strong chemical bond between the implant and bone.[44] This interfacial bond is formed as the result of ion exchange which occurs between Na^+ ions from the glass and H_3O^+ ions from the surrounding fluid, leading to the formation of a polycondensed surface silanol gel layer, the release of soluble Si^{4+} species in the form of silicic acid, and ultimately, the precipitation of a carbonated hydroxyapatite.[45] After the bond between the implant and tissue has been formed, further degradation of the glass surface occurs, releasing ionic dissolution products which have been shown to stimulate osteogenesis *in vitro* by inducing the proliferation and differentiation of osteoblasts.[202]

In addition to promoting bone-growth properties, BGs can be formulated to release ions which exhibit anti-bacterial properties. Zn was included in the glass series for its bone-promoting properties[174], and because it has exhibited toxicity towards pathogenic bacteria which are known to cause infections at the site of implantation, such as *Staphylococcus aureus* (*S. aureus*, Gram +ve), and *Escherichia coli* (*E. coli*, Gram –ve).[176] In the experimental glasses, *TGa-1* and *TGa-2*, Ga was substituted for Zn in respective concentrations of 8 and 16 mol%, in an attempt to elicit some of the therapeutic abilities expressed by the pharmaceutical form gallium nitrate ($Ga(NO_3)_3$), through the release of ionic Ga^{3+}. The therapeutic effects elicited by ($Ga(NO_3)_3$) include bone-promoting properties, such as reduced Ca in the bloodstream of cancer patients[181,182] and reduced serum alkaline phosphatase (ALP) in patients with Paget's disease of bone[124], bactericidal effects against both Gram (+ve) strains such as *Mycobacterium tuberculosis*[125] and Gram (-ve) strains such as *Pseudomonas aeruginosa*[126], as well as a wide range of anti-cancerous properties.[99,101,102,105,106,110] Implants intended to promote osteostimulation, such as those containing BGs, are designed to encourage the adherence and proliferation of bone-forming osteoblast cells, but unfortunately, can also allow for bacterial and fungal adhesion, leading to implant-

associated infections. These infections can have serious consequences, including prolonged hospitalization with systemic anti-biotic treatment, multiple revision procedures, amputation, and potentially even death.[232] In addition to the complications introduced by implant-associated infections, it has been proven that the use of anti-biotics can promote the evolution of drug-resistant bacterial strains such as Methicillin-resistant *S. aureus* (MRSA)[233], and the development of these strains has prompted the need for different methods of combatting infection. BGs are an intriguing candidate for bone void-filling materials, which can also provide bactericidal effects at the implant site, as it has been shown that the adhesion of bacterial strains such as *E. coli* and *S. aureus* to BG surfaces results in cell death[234,235], and that liquid BG extracts can also decrease bacterial viability.[236] BGs have also been shown to inhibit the survival of the opportunistic fungus *Candida albicans* (*C. albicans*)[237], furthering their potential for these applications.

Despite the ability of BGs to form chemical bonds with bone and subsequently release beneficial ions, the mechanism by which they are delivered and maintained in a specific location still requires much improvement. Materials such as glass-ceramic scaffolds[210,212] and glass-ionomer/polyalkenoate cements[214,215] have been thoroughly studied for skeletal restoration applications, but still exhibit limitations, such as delayed setting times[217] and harmful exothermic reactions.[218] To address these limitations, polymer hydrogels can be employed as matrix materials. Hydrogels can be defined as three-dimensional networks of hydrophilic polymers which can absorb considerable amounts of water[238], and have been used in a wide range of biomedical applications, ranging from cosmetics and contact lenses, to replacement materials for skin, ligaments, and bone, due to the hydrophilicity, permeability, and biocompatibility which they have exhibited.[239-242]. These materials can be tailored to cross-link virtually instantaneously without an exothermic reaction, while simultaneously expressing an ability to fill irregular skeletal defects without the need for pre-implantation shaping[236], which can potentially allow for the direct injection, and subsequent setting, into bone void sites. In addition, the hydrogel carrier can localize the release of ions from the glass particles, and potentially be tailored to provide sustained release, which can be beneficial for specific applications.

Currently, we have synthesized degradable hydrogels consisting of CMC and Dex, which rapidly cross-link *in situ* via hydrazone bond formation (Hudson *et al.*[162]), and seeded various amounts of Ga-containing BG particles throughout the polymeric network to obtain BG-hydrogel composites. The aim of this segment of the investigation is to incubate the BGs and BG-hydrogel composites in aqueous media for periods of 1, 7, and 30 days, and evaluate the *in vitro* anti-bacterial efficacy of the respective extracts against *E. coli* and *S. aureus*, as well as the anti-fungal efficacy against *C. albicans*, using both the broth dilution method, and to more comprehensively evaluate the anti-microbial potential of the BG-hydrogel composites using the agar diffusion method.

IIIB. Materials & Methods

1. Glass Synthesis

The powdered mixes of analytical grade reagents (Fisher Sci., PA, USA) were mixed using silica beads, and then oven dried (100ºC, 1 h) and fired (1500ºC, 1 h) in platinum crucibles and shock quenched into water. For studies utlizing BGs, the resulting frits were dried, ground using a Gy-Ro Mill (Glen Creston Ltd, South West London, UK) in 10 second intervals at 3400 rpm, and sieved to retrieve glass powders with a maximum particle size of 45 μm (Table 8). For studies utilizing BG-hydrogel composites, the resulting frits were further ground to obtain glass powders with a maximum particle size of 10 µm (Table 5) to achieve efficient distribution throughout the polymer network.

Table 8. Particle Size (µm) Distribution (BG Extracts)

	Mean	**S.D.**	**d10**	**d50**	**d90**
Control	11.1	4.7	7.0	9.6	17.3
TGa-1	10.3	3.9	6.9	9.1	15.4
TGa-2	10.2	3.8	6.9	9.0	15.1

2. Polymer Functionalization, Hydrogel Synthesis, & Glass-Hydrogel Composite Synthesis

See Section IIB.

3. Glass Characterization

3.1. Particle Size Analysis

See Section IB.

3.2. Ion Release Profiles

Powder samples (n = 3) were weighed to contain 1 m^2 of glass per incubation sample (Keenan *et al.*[243]), and were then submerged in PBS for periods of 1, 7, and 30 days. After the incubation times were complete, the aqueous solution from each sample was removed and filtered using Amicon® Ultra-4 Centrifugal Filters (Merck KGaA, Darmstadt, Germany). Dilutions of each extract were then prepared (1:100), and ion

release analysis was performed. Solutions were analyzed for Na, Ca, Si, Zn, and Ga content. The ion release profile of each glass was measured using Inductively Coupled Plasma – Optical Emission Spectroscopy (ICP-OES) on a Perkin-Elmer Optima 8000 (Perkin Elmer, MA, USA). ICP-OES calibration standards for Ca, Si, Na, Zn and Ga ions were prepared from stock solutions on a gravimetric basis. Three target calibration standards were prepared for each ion, and PBS was used as a control.

4. Biological Evaluation of BGs and BG-Hydrogel Composites

4.1. Liquid Broth Analysis

The anti-bacterial efficacy of the BG series, and BG-hydrogel composites, was evaluated against *E. coli* (*ATCC 8739*, LB broth) and *S. aureus* (*strain UMAS-1*, TSB broth), while the anti-fungal efficacy was evaluated against *C. albicans*, using the broth dilution method. Two sets of BG sample extracts (n = 3, 1 m^2 glass surface area) were obtained by incubating *Control*, *TGa-1*, and *TGa-2* samples in 10 ml ultrapure water, and 10 ml PBS, for periods of 1, 7, and 30 days. For BG extracts, 50 µl/ml and 100 µl/ml of each extract was removed and added to growing experimental cultures. Extracts for BG-hydrogel composites (n = 3) were obtained by incubating samples in 1 ml PBS for periods of 1, 7, and 30 days, and 50 µl/ml of each extract was then removed and added to growing experimental cultures. Samples were then incubated, along with a *growing control* and *sterile broth*, for 24 hours in an incubator at 37ºC. After 24 hours, the samples were seeded into a 96 well-plate and measured at a wavelength of 570 nm using a µQuant Plate Reader (Bio-Tek Instruments, Inc., VT, USA).

4.2. Agar Diffusion Analysis

The anti-bacterial efficacy of the BG-hydrogel composites was evaluated against *E. coli* (*ATCC 8739*, LB broth and agar) and *S. aureus* (*strain UMAS-1*, TSB broth and agar), while the anti-fungal efficacy was evaluated against *C. albicans*, using the agar diffusion method. Relevant broth and agar were used for the culture of each different microbe, which were grown aerobically at 37ºC. Agar disc-diffusion plates were prepared by pouring 20 ml liquid agar, creating 3 equally-spaced wells in each plate by removing 6 mmϕ cut-outs using a plastic mold, crosslinking BG-hydrogel discs (n = 3) in the wells,

and then pouring an additional 6 ml liquid agar to cover the discs (Figure 39). Sterile swabs were then dipped in a 1/50 dilution of the appropriate 24 hr culture of bacteria or fungus, and spread across the plates. Plates were then incubated for 24 hr. Inhibition zones were calculated using *Equation* (1):

$$Inhibition\ Zone\ (mm) = \frac{Halo\phi - Disc\phi}{2}, \quad (1)$$

where the $Halo\phi$ is the diameter of the inhibition zone, and the $Disc\phi$ is the diameter of the test material. Plates were imaged using a Synbiosis Protocol 3 colony counter (Synoptics Ltd., Cambridge, UK).

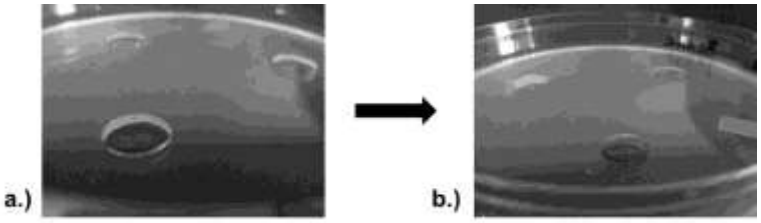

Figure 39. Agar diffusion plates with a.) Wells cut out of agar, and b.) Wells filled with *Blank* hydrogels.

5. Statistical Analysis

Broth dilution data for the BG series and the BG-hydrogel composites are presented as means ± standard deviations, and represents data from 3 individual extract replicates per BG and BG-hydrogel composite, per incubation interval. Agar diffusion data represents 3 BG-hydrogel composite discs per microbe. One-way analysis of variance (ANOVA) was used to compare broth dilution data in relation to incubation time, and Ga-content, of both the BG series, and the BG-hydrogel composites. One-way analysis of variance (ANOVA) was also used to compare agar diffusion data in relation to Ga-content. Comparison of relevant means was performed using the post hoc Bonferroni test. Differences between groups were deemed significant when $p < 0.05$.

IIIC. Results

1. Ion Release

Prior work using this glass series focused on the characterization of extracts obtained after incubation in ultrapure water. In the current study, BG extracts obtained after incubation in both ultrapure water and PBS are utilized to study their effectiveness against *E. coli*, *S. aureus*, and *C. albicans*, which is the reason for the characterization of BG ion release in PBS after 1, 7, and 30 days. The only constituent ions which were found to have released from the glass structures in significant amounts into PBS over 30 days were Si^{4+} and Ga^{3+}, and these profiles can be seen in Figure 40. Figure 40a shows that all 3 glasses exhibited a similar trend across the three time periods for Si^{4+} release, with an increase from 68, 92, and 88 mg/L after 1 day, to 91, 102, and 91 mg/L after 7 days, and then a decrease to 72, 79, and 64 mg/L after 30 days for *Control*, *TGa-1*, and *TGa-2* glasses, respectively. Although Figure 40b shows that the two Ga-containing glasses exhibited similar release profiles over the three time periods, lower Ga^{3+} concentrations were released from *TGa-1* after 1, 7, and 30 days (10, 38, and 42 mg/L, respectively), than from *TGa-2* (26, 75, and 78 mg/L, respectively), which differed from the Si^{4+} release profiles where *TGa-1* exhibited the highest release totals after each time period.

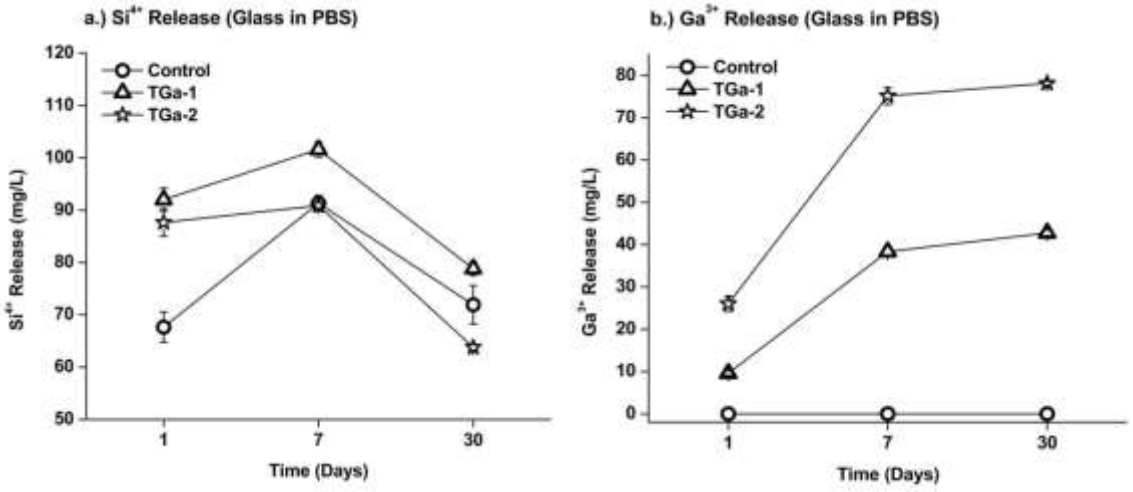

Figure 40. Ion release profiles for a.) Si^{4+} and b.) Ga^{3+} for glasses incubated in PBS for 1, 7, and 30 days.

2. Liquid Broth Analysis

Liquid broth analysis was conducted using liquid extracts obtained from the incubation of Control, TGa-1, and TGa-2 glasses in both ultrapure water and PBS, for periods of 1, 7, and 30 days. For BG sample extracts, two different concentrations of 50 µl/ml and 100 µl/ml were added to growing experimental cultures to determine if the extracts influenced bacterial viability in a dose-dependent manner. Figure 41 displays the efficacy of BG extracts against E. coli, where it is seen that none of the extracts obtained from incubation in water inhibited E. coli viability. However, for extracts obtained after incubation in PBS, all three glass types exhibited inhibitory effects towards *E. coli* viability. With the addition of 50 µl/ml of extracts obtained after 7 days of incubation in PBS, *TGa-1* and *TGa-2* decreased viability to 83% and 76%, respectively. The addition of 100 µl/ml of extracts obtained after incubation in PBS resulted in no significant decrease in viability for *Control* after 30 days, while *TGa-1* and *TGa-2* extracts respectively decreased *E. coli* viability to 62% and 58% after 7 days, and 76% and 84% after 30 days. Extracts obtained from the incubation of glass-hydrogel composites containing 0.05, 0.10, and 0.25 m^2 of *Control*, *TGa-1*, and *TGa-2* glass in PBS were also obtained over periods of 1, 7, and 30 days, and 50 µL/mL doses of each extract were then added to growing cultures of *E. coli*. As can be seen in Figure 42, extracts obtained from composites containing 0.05 and 0.25 m^2 glass produced no inhibition in *E. coli* viability, while composites containing 0.10 m^2 glass slightly inhibited viability, except for extracts obtained after 30 days from the composites containing 0.10 m^2 *TGa-2* glass, which increased viability.

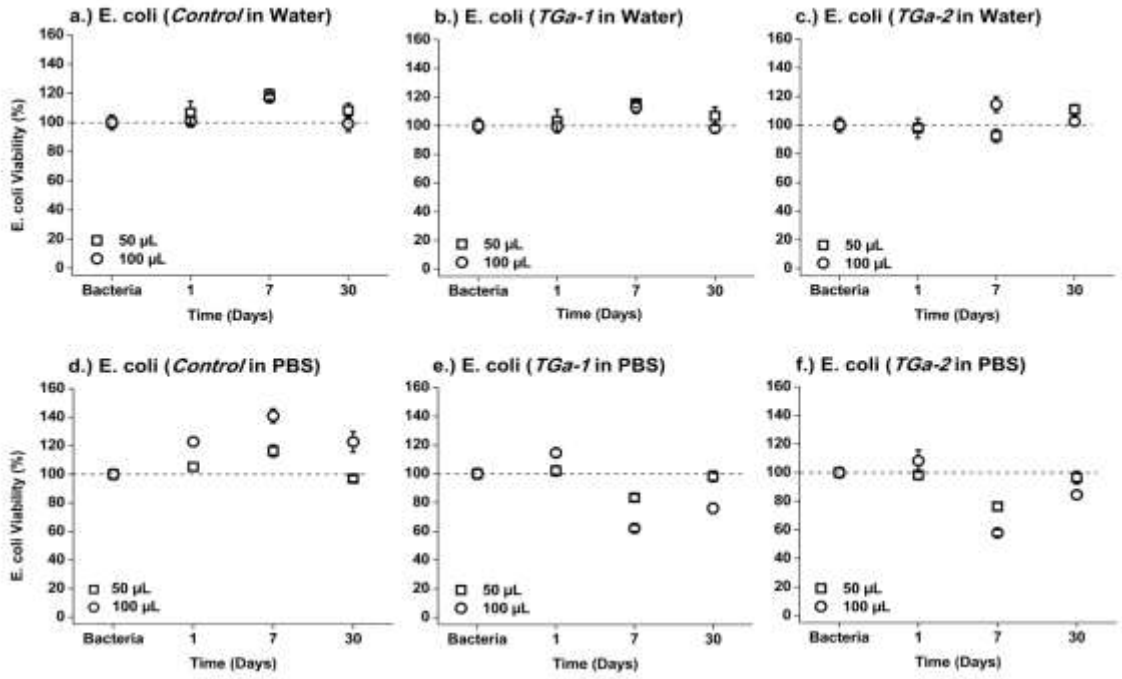

Figure 41. Anti-bacterial evaluation of BG series extracts obtained after incubation for up to 30 days in a,b,c.) Water and d,e,f.) PBS against *E. coli.*

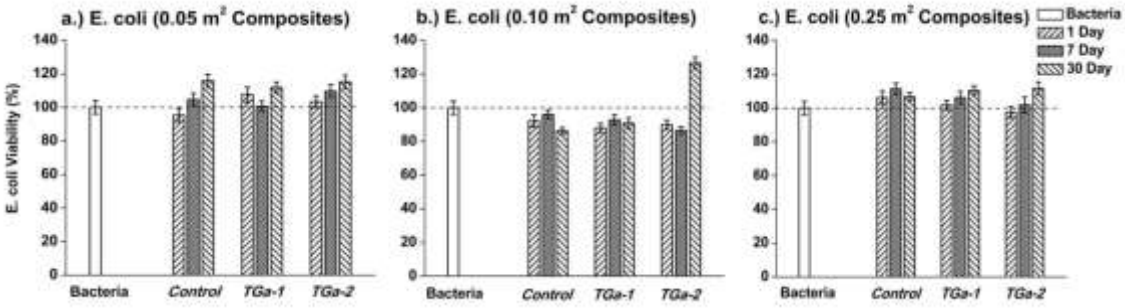

Figure 42. Anti-bacterial evaluation of extracts obtained from BG-hydrogel composites containing a.) 0.05, b.) 0.10, and c.) 0.25 m^2 glass against *E. coli*.

The efficacy of BG extracts against *S. aureus* is displayed in Figure 43, where it is evident that none of these extracts produce inhibitory effects on *S. aureus* viability after 1, 7, or 30 days. Figure 44 exhibits the results of liquid broth analysis conducted using extracts obtained from the BG-hydrogel composites, and shows that, like the BG extracts, none of the composite extracts significantly inhibit *S. aureus* viability after 1, 7, or 30 days.

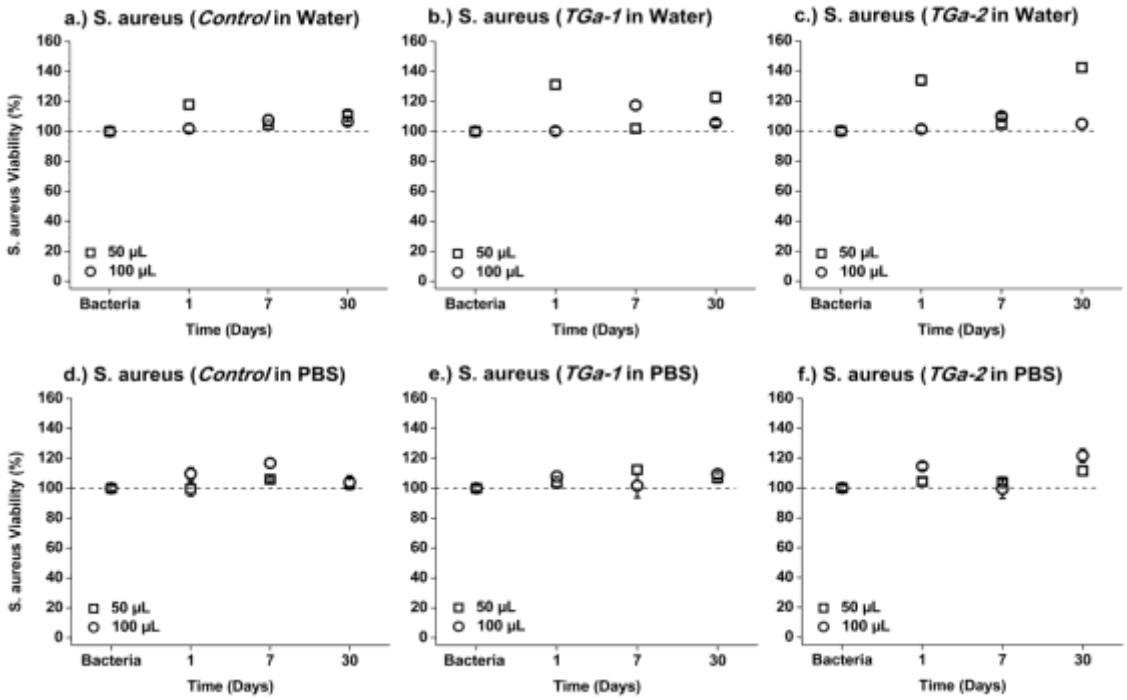

Figure 43. Anti-bacterial evaluation of BG series extracts obtained after incubation for up to 30 days in a,b,c.) Water and d,e,f.) PBS against *S. aureus*.

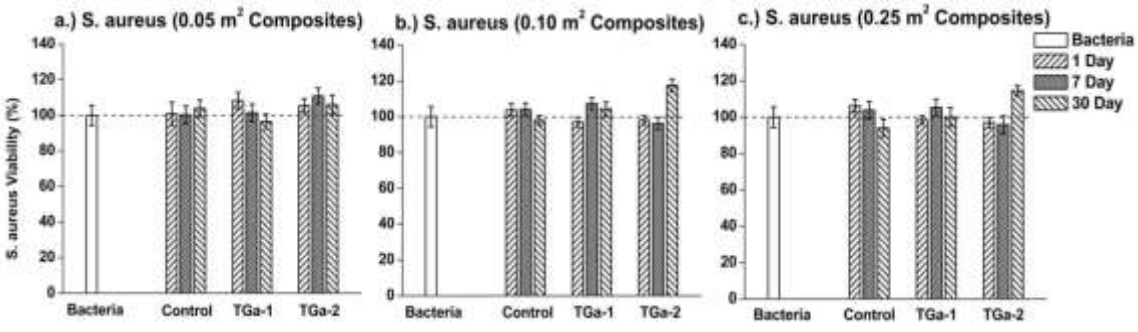

Figure 44. Anti-bacterial evaluation of extracts obtained from BG-hydrogel composites containing a.) 0.05, b.) 0.10, and c.) 0.25 m^2 glass against *S. aureus*.

The efficacies of both the BG extracts, and the extracts obtained from the glass-hydrogel composites, were also evaluated against the fungus *C. albicans*, and although total inhibition was not observed for any of the extracts, each extract did exhibit some anti-fungal ability. Figure 45 presents the liquid broth data for the BG extracts, and reveals that while both *Control* and *TGa-1* extracts obtained after incubation in both water and PBS inhibit *C. albicans* viability after 30 days, the 100 µL dose of *TGa-2* extracts obtained after incubation in PBS inhibit viability after 1, 7, and 30 days, resulting in 64% viability produced by the 30 day extracts. For extracts of *TGa-2* obtained after incubation in ultrapure water, a minimum in viability was observed after 7 days for both dosages (76% and 38% for 50 µL and 100 µL doses, respectively), while viabilities then increased to 84% and 73% after 30 days for 50 µL and 100 µL doses, respectively. The results for extracts obtained from the glass-hydrogel composites can be seen in Figure 46, and it can be seen that for each loading of each type of glass, a decrease in *C. albicans* viability is observed from 1 to 30 days, with *TGa-2* composite extracts exhibiting the lowest viabilities for each loading, with 79%, 79%, and 77% viability for 0.05, 0.10, and 0.25 m^2 composites, respectively.

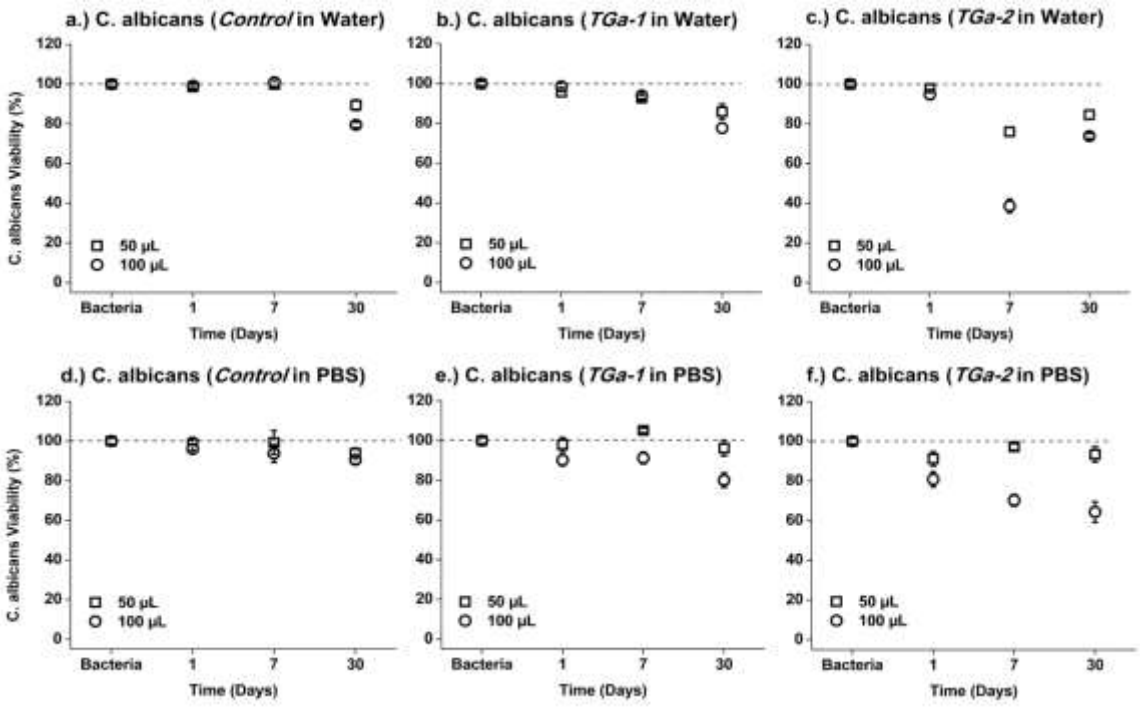

Figure 45. Anti-fungal evaluation of BG series extracts obtained after incubation for up to 30 days in a,b,c.) Water and d,e,f.) PBS against *C. albicans*.

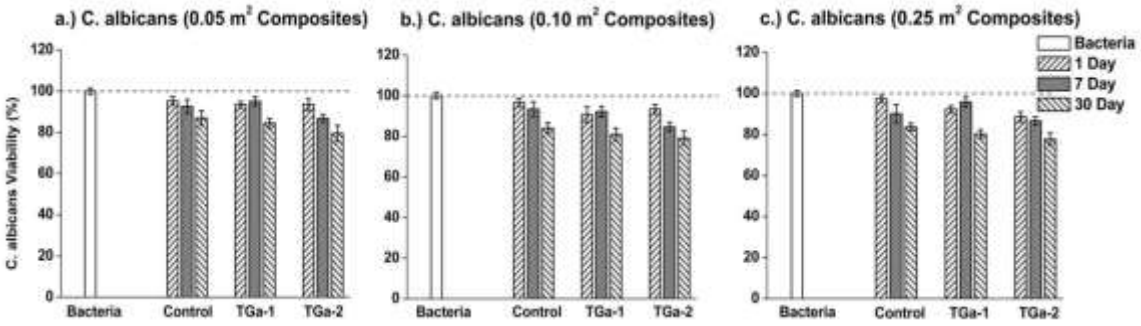

Figure 46. Anti-fungal evaluation of extracts obtained from BG-hydrogel composites containing a.) 0.05, b.) 0.10, and c.) 0.25 m^2 glass against *C. albicans*.

3. Agar Diffusion

Agar diffusion testing using glass-hydrogel composites which were cross-linked *in situ* inside wells which were excised from agar plates, and the sample images can be seen in Figure 47, with the representative numerical data for the resultant inhibition zones shown in Figure 48. It was observed that each of the glass-containing composites inhibited *E. coli* to some degree, with most of the composites producing average inhibition zones of 2 mm or less, although the most effective inhibition was observed for composites containing 0.10 m^2 *Control* glass, which produced an average inhibition zone of 8.3 mm. The composites were less effective against *S. aureus*, with only those containing 0.05 m^2 *TGa-2*, and 0.10 m^2 *Control*, *TGa-1*, and *TGa-2* glass producing inhibition zones. The composites containing 0.10 m^2 *Control* glass were once against the most effective, producing average inhibition zones of 7.5 mm. As was seen in the broth dilution studies, these glass-hydrogel composites most effectively inhibited *C. albicans*, with all composites exhibiting inhibition except for those containing 0.05 m^2 *Control* and *TGa-1* glasses. Although the numerical data does not as effectively represent the increased efficacy of these composites against *C. albicans* due to isolated surviving colonies which resulted in lower calculated inhibition zones, it can be seen in the images that nearly total inhibition was achieved by composites containing 0.10 m^2 glass, as well as those containing 0.25 m^2 *Control* glass. Additionally, significant inhibition was achieved by composites containing 0.05 m^2 and 0.25 m^2 *TGa-2* glass.

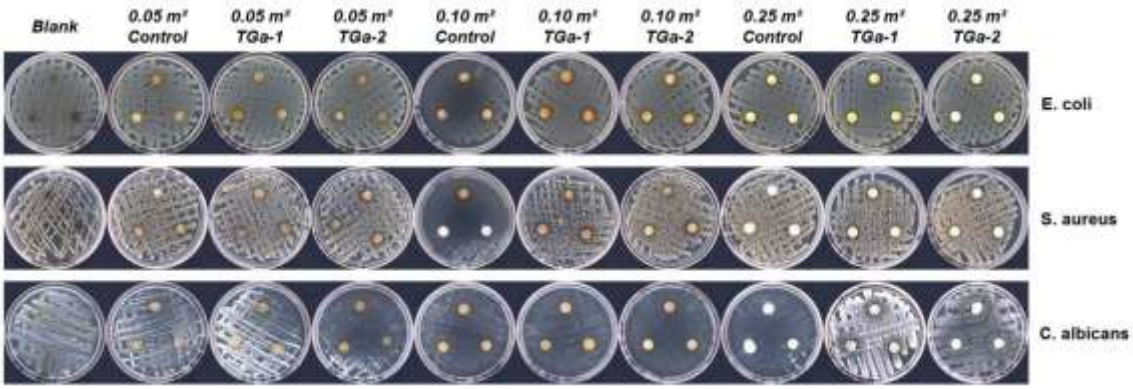

Figure 47. Anti-microbial evaluation of BG-hydrogel composites using the agar diffusion method against *E. coli*, *S. aureus*, and *C. albicans*.

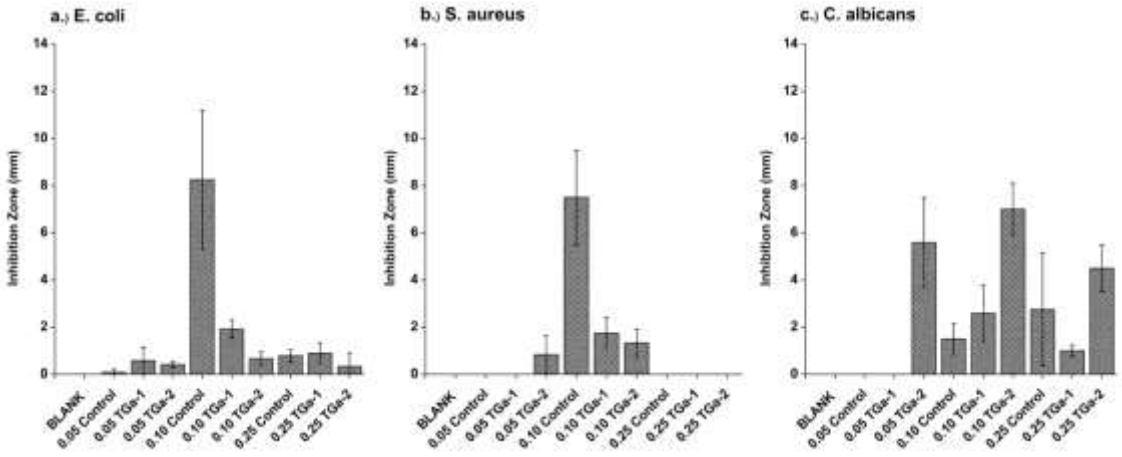

Figure 48. Inhibition zone measurements of each BG-composite against a.) *E. coli*, b.) *S. aureus*, and c.) *C. albicans*.

IIID. Discussion

BGs are materials which possess the ability to react with physiological fluids upon implantation into the body and form chemical bonds with bone. These glasses can be formulated to contain multiple elements which, upon dissolution, can provide many different therapeutic effects. The delivery of BG particles is an issue that has garnered interest for decades with several advancements having been made, however, there is still much room for improvement. Polymeric hydrogels are of particular interest for this application, as they can be engineered to possess a scaffold-like structure which can allow for cell proliferation and survival.[227] These materials can also be used in composite materials such as CMC-hydroxyapatite composites, which can provide enhanced osteoconductivity[223], and Dex gels seeded with bone morphogenic protein(BMP)-loaded microspheres, which can allow for controlled release kinetics of biomolecules.[224] In the current study, CMC-Dex hydrogels were employed, which were previously shown to act as carriers for the anti-fungal agent Amphotericin B to provide fungicidal effects against *C. albicans*[162], and were seeded with Ga-containing BGs to determine if the release of ionic species from these composite materials could provide anti-bacterial and anti-fungal effects.

Prior work had characterized the release of constituent ions from the BG series after incubation in ultrapure water[243], but in order to more thoroughly compare the BG extracts to the BG-hydrogel composite extracts, BG extracts were also obtained after incubation in PBS for 1, 7, and 30 days, and ion release was characterized using ICP-OES. Unlike the extracts obtained in ultrapure water, which exhibited release of each constituent element over 30 days, only Si^{4+} and Ga^{3+} were released from the glass particles into PBS. As was seen in prior work, *TGa-2* released the largest quantity of Ga^{3+} after 1, 7, and 30 days. However, in comparison to prior work where *Control*, *TGa-1*, and *TGa-2* released 7, 14, and 31 mg/L of Si^{4+} after 1 day, and 1, 10, and 30 mg/L after 30 days in ultrapure water, respectively, in the current study, *Control*, *TGa-1*, and *TGa-2* released 68, 92, and 88 mg/L of Si^{4+} after 1 day, and 64, 79, and 72 mg/L after 30 days in PBS, respectively, suggesting an increase in reactivity between particle surfaces and solution. This may be attributed to the presence of Na^{+} and K^{+} ions in PBS, which may have increased the rate of interaction of the fluid with negatively charged surface groups of the glass particles,

thus resulting in an increased dissolution rate. Moreover, since PBS possesses a higher pH (~7.4) than ultrapure water (~5.4) which is further from the isoelectric point of SiO_2 (~1.7-3.5)[229], the increased charge discrepancy may have led to increased polarization of Si-containing groups present on the surface of the glass particles, thus resulting in increased Si^{4+} release. *Control*, *TGa-1*, and *TGa-2* also all exhibited a decrease in Si^{4+} release from 7-30 days, which was also observed in prior work, and was attributed to precipitation of ions out of solution and onto BG particle surfaces.*TGa-1* released more Si^{4+} after 1, 7, and 30 days than *Control* and *TGa-2*, and no decrease in Ga^{3+} release was observed for either *TGa-1* or *TGa-2* from 7-30 days, suggesting that only Si^{4+} precipitated out of solution, while Ga^{3+} did not. It was observed that Si^{4+} release from *TGa-1* decreased from 101 to 79 mg/L after 7 and 30 days, respectively, while release from *TGa-2* decreased from 91 to 72 mg/L, clearly indicating precipitation out of solution. However, it was observed that Ga^{3+} release from *TGa-1* increased from 10 to 38 mg/L from 1-7 days, and only from 38 to 42 mg/L from 7-30 days, while release from *TGa-2* increased from 26 to 75 mg/L from 1-7 days, and only from 75 to 78 mg/L from 7-30 days, implying that the release of Ga^{3+} from both Ga-containing glasses slowed between 7-30 days, which further suggests that Si^{4+} ions precipitated out of solution and onto the BG particle surfaces, resulting in a thicker silica-rich surface layer which slowed the release of Ga^{3+} from the glass structure and into solution.

Liquid broth analysis was conducted using 50 and 100 µL aliquots of liquid extracts of BGs obtained after incubation in ultrapure water and PBS, as well as 50 µL aliquots of extracts obtained from BG-hydrogel composites after incubation in PBS, for periods of 1, 7, and 30 days. For BG water extracts, no inhibitive activity was exhibited towards *E. coli* or *S. aureus* over the 30 day period. However, extracts of all 3 glasses did display some anti-fungal ability towards *C. albicans*, with *TGa-2* extracts obtained after 7 days of incubation displaying the greatest efficacy. Prior work utilized these extracts to characterize the ion release of this glass series[243], and revealed that over a 30 day incubation period in ultrapure water, the release of Na^+ from each of the glasses was comparable at each time interval, *TGa-1* and *TGa-2* released Ga^{3+} while the non-Ga-containing *Control* did not, and *TGa-2* released at least twice the amount of Ca^{2+} and Si^{4+} than *Control* and *TGa-1* released at each time interval. Since each glass exhibits some

inhibition toward *C. albicans* despite the absence of Ga^{3+}-release from *Control*, according to the previously characterized ion release information, the anti-fungal ability may be attributed to the release of either Ca^{2+} or Si^{4+}. For BG extracts obtained in PBS, *S. aureus* was once again uninhibited, however, these extracts did express some inhibitive ability towards the viability of both *E. coli* and *C. albicans*. This is not a condemning result, as Gram +ve bacteria such as *S. aureus* are known to lack an outer membrane, but possess a simple, thick peptidoglycan cell wall, which causes these bacteria to be naturally more resistant to anti-microbials than Gram –ve bacteria like *E. coli*, as these microbes possess more complex, yet much thinner barriers to the outside environment.[171] While the viability of neither *E. coli* nor *C. albicans* was hindered by the *Control* extracts, *TGa-1* and *TGa-2* extracts exhibited some inhibitive ability towards both strains, with increased efficacies displayed by the 100 µL doses compared to the 50 µL doses after 7 and 30 days against *E. coli*, and after 1, 7, and 30 days for *C. albicans*. For both *TGa-1* and *TGa-2*, a decrease in *E. coli* viability was observed from 1-7 days, while viability increased from 1-30 days. The current ion release data revealed that these glasses exhibited both an increase in Si^{4+} release from 1-7 days and a decrease in Si^{4+} release from 7-30 days, while Ga^{3+} release continually increased over both periods, suggesting that Si^{4+} concentration in solution may have more influence on *E. coli* viability than Ga^{3+} concentration. However, for *C. albicans*, the addition of 100 µL aliquots of both *TGa-1* and *TGa-2* extracts obtained after 30 days of incubation resulted in the lowest viabilities of any of the time intervals, suggesting that for this strain of fungus, the concentration of Ga^{3+} in solution may hold more influence over cell viability than Si^{4+} concentration. Interestingly, the results of liquid broth analysis using the extracts obtained from the BG-hydrogel composites did not support the inferences made from the BG extract data. Prior work characterized the ion release of each of these composites, and found that both glass composition and glass loading within the composites affected ion release, with the most notable trends including increased Si^{4+} release from 1-30 days for composites containing 0.05 m^2 *Control*, *TGa-1*, and *TGa-2*, 0.10 m^2 *Control* and *TGa-1*, and 0.25 m^2 *TGa-1* and *TGa-2*, and increased Ga^{3+} release from 1-30 days for all composites containing *TGa-1* and *TGa-2*. Additionally, the release of Zn^{2+} was observed after 30 days for composites containing 0.05 m^2 *TGa-1* and *TGa-2*,

0.10 m^2 *Control*, *TGa-1*, and *TGa-2*, and 0.25 m^2 *Control* and *TGa-2*, while all composites containing 0.25 m^2 glass exhibited Ca^{2+} release over each of the time intervals, with a maximum after 30 days. Considering these prior results, one would expect the BG-hydrogel composite extracts to possess greater efficacy against both *E. coli* and *S. aureus* than both types of BG extracts, as Zn has been shown to inhibit both of these bacterial species[176], and Zn^{2+} release was observed for several of the composites, while no release was observed for the glasses in either incubation media. Additionally, many of the composites released higher concentrations of Si^{4+} at respective time intervals than the BGs. However, Ga^{3+} release from composites containing *TGa-1* and *TGa-2* was minimal ($\leq$ 5 mg/L) after 1, 7, and 30 days, although increased release was observed from 1-30 days, while these glasses by themselves released larger quantities in both water and PBS. This information suggests that perhaps a form of synergy exists between Si^{4+} and Ga^{3+} ions, which allows for more efficient anti-bacterial activity than when both ions are not present in solution together. The idea of synergistic anti-bacterial properties between metal ions has been previously proposed in the literature for ions such as Zn^{2+} and Ce^{3+},[244] where it was suggested that the different ions may have different attack target sites on the cell membranes of bacteria, resulting in more bactericidal effect when both ions are present. Additionally, it was also proposed that the ions may interact with each other in solution, producing more hydroxylic free radicals, which are extremely reactive and can also inhibit bacterial growth. Although these results do not display complete colony reduction for any of the extracts against either bacteria or fungus, these results are encouraging as they exhibit *in vitro* the ability of ions dissociated from the glass particles to reduce the viability of both *E. coli* and *C. albicans*. This is significant because prior studies using 45S5 Bioglass® particulate concluded that BGs possess anti-bacterial abilities against common bacteria such as *E. coli*[234] and *S. aureus*[235], but that these effects were dependent on both the high pH of solution, and the adhesion of microbes to the particle surfaces, as this adhesion would result in the release of a high Ca^{2+} concentration in the proximity of the plasma membrane, which would distort the membrane's electrochemical potential gradient and ultimately result in cell death. To further evaluate the anti-bacterial and anti-fungal potential of this series of BGs, the authors intend to re-conduct the assays using glass particulates, to determine if, in addition to reducing the

viability of microbes by ionic dissolution products, this BG series can also allow for the adhesion of microbes, and further reduce their viability.

Agar diffusion analysis was also conducted against all three microbial strains, using BG-hydrogel composites which were injected directly into pre-formed wells in agar, and incubated post-inoculation for 24 hours. These studies concurred with the liquid broth data, as several of the BG-hydrogel composites produced small inhibition zones in *E. coli*, while several composites produced larger inhibition zones in *C. albicans*, with near complete colony reduction observed for multiple samples. However, there were also some stark differences observed in these studies, such as the appearance of inhibition zones in *S. aureus*, and the dominant anti-microbial ability of composites containing 0.10 m^2 *Control* glass against *E. coli*, *S. aureus*, and *C. albicans*. This may be explained by prior work by the authors, which characterized the ion release of these BG-composites and found that for each glass-loading level, composites containing *Control* glass released significantly more Si^{4+} than *TGa-1* and *TGa-2* composites after 24 hours, with a maximum of 157 mg/L observed from 0.10 m^2 *Control*, while minimal Ga^{3+} ($\leq$ 3 mg/L) was released from the Ga-containing composites. Although the liquid broth studies suggested that the release of Si^{4+} was not solely responsible for anti-microbial activity, the results of prior work suggest that composites containing 0.10 m^2 *Control* glass exhibit the fastest rate of glass dissolution, and with these composites being incubated in agar with bacteria seeded in fixated positions directly above, rather than aqueous media with bacteria seeded in solution, perhaps these composites released ionic dissolution products at a higher rate than the other composites, resulting in increased microbial inhibition.

IIIE. Conclusion

In summary, throughout this section we discovered that:

- The release of dissolution products from the glasses is highly dependent on the medium in which they are submerged, exhibiting different trends between incubation in ultrapure water and PBS
- None of the liquid extracts from either the BGs or the composites inhibited *S. aureus* viability
- Both BG and composite extracts exhibited inhibitive properties toward *E. coli* and *C. albicans* viabilities
- Agar diffusion studies with composites cross-linked *in situ* into agar which was then covered with colonies exhibited more effective inhibition of *C. albicans* than liquid broth studies
- Composites also exhibited a small degree of inhibition towards *S. aureus* in the agar diffusion studies

In this segment of the study, ion release profiles were first characterized for BG particles incubated in PBS for periods of up to 30 days, and revealed that only Si^{4+} and Ga^{3+} were released in significant concentrations. Broth dilution studies revealed that none of the liquid extracts inhibited *S. aureus* viability, while some inhibitive effects were exhibited by the extracts of both the BGs, and the BG-hydrogel composites, against both *E. coli* and *C. albicans*, with the greatest reduction in viability observed for BG extracts against the fungus. Agar diffusion studies further exhibited the anti-fungal ability of these materials, while also suggesting that these materials possess anti-bacterial potential when placed in a more viscous environment than aqueous media. The results of this study suggest that Ga-containing BGs and BG-hydrogel composites have potential as anti-bacterial and anti-fungal agents, which combined with the results of prior work, further suggests their potential as bone-void filling materials.

Upon completion of the third portion of this project, the Ga-glass series had been fully characterized, both structurally[154] and physically, glass-hydrogel composites had been synthesized and physically characterized, both the glasses and composites had exhibited *in vitro* cytocompatibility with fibroblasts and osteoblasts, and the *in vitro* anti-

bacterial and anti-fungal efficacy of both the glasses and the composites had been extensively evaluated. As the initial three portions of this study combined to suggest the applicability of these materials as multi-functional bone-filling materials, the fourth and final segment of this project then aimed to obtain a deeper understanding of the molecular structures of the glass-hydrogel composites, and to evaluate the *in vitro* efficacy of their extracts against cancerous MG-63 osteosarcoma cells.

Part IV: Structural Characterization and Anti-Cancerous Potential of Ga-Bioactive Glass/Polymer Hydrogel Composites

Keenan T.J., Placek L.M., Coughlan A., Hall M.M., Wren A.W., "Structural Characterization and Anti-Cancerous Potential of Ga-Bioactive Glass/Polymeric Hydrogel Composites" *Carbohydrate Polymers* (Under Peer Review).

The fourth and final part of this study aimed to obtain a more in-depth understanding of the molecular structure of these glass-hydrogel composite materials. As one of the primary intentions of included Ga in the glass series was its potential anti-cancerous effects, the cytotoxicity of liquid extracts from these materials was also evaluated against MG-63 osteosarcoma. The results in this section include:

- Transmission electron microscopy micrographs of the composites
- DTA thermograms of the *Blank* hydrogel and the glass-gel composites
- ^{13}C cross-polarization magic angle spinning nuclear magnetic resonance (^{13}C CP/MAS-NMR) spectra for both the unfunctionalized and functionalized polymers, the *Blank* hydrogel, and the glass-gel composites
- Cell viability analysis (MG-63) using liquid extracts from both the glass series and the glass-gel composites

In this segment, TEM confirmed what was previously observed with SEM, showing that glass particles were present within the composites, although particle agglomeration was observed. Thermal analysis revealed that the composite materials had multiple glass transition temperatures (T_g), and melting temperatures (T_m), and that glass composition and content did have small effects on both T_g and T_m. MAS-NMR revealed that both CMC and Dex were successfully functionalized, that cross-linking occurred in the hydrogels and composites, and that glass addition did slightly alter bonding environments. Cell viability analysis suggested that extracts of composites containing glass with the largest Ga-content (16 mol%), significantly decrease MG-63 viability after 30 days of incubation. This final portion of the study successfully characterized this composite series, and demonstrated their potential for anti-cancerous applications, further suggesting their potential for bone void-filling applications.

IVA. Introduction

Bone is an extremely complex, dynamic, composite tissue, in which defects can occur due to trauma, infection, or tumor resection which are too large for the body to repair without assistance[198], and in order to correct these flaws, complex materials must also be synthesized to perform in a dynamic manner. One such class of materials is known as bioactive glasses (BG), which were first formulated by Hench *et al.*[201], possess a low glass network-former and high glass network-modifier content , which upon implantation into the body, allows for a series of surface reactions to occur in order for the material to form a strong chemical bond with host tissue, and then the subsequent dissolution of the material over time. BGs are of interest in defect-filling applications because their dissolution products, which are released over time from the eroding glass network, can stimulate positive responses in the host tissue, such as bone-promoting properties[202], and can also provide additional therapeutic effects, such as anti-bacterial[203,204], and possibly, anti-cancerous abilities. In the current study, a BG series ($0.42SiO_2$-$0.10Na_2O$-$0.08CaO$-$(0.40 - x)ZnO$-$(x)Ga_2O_3$) was formulated, in which ZnO was substituted with up to 16 mol% Ga_2O_3. This glass composition has been previously shown to allow for dissolution of the glasses upon submersion in aqueous media over periods of up to one year, to allow for Ca/P-containing depositions to form on the surface, and to promote the survival of MC3T3-E1osteoblasts.[245] Each constituent of this series has been shown to play a role in either bone metabolism, or the establishment of an interfacial bond between implant and bone, including: (1) Si, which not only acts as the primary glass network-former, but is also a key element in the formation and calcification of bone tissue[205,206]; (2) Na, which acts as the primary glass network-modifier and exchanges with H_3O^+ ions in solution, beginning the process of forming a chemical bond between implant and host[208]; (3) Ca, which can increase the expression of insulin-like growth factors, which are responsible for osteoblast proliferation[209]; (4) Zn, which was included for its osteostimulative[174] and anti-bacterial[176] properties; and (5) Ga, which was incorporated in an attempt to harness some of the bone-promoting[120,123,124], anti-bacterial[125,126], and anti-cancerous[99-101,106] properties exhibited by the pharmaceutical gallium nitrate ($Ga(NO_3)_3$), from the ionic form (Ga^{3+}), upon dissolution from the glass network.

Despite the ability of BGs to chemically bond to tissue, and to release therapeutic ions into the local environment over time, the challenge of developing a sufficient mechanism to deliver these materials to a defect site, and maintain their positioning for extended periods of time, is still an area which requires much more work. Some progress has been made with the development of glass-ceramic scaffolds[210-212] and glass-ionomer/polyalkenoate cements[213-216], however, these methods still suffer major drawbacks, such as the requirement for pre-implant machining, extended setting times[217], and potentially necrosis-inducing exothermic reactions during the setting process.[240] Ideally, one would like to obtain a matrix material which can not only allow for easy delivery of BG particles to a bone defect site of any shape without prior shaping, and maintain that position for a long period of time, but also act as a scaffold upon which bone-forming osteoblast cells can attach and deposit new host tissue, without the risks posed by long setting times and exothermic reactions. One class of materials which can potentially be manipulated to satisfy each of these requirements is called polymer hydrogels, which are defined as three-dimensional networks of hydrophilic polymers which can absorb and retain significant amounts of water.[238] Polymer hydrogels have been used in a wide range of applications, including drug-delivery, cosmetics, contact lenses, corneal implants, and in the replacement of tissues such as skin, tendons, ligaments, and bone, because of the excellent hydrophilicity, permeability, and biocompatibility they have displayed.[239-242,246] Of particular interest for biomaterials applications in the modern age are hydrogels made from natural polymers because of their natural abundance, biocompatibility, and biodegradibility.[247-250] Of the many natural polymers, cellulose and dextran are of particular interest for several reasons. Cellulose is the most abundant polysaccharide available worldwide[251], which translates to a relatively low cost compared to some other materials, consisting of many β-1,4 linked D-glucose units[252,253], and has proven effective as a constituent of composite materials, such as hydroxyapatite/cellulose composites for enhanced osteoconductivity.[223] Dextran (Dex) is a homopolysaccharide consisting of straight chains of D-glucose units with α-1,6 linkages, with branches most commonly stemming from α-1,3 linkages[166], and has also proven to be an effective component in composite materials like Dex gels seeded with bone morphogenic protein (BMP)-loaded polyethylene glycol (PEG) microspheres for

BMP-delivery.[224] Additionally, prior work has been conducted by Hudson *et al.*, in which the water-soluble cellulose derivative sodium carboxymethyl cellulose (CMC) was functionalized with hydrazine groups and cross-linked via hydrazone bond formation to conjugates of Dex, which was first modified with aldehyde groups, and the anti-fungal Amphotericin B (AmB), to obtain hydrogel composites which were shown not to cause tissue toxicity in mice, and also exhibited anti-fungal efficacy against *C. albicans*.[162]

Currently, composites have been synthesized consisting of degradable CMC/Dex hydrogels impregnated with various loadings of Ga-BG particles, which have been previously characterized by the authors to determine their swelling and solubility characteristics, their compatibility with fibroblasts and osteoblasts, and their potential as anti-bacterial and anti-fungal agents. This study aims to structurally characterize these composites through the use of transmission electron microscopy (TEM), differential thermal analysis (DTA), and ^{13}C cross-polarization magic angle spinning nuclear magnetic resonance (CP/MAS-NMR), and to determine the anti-cancerous potential of liquid extracts obtained from these composites against MG-63 osteosarcoma.

IVB. Materials & Methods

1. Glass Synthesis

See Section IIB.

2. Polymer Functionalization, Hydrogel Synthesis, & Glass-Hydrogel Composite Synthesis

See Section IIB.

3. Composite Characterization

To prepare glass/hydrogel composites for structural characterization, samples were first frozen at -80ºC and then lyophilized using a Labconco FreezeTriad Freeze Drying System (Labconco, USA). Composites were then thinly sliced and ground to a powder (Figure 49).

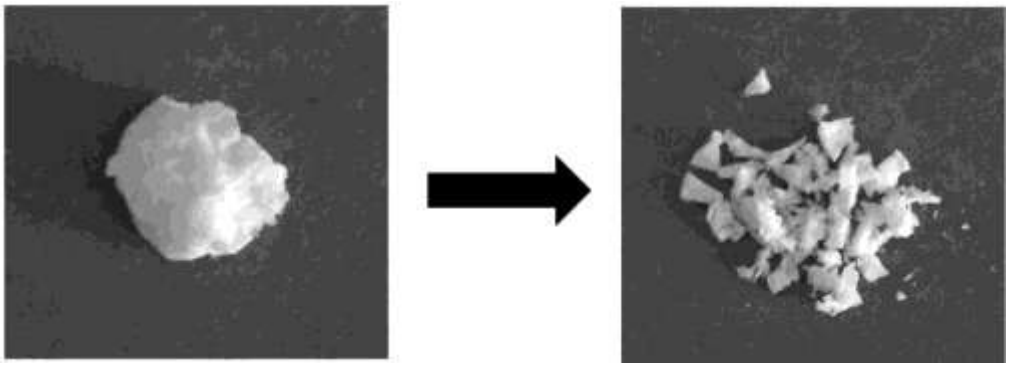

Figure 49. Grinding of BG-hydrogel composites.

3.1. Transmission Electron Microscopy (TEM)

TEM specimens were first placed on a copper single tilt holder (FEI) and then placed into the instrument. TEM was conducted using a FEI Titan ETEM 80-300 electron microscope (FEI Company, Hillsboro, OR, USA), equipped with a Gatan imaging filter (GIF), and operated at an accelerating voltage of 300 kV. The Imaging Mode was undertaken as energy filtered zero loss images with an energy slit width of 10 eV. This was done to ensure that 300±5 eV electrons are used to form each image, and all other inelastically scattered electrons were removed.

3.2. Thermal Analysis

A SDT Q600 Simultaneous Thermal Gravimetric Analyser-Differential Scanning Calorimetry (TGA-DSC) (TA Instruments, DE, USA) was used to obtain a thermal profile of each composite, specifically the glass transition temperature (T_g) and crystallization temperatures. A heating rate of 10ºC/min was employed in an air atmosphere (100 mL/min) using alumina as a reference in a matched platinum crucible. Sample measurements were carried out every 0.5 seconds between 30˚C and 650˚C. TA Universal Analysis software (TA Instruments, DW, USA) was used to plot and obtain the temperatures of interest.

3.3. ^{13}C Cross-Polarization Magic Angle Spinning Nuclear Magnetic Resonance (^{13}C CP/MAS-NMR)

^{13}C CP solid state NMR analysis was performed at a frequency of ~150.96 MHz (BF=-150.9581280 with transmitter set to 100ppm) on a Bruker AVIII 600MHz widebore spectrometer equipped with a 4mm HXY MAS probe configured with RF channels for ^{1}H and ^{13}C temperature regulated to 298K. The spin rate was always kept at 8 kHz. A pulse width of 1H 2.5us (90 and 100kHz tppm 15-based decoupling during detection) was used, with a contact time of 1ms 13C (with a B1 field of 66kHz), and an acquisition time of 25 ms. The recycle time was 3s. Spectra were obtained with a width of ~414 ppm, and 4096 scans were conducted for each experiment. The proper contact time was chosen after several trials with *Blank* hydrogels. A 20Hz Gaussian apodization function was also applied to the time domain prior to Fourier transformation.

4. Biological Evaluation

4.1. Obtaining Liquid Extracts

To obtain BG extracts, powder samples (n = 3), whose particle size information is displayed in Table 8, were weighed to contain 1 m^2 of glass per incubation sample (Keenan *et al.*[245]), and were then submerged in 10 ml ultrapure water for periods of 1, 7, and 30 days. To obtain BG-hydrogel composite extracts, samples (n = 3) were submerged in 1 ml PBS for periods of 1, 7, and 30 days. After the incubation times were complete,

the aqueous solution from each sample was removed and filtered using Amicon® Ultra-4 Centrifugal Filters (Merck KGaA, Darmstadt, Germany).

4.2. Methyl Tetrazolium (MTT) Assays

The established cell line MG-63 Osteosarcoma (ATCC®-CRL-1427™) was used in this study. MG-63 osteosarcoma were cultured in EMEM (ATCC®-30-2003™), which included L-glutamine and was supplemented with 10 vol% FBS. Cells were maintained on a regular feeding regime in a cell culture incubator at 37˚C, with a 5% CO2/95% air atmosphere. Cells were then seeded into 96 well plates at a density of 10,000 cells per well and incubated for 24 hours prior to the addition of liquid extracts. The cytotoxicity of BG and BG-hydrogel composite extracts were evaluated using the Methyl Tetrazolium (MTT) assay. 10 µl aliquots of undiluted extract were added into wells containing cells in culture medium (100 µl), and incubated for an additional 24 hours. 10 µl of the MTT assay was then added to each well and incubated for an additional 4 hours. After 4 hours, the cultures were removed from the incubator, and the resultant formazan crystals were dissolved by first removing all of the aqueous media from each well, and then adding 100 µl of MTT Solubilization Solution (10% Triton x-100 in Acidic Isopropanol. (0.1 n HCI)). Once the crystals were fully dissolved, the absorbance was measured at a wavelength of 570 nm using a µQuant Plate Reader (Bio-Tek Insturments, Inc., VT, USA). 10 µl aliquots of ultrapure water and PBS were used as control additions for BG and BG-hydrogel composite assays, respectively, and cells were assumed to have metabolic activities of 100%. BG, *Blank* hydrogel, and BG-hydrogel composite extracts in media without cells were also tested, and were found not to interfere with the MTT assay.

5. Statistical Analysis

Cell viability data are presented as means ± standard deviations, and represent data from 3 individual extract replicates per BG or BG/hydrogel composite, per incubation interval. One-way analysis of variance (ANOVA) was used to compare the cytotoxicity of the composite extracts against MG-63 osteosarcoma in relation to 1) incubation time, and 2) Ga-content. Comparison of relevant means was performed using

the post hoc Bonferroni test. Differences between groups were deemed significant when $p < 0.05$.

IVC. Results & Discussion

1. Structural Characterization

1.1. TEM Analysis

TEM was utilized to observe the dispersion of the glass particles in the glass-hydrogel composites, and the resulting micrographs can be seen in Figure 50. Figure 50a shows that the non-Ga-containing *Control* glass is more evenly distributed within the hydrogel network, while Figures 50b and 50c suggest that the particles of the Ga-containing *TGa-1* and *TGa-2* glasses agglomerated slightly more than *Control*.

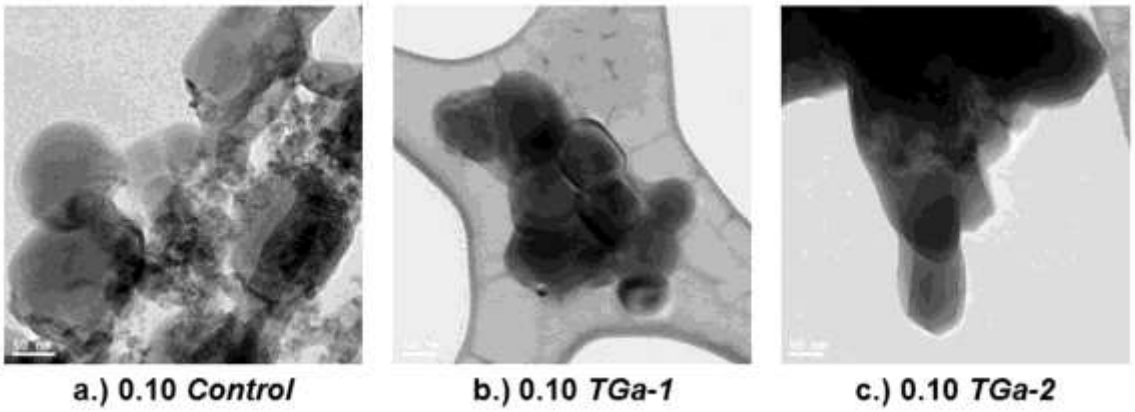

Figure 50. TEM micrographs of BG-hydrogel composites containing 0.10 m^2 a.) *Control*, b.) *TGa-1*, and c.) *TGa-2*.

1.2. Thermal Analysis

Analysis by DTA was conducted to provide insight to structural differences which may exist between the *Blank* CMC/Dex hydrogel, and the various BG-hydrogel composites, based upon the behavior of the samples as a function of temperature, and these results are presented in Figure 51. As can be seen for the *Blank* hydrogel, there are transitions which occur at 192ºC and 322ºC, followed by a large exothermic peak at 452ºC, and then a broad exothermic shoulder at 458ºC. For each of the composite samples, the initial transition can also be observed between 190-197ºC, and this transition likely corresponds to the occurrence of some complex reactions involving Dex, such as

melting, isomerization, and transglycosylation.[254] The composite samples also exhibit the second transition that was observed in the *Blank* gel, and these transitions can be seen in the range of 322-339ºC. This transition is likely indicative of the decomposition of CMC, which has been observed near 290ºC in prior work[240], however, in the current study we have reported the midpoint temperature of the transitions, and not the temperatures where the transition initiated, which ranged from 285-295ºC. Most of the composites then exhibit an intense exothermic peak between 437-455ºC, followed closely by a broad exothermic shoulder between 453-464ºC. It can be seen in Figures 51k-n, which display the residual weight fraction (%) as a function of time, that the intense exothermic peaks correlate with sharp increases in the rate of weight loss, while the broad exothermic shoulders correlate with a temporary halt in weight loss, which is again followed by rapid weight loss. These figures also show that for all samples, weight loss does not occur above ~480ºC, and composites containing larger amounts of glass retain higher residual weight fractions. These factors combine to suggest that the exothermic peak and shoulder are indicative of decomposition reactions due to oxidation, and at temperatures above the maximum heighth of the shoulder, any remaining organic components are converted to CO_2 (g) until only the glass particles remain beyond ~480ºC. Figures 51k-n also display clear increases in the rate of weight loss after the first two transitions for all samples other than the composite containing 0.25 m^2 *Control* glass, which also displays only a single broad exotherm in Figure 51d. This sample displays a very slight increase in the rate of weight loss after the transition temperature associated with Dex, but still displays an increase in the rate of weight loss after the transition associated with CMC which is comparable to other composite samples, which combined with the single broad exothermic peak, may suggest that perhaps this sample contains a higher CMC-content than the others, resulting in the disappearance of the distinct exothermic shoulder, and thermal properties more characteristic of CMC than a hydrogel consisting of both CMC and Dex. The weight loss information presented in Figures 51k-n also shows that composites containing 0.05 m^2 glass lost weight in a manner nearly identical to the *Blank* hydrogel, while composites containing 0.25 m^2 glass displayed more distinct decreases in the rate of weight loss at temperatures immediately above those at which intense exothermic features were observed. Additionally, composites containing 0.10 or 0.25 m^2

TGa-1 or *TGa-2* exhibited increases in the rate of weight loss immediately prior to the temperatures at which their intense exothermic peaks occurred, while composites containing 0.10 or 0.25 m^2 *Control* did not. This suggests that there may be an interaction occurring between the Ga-containing glass particles and the polymer matrix, which translates to more rapid degradation of a specific group of organic components during the first intense exothermic reaction. Prior work with this glass series has demonstrated that the Ga-containing glasses exhibit more rapid dissolution in aqueous media than the *Control* glass[245], suggesting that these glass particles possess more reactive surfaces, which may have resulted in the interaction of polar groups present on these surfaces with charged or unreacted moieties within the polymer matrix.

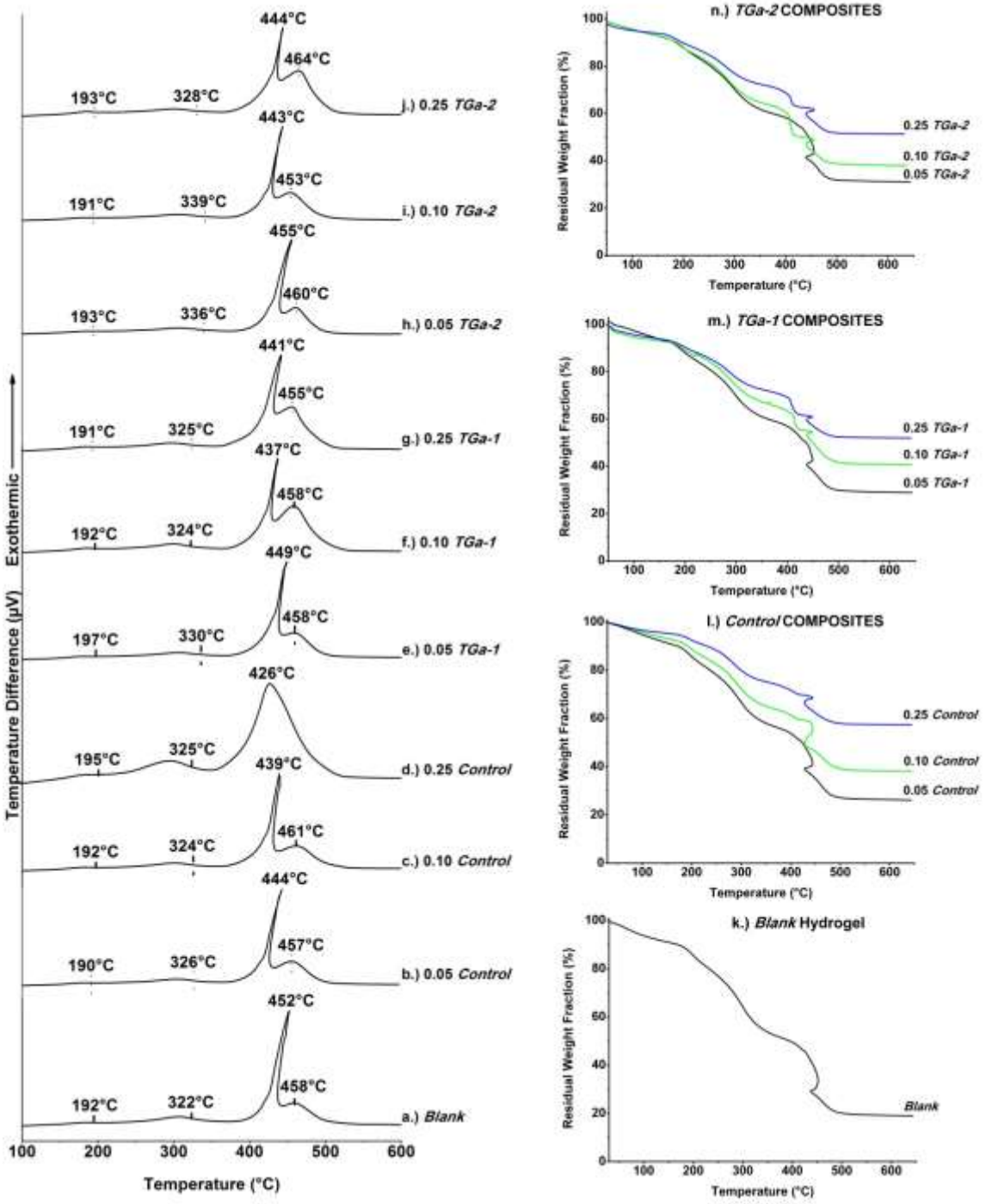

Figure 51. DTA thermograms of composites displaying a.-j.) Temperature Difference (µV) and k.-n.) Residual Weight Fraction (%) as a function of temperature (ºC).

1.3. ^{13}C CP/MAS-NMR

^{13}C CP/MAS-NMR spectroscopy is considered one of the most powerful tools for characterizing the composition and sequence of polysaccharide units.[255,256] For several years, the application of solid-state NMR techniques was restricted due to poor resolution, which was caused by line broadening due to chemical shift anisotropy and the direct dipolar interaction of polar molecules.[256] This problem was addressed through the development of magic angle spinning (MAS)[257,258], and the combination of MAS with cross-polarization was then found to enable the narrowing of spectral lines and the enhancement of signal.[259] Although ^{13}C CP/MAS-NMR can be conducted with an absolute standard intensity reference, which represents a known number of nuclei in an NMR spectrum, and thus can be used for quantitative analysis[260], this method can be extremely difficult and is complicated for the analysis of a single polysaccharide sample, let alone composite samples consisting of multiple functionalized polysaccharides. As a result, ^{13}C CP/MAS-NMR was used in this study strictly as a qualitative technique, to help determine if the polymers were successfully functionalized, to identify the presence of cross-links in the CMC/Dex hydrogels, and to investigate whether glass content or composition affected the chemical states present within the materials.

Prior to studying the functionalization and subsequent cross-linking of the polysaccharides, CMC was first analyzed as-received from the supplier. In Figure 52c, the spectrum obtained for CMC (sodium salt) is shown, with several distinct peaks present. As was previously determined by de Nooy *et al.*, the resonance of the substituent carboxylate carbon (C-8) is observed at 178 ppm, while the resonance due to the anomeric C-1 carbon atom of the glucosyl unit is observed at 104 ppm.[261] The other substituent carbon (C-7) expresses several resonances, which can be observed in combination with resonances due to C-2 at 125 and 20 ppm, and in the very intense resonance peak observed at 74 ppm, which is due to the overlap of C-2, C-3, C-4, C-5, and C-7 resonances.[262] Additionally, a resonance due to C-4 is also observed at 82 ppm, while the resonance due to C-6 can be seen at 62 ppm.[261] Figure 52d exhibits the spectrum obtained for CMC which had been functionalized with AAD to obtain CMC-ADH, and confirms that successful functionalization occurred as new resonance peaks were observed at 16, 25, 35, 44, and 161 ppm. The peaks at 25 and 35 ppm are likely

attributable to newly introduced methylene carbons[261], while the peak at 44 ppm is likely characteristic of the hydrazine groups.[263] Additionally, a more prominent shoulder can be observed in the resonance peak representative of the anomeric C-1 carbon. The presence of this shoulder at 98 ppm in the CMC-ADH spectrum suggests that this functionalization not only attached new groups to CMC, but as a result, also caused a change in the orientation (axial vs. equatorial) and/or chemistry (internal/non-reducing vs. chain end/reducing) of the C-1 carbon.[264]

Dex was also analyzed using ^{13}C CP/MAS-NMR in both the as-received form, and the functionalized form. Figure 52a displays the spectrum obtained for Dex, where it can be seen that there are only two distinct resonance peaks present, and one prominent shoulder. As with CMC, the most intense peak at 72 ppm is indicative of overlapping resonances of the C-2, C-3, C-4, and C-5 carbons, with the peak at 65 ppm representing the resonance of the C-6 carbon.[264] However, unlike CMC, Dex is comprised of D-glucose units with α-1,6 linkages rather than β-1,4 linkages, and this is exhibited by the downshift of the anomeric C-1 carbon peak to 98 ppm, which is indicative of α-C-1 carbons.[265] Dex was then oxidized to obtain Dex-CHO, and this functionalization is confirmed by Figure 52b, which displays a transition from a well-defined individual peak for the C-1 carbon, to a broadened peak representative of several different overlapping resonances, ranging from 87-101 ppm. Additionally, a new peak is observed at 80 ppm. As with CMC, the divergence of the C-1 peak suggests changes in orientation and/or chemistry at that position, while the peak at 80 ppm, along with the shoulder present at 87 ppm, suggest the introduction of non-anomeric carbons involved in glycosidic linkages[261], which suggests that some of the newly added aldehyde groups may be acting as junctions between chains.

After the functionalization of CMC and Dex was completed, these polymers were then cross-linked to form a hydrogel via hydrazone bonds. The ^{13}C CP/MAS-NMR spectrum for the CMC/Dex hydrogel can be seen in Figure 52e, where features from both the CMC-ADH and Dex-CHO spectra can be easily recognized. The diagnostic C-1 peak suggests a larger presence of α-glycosidic linkages are present in the gel than β-linkages (which is expected, as the Dex-CHO:CMC-ADH ratio is 2.4:1 by weight), although both are clearly present, as the broad peak stretches from roughly 87-106 ppm. The

broadening of this peak, as well as the broadening of the peak located at 80 ppm, may also suggest the participation of these carbon atoms in cross-linking, as the broadening of NMR peaks is an indication of a decrease in molecular motion.[266] The peaks at 125 and 179 ppm which are indicative of the substituent C-7 and C-8 carbons of CMC are also observed, as well as the multiple peaks ranging from 16-44 ppm, which were identified as resonances for methylene carbons and hydrazine groups introduced during CMC-functionalization. However, these peaks appear broader in the CMC/Dex hydrogel spectrum, in part due to the lower concentration of CMC, but this characteristic is also likely another indicator of participation in cross-linking, which is expected, as these two polymers were functionalized with the intention of cross-linking occurring between the introduced functional groups. In addition, one orientation of hydrazone bond has been shown to express most of it's characteristic resonance peaks between 16-47 ppm[263], which further suggests that these two polymers were successfully cross-linked.

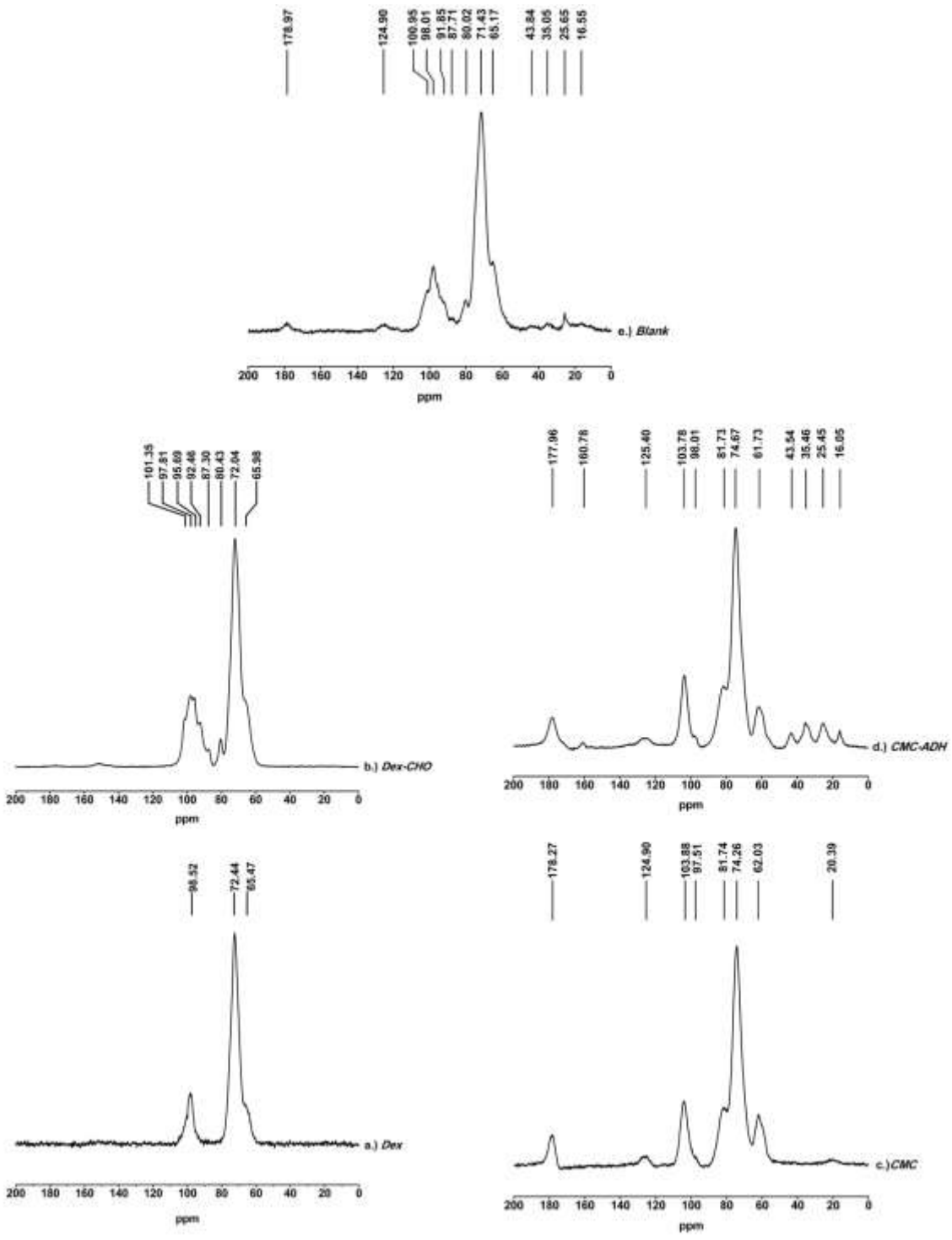

Figure 52. ^{13}C CP/MAS-NMR spectra of a.) Dex and the functionalized form b.) Dex-CHO, c.) CMC and the functionalized form d.) CMC-ADH, and the cross-linked e.) *Blank* hydrogel.

The focus of this study was to not only functionalize these polymers and cross-link them to form hydrogels, but to also incorporate BG particles to create glass-hydrogel composites, and determine if either BG-content or concentration alters chemical environments present within the materials. Figure 53 presents the ^{13}C CP/MAS-NMR spectra for several composites containing different amounts of either *Control*, *TGa-1*, or *TGa-2*, and it can be seen that these spectra display very little deviation from the spectrum generated by the *Blank* hydrogel, with the main C-1 resonance peak remaining centered at 98 ppm for all composites, and that only subtle differences exist between different composites. Between the composites containing 0.05 m^2 and 0.10 m^2 BG, there are no significant differences which are clearly evident, however, the composite containing 0.25 m^2 *Control* glass does exhibit a shoulder in the C-1 resonance peak at 103 ppm which is more pronounced than the shoulders displayed by the other composites. Although this is not as significant as the appearance of a new resonance peak, or the disappearance of a previously observed one, this does suggest that this composite contains more C-1 carbons which are a component of β-linkages, which would suggest that this composite is slightly more rigid than the others. This may be the result of an interaction between polar surface groups present on the surfaces of the BG particles and the functional groups present on the polysaccharide chains, however, since no new resonance peaks are observed between the *Blank* hydrogel and composite spectra, it is more likely that a synthesis error occurred, and this sample simply contained a slightly higher concentration of CMC-ADH than the other composites. Combined with the TEM micrographs, which showed that *Control* particles were more evenly distributed throughout the polymer network while *TGa-1* and *TGa-2* particles exhibited a slightly higher tendency to agglomerate, the information provided by the ^{13}C NMR spectra suggests that glass particles are physically trapped within the BG-hydrogel composite network, and that future work should be conducted to determine whether there are different interactions occurring between the surfaces of *Control* particles than the surfaces of *TGa-1* and *TGa-2* particles, thus resulting in slight differences in their respective dispersions throughout the network.

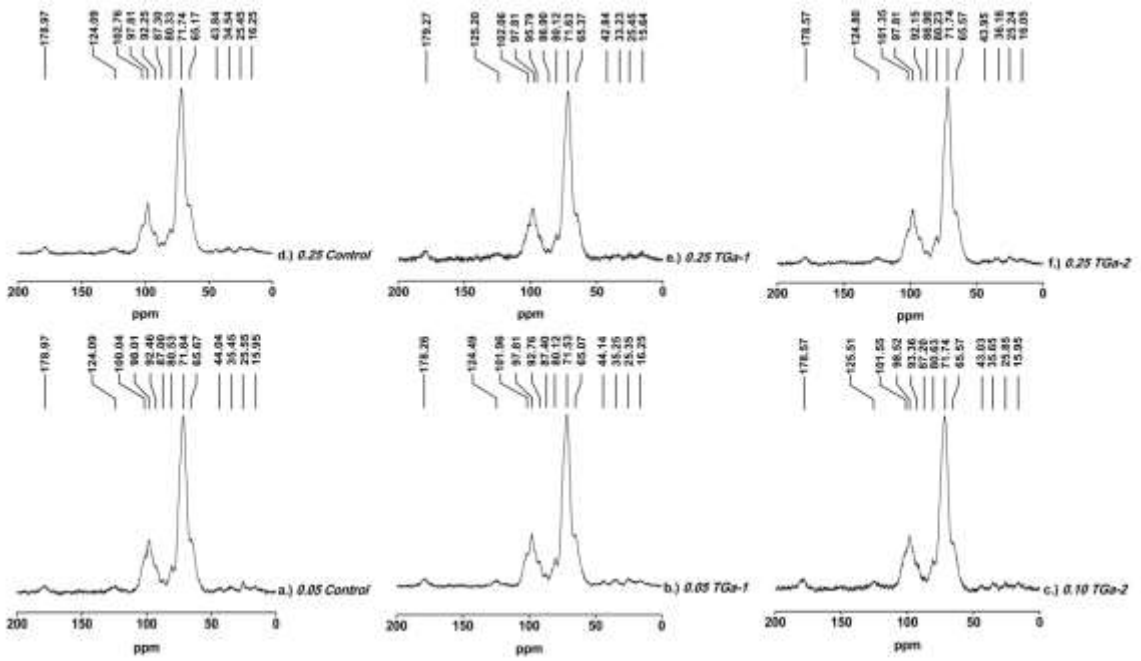

Figure 53. ^{13}C CP/MAS-NMR spectra of BG-hydrogel composites containing 0.05 m^2 a.) *Control* and b.) *TGa-1*, 0.10 m^2 c.) *TGa-2*, and 0.25 m^2 d.) *Control*, e.) *TGa-1*, and f.) *TGa-2*.

1.4. Biological Evaluation

Cell viability analysis was conducted using liquid extracts which were obtained by incubating BG powder samples in ultrapure water, and by incubating *Blank* hydrogels and BG-hydrogel composites in PBS. Figure 54 presents the *in vitro* cytotoxic capability of the BG extracts towards MG-63 osteosarcoma after incubation periods of 1, 7, and 30 days, and illustrates that *TGa-2* extracts obtained after 30 days decrease MG-63 viability to 79%, which is a significant decrease in comparison to the *control cells* (p = 0.048). Similar results are observed in Figure 55, which presents cell viability data for the BG-hydrogel composites. As with the BG extracts, extracts obtained from composites which contained the largest amount of the *TGa-2* glass exhibited the greatest decrease in MG-63 viability, decreasing cell survival to 69% after 30 days. This decrease induced by composites containing 0.25 m^2 *TGa-2* after 30 days of incubation was significant in comparison to the *control cells* (p = 0.003), *Blank* hydrogels (p = 0.032), 0.25 m^2 *Control* composites (p = 0.000), and 0.25 m^2 *TGa-1* composites (p = 0.000). These results are

particularly encouraging as not only does this study show that *TGa-2* extracts from BG and from BG-hydrogel composites both have the ability to reduce MG-63 osteosarcoma viability, but prior work by the authors also demonstrated that none of these BG extracts, nor BG-composite extracts, decrease MC3T3-E1 osteoblast viability over a period of 30 days, suggesting that these ionic dissolution products may be able to deter the growth of cancerous bone cells without negatively affecting the growth of healthy bone cells. This phenomenon may be explained by the similarities between Ga and ferric iron (Fe(III)), including ionic radii and electronegativity, which allow Ga to be incorporated into cells both dependently[137], and independently[132,133] of the transferrin receptor-facilitated pathway. This is important because it is well known that rapidly dividing cancer cells display increased Fe metabolism compared to normal healthy cells[129,267], and Ga presence interrupts Fe metabolism in two ways. First, if the external sites where cells process Fe-transferrin complexes are already occupied by Ga-containing complexes, then the cell physically does not have the ability to process as much Fe as when Ga-complexes are not present.[138] Secondly, it has been shown that Ga presence within the cell disrupts the recognition of Fe-transferrin complexes by endosomes, resulting in a decreased amount of Fe being dissociated from the transferrin complexes, and therefore, decreased Fe metabolism.[138] Together, these two factors act to inhibit the Fe-dependent function of the enzyme ribonucleotide reductase[111], which ultimately results in the inhibition of DNA synthesis[140]. Since cancer cells uptake larger amounts of Fe than normal cells, and Ga has been shown to be taken up in similar fashion, this may be the reason why normal osteoblasts were not negatively affected by Ga-containing extracts, while the viability of cancerous osteosarcoma cells decreased. Further work will be conducted in which the MTT assay of MG-63 osteosarcoma will be carried out in the presence of BG particles, and BG-hydrogel composites, to determine if contact with these surfaces induces further cytotoxicity through increased local pH and ionic concentration, as has been seen with different strains of bacteria.[234,235]

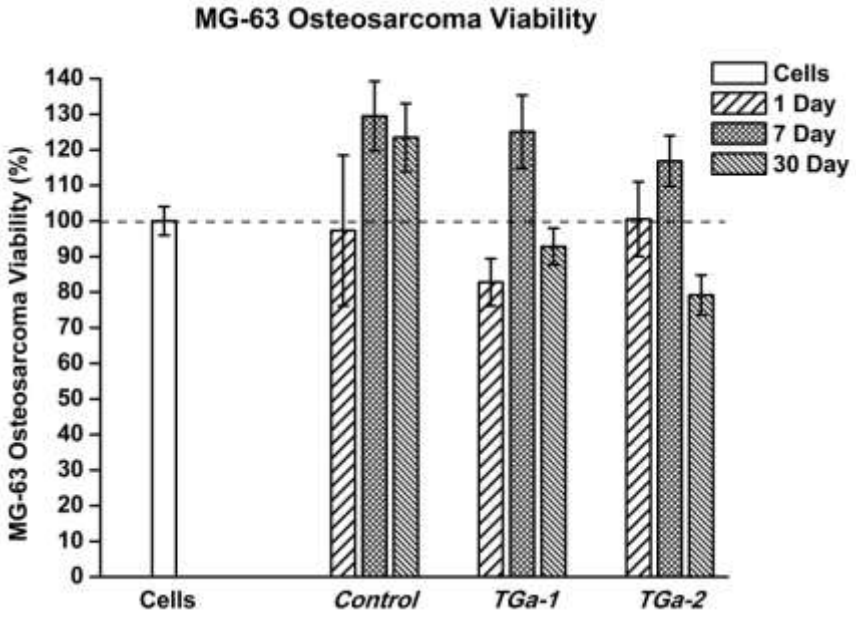

Figure 54. MG-63 osteosarcoma viability for extracts obtained from *Control*, *TGa-1*, and *TGa-2* glasses after incubation periods of 1, 7, and 30 days.

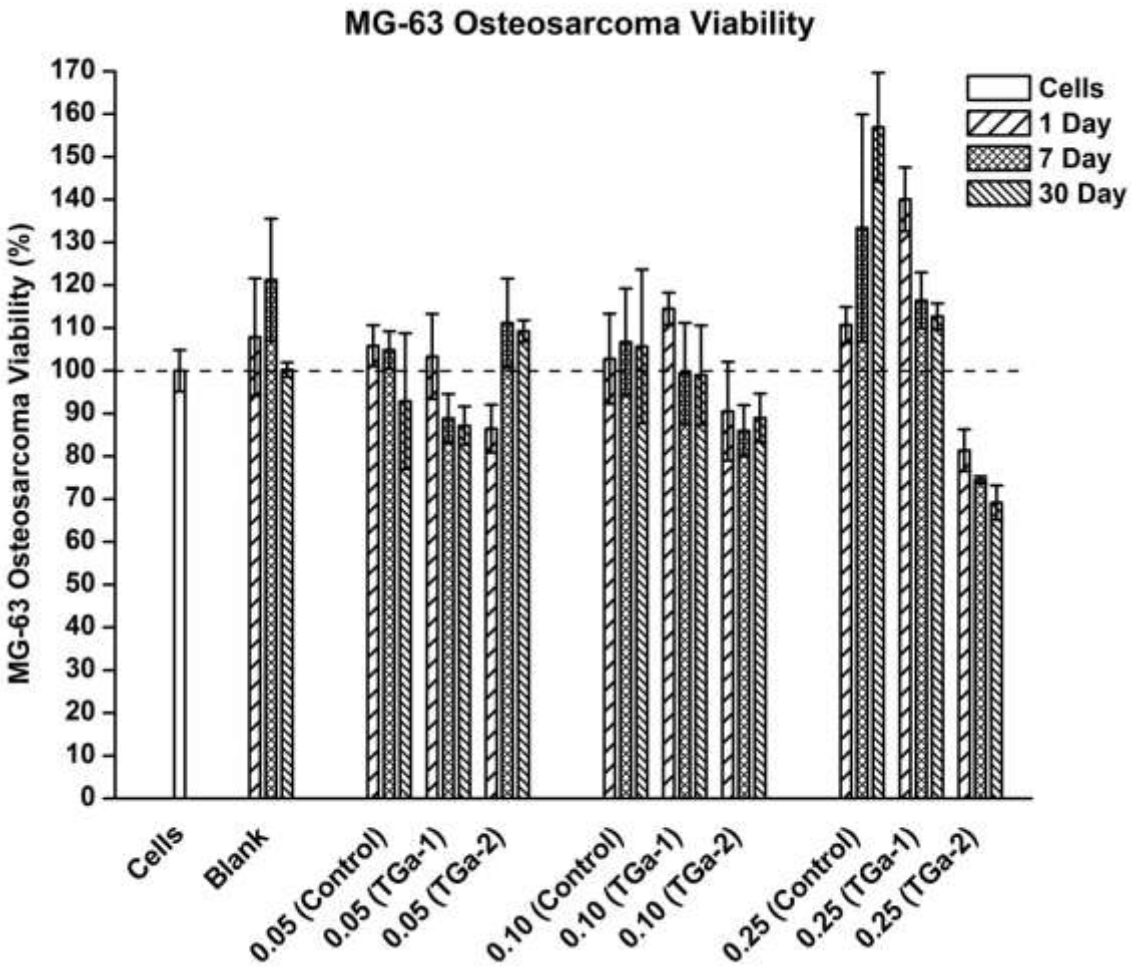

Figure 55. MG-63 osteosarcoma viability for extracts obtained from *Blank* hydrogels and BG-hydrogel composites after incubation periods of 1, 7, and 30 days.

IVE. Conclusion

In this fourth and final section, we successfully:

- Confirmed the presence of glass particles within the polymer network using TEM, with some agglomeration observed
- Conducted thermal analysis which suggested that both Ga-inclusion and increased glass content (> 0.05 m^2/batch), resulted in more rapid degradation of the polymer network at high temperatures
- Utilized ^{13}C CP/MAS-NMR to confirm the functionalization of the polymers, confirm the formation of cross-links via hydrazone bonds, and to suggest that glass particles are physically entrapped within the polymer network
- Evaluated the cytotoxicity of liquid extracts towards MG-63 osteosarcoma, and determined that the *TGa-2* glasses and glass-hydrogel composites containing *TGa-2* exhibited the greatest efficacy

In the final portion of this study, we confirmed the ability to load Ga-containing BG particles into CMC/Dex hydrogels, although some agglomeration of glass particles did occur. Thermal analysis suggested that glass content and composition did slightly influence the rate of decomposition reactions, which may be indicative of interactions occurring between the BG surfaces and the polymer matrix. However, the functionalization and subsequent cross-linking of the polymers was confirmed using ^{13}C CP/MAS-NMR spectroscopy, which also suggested that glass content and composition may have a slight influence on the structure of the composites, although it is more plausible to infer that BG particles are entrapped within pores of the matrix, rather than chemically reacting with the hydrogel. Additionally, liquid extracts obtained after 30 days of incubation from both BG particles and BG-hydrogel composites containing *TGa-2*, which possessed the highest Ga-content, demonstrated *in vitro* efficacy towards MG-63 osteosarcoma. This final segment demonstrated that we had indeed successfully functionalized CMC and Dex, and synthesized hydrogel composites impregnated with Ga-containing BG particles, while also demonstrating that extracts from these composites

did possess anti-cancerous potential, further suggesting the possibility of using these materials in bone void-filling applications.

CONCLUSION

This project was designed to be a comprehensive study which centered around a Ga-containing bioactive glass series which possessed, as suggested by prior characterization work, potential in bone void-filling applications. To fully evaluate the *in vitro* characteristics of this glass series, and to develop and characterize a delivery mechanism for these glasses, this study was divided into 4 segments. In the first, the glasses exhibited bioactivity through the appearance of Ca/P deposits on their surfaces after incubation in SBF, as well as long-term solubility of the glasses in ultrapure water, from which liquid extracts proved harmful towards L-929 fibroblasts beyond 30 days, but produced no inhibitory effects against MC3T3-E1 osteoblasts after incubation periods of up to 365 days. Next, the polysaccharides CMC and Dex were functionalized to obtain CMC-ADH and Dex-CHO, and these functionalized polymers were cross-linked in the presence of particles of the Ga-glass series to obtain glass-hydrogel composites. At this point the physical properties of the composites were characterized, solubility analysis showed that the composites effectively released the desired glass dissolution products into PBS, and liquid extracts from these solubility studies proved to be harmless towards fibroblasts and osteoblasts. In the third segment, the *in vitro* efficacies of both the glass and the glass-gel composites towards *E. coli*, *S. aureus*, and *C. albicans* were evaluated, with liquid extracts from both the glasses and gels proving somewhat effective in inhibiting *E. coli* and *C. albicans*, and composites cross-linked *in situ* into agar plates proving slightly effective against both *S. aureus* and *E. coli*, and extremely effective against *C. albicans*. Finally, to confirm the functionalization of the polymers and to gain insight into the structural configuration of the composites, thermal analysis and ^{13}C CP/MAS-NMR were conducted, revealing that the polymers had been successfully functionalized, that Ga-inclusion and increased glass content lead to an increased rate of degradation of the polymer network at high temperatures, and that the glass particles were most likely physically entrapped within the network, rather than chemically conjugated. The final test was to evaluate the *in vitro* anti-cancerous abilities of these materials, and both the *TGa-2* glass, and the composites containing the *TGa-2* glass, exhibited potential inhibitory properties towards MG-63 osteosarcoma cells. Overall, this

study proved that incorporating Ga_2O_3 into bioactive glass formulations does allow for the elicitation of some of the same therapeutic effects as the pharmaceutical $Ga(NO_3)_3$ upon dissolution of Ga^{3+} from the glass network, and that these glasses can be combined with polymer hydrogels to form composites, which also demonstrate the ability to elicit these therapeutic effects. The success exhibited throughout these *in vitro* studies suggests that these materials have potential in bone void-filling applications, and offers ample evidence suggesting that these composites are worthy candidates for future *in vivo* studies.

FUTURE WORK

As was previously stated, these materials have been thoroughly characterized in the *in vitro* setting, and the bulk of the future work should be conducted *in vivo*, primarily involving rat models to determine if these composites actually provide some of the therapeutic effects that were observed in this study, once they are placed inside a living host. However, at this time, *in vivo* work of this magnitude cannot be conducted at Alfred University, but there are a few *in vitro* studies which could be carried out. In the current study, the cytotoxicity of these materials towards MG-63 osteosarcoma was discussed, however, there are other forms of bone cancer against which these materials have potential. Included in the appendix are the results for cytotoxicity tests conducted using NCI-H929 myeloma cells, which also suggested that *TGa-2* liquid extracts were most effective for the glass samples, while composites containing 0.25 m^2 *TGa-1* were the most effective inhibitors out of the composites examined, but these cells are grown and used in suspension as they are cancerous blood plasma cells, which makes accurate data collection much more difficult than when using cells which attach to material surfaces. Myeloma cytotoxicity results from the current study are included in the appendix and not in the published studies because they contain large errors, so future work could focus on altering experimental parameters and re-conducting this work in order to obtain data with less error. Additionally, the anti-bacterial and anti-fungal work conducted in the current study strictly utilized liquid extracts for evaluation of the glass series, and although some inhibition was exhibited by these extracts, the literature suggests that the incubation of bacteria in physical contact with bioactive glass surfaces yields much greater inhibition, making it desirable for further anti-bacterial and anti-fungal evaluation to be conducted by incubating particles of this Ga-containing glass series in contact with *E. coli*, *S. aureus*, and *C. albicans*.

APPENDIX

AI. Nuclear Magnetic Resonance (NMR) Fundamentals

AI1. NMR Background

Magnetic resonance is based on the interaction between an external magnetic field and a magnetically active nucleus that possesses spin. As a result of possessing spin, these nuclei have an angular momentum and a magnetic moment.[163] When a nucleus is placed in a magnetic field, there are two phenomena which are observed known as Zeeman splitting and nuclear precession. Zeeman splitting results in the creation of $2I + 1$ magnetic energy states, where I = the spin quantum number. When the atomic mass and number are even numbers, $I = 0$, and as a result, these nuclei do not express multiple energy levels when exposed to a magnetic field. This is why ^{12}C nuclei are NMR-inactive, while ^{13}C nuclei are NMR-active. The angular momentum in the static external magnetic field (B_0) undergoes the Larmor precession about the field direction. Equation 2 describes this procession, which occurs with a frequency of:

$$\omega_0 = \gamma B_0 , \tag{2}$$

where γ = the magnetogyric ratio (which is the ratio of the properties angular momentum and the magnetic moment) . This spinning angular momentum allows for magnetization of the nucleus. This can be envisioned as rotating system of coordinates, with x- and y-axes which rotate with the frequency (ω_0) about a z-axis, which is the field direction of the static magnetic field (B_0). A second magnetic field (B_1) is then introduced, which can be set to oscillate at a specific radio frequency (RF). These specific RFs or "resonances" are used to observe magnetic characteristics of particular nuclei (^1H, ^{13}C, ^{29}Si, etc.) in a material. After a 90º pulse of B_1, the magnetization (μ_i) of the magnetic nuclei becomes fixed in the xy plane, and this transverse magnetization induces a signal decay or "free induction decay (FID)". A Fourier transformation can then be conducted on the FID, yielding a spectrum.[266]

AI2. Spin-Lattice and Spin-Spin Relaxation

In an external magnetic field (B_0), the equilibrium magnetization of a sample is aligned along the z-axis. If an RF pulse excites the spin system, this alignment is

disturbed and subsequently, the z-component of the sample's magnetization (M_z) decreases. In order for the system to return to equilibrium, excess energy must be dissipated. Bloch's equation (Equation 3) can be used to describe the rate at which a system returns to equilibrium[268], and it is written as:

$$\frac{dM_z}{dt} = -\frac{(M_z - M_0)}{T_1}, \quad (3)$$

where M_0 = the equilibrium magnetization of a sample, and T_1 = the spin-lattice relaxation time. Once equilibrium has been disrupted, the magnetization of a sample may have components in the xy plane, and these components will also eventually return to equilibrium. Bloch's equation can also be used to describe this phenomenon[268], as seen in Equation 4:

$$\frac{dM_{xy}}{dt} = -\frac{M_{xy}}{T_2}, \quad (4)$$

where T_2 = the spin-spin relaxation time, and is a characteristic time of specific molecular motions. The rate of xy relaxation may be larger than the rate of relaxation in the z-direction, but it may never be smaller. If the FID decays at a rapid pace, that means the xy relaxation rate is high, and this will be reflected as a broadening in the spectrum.

AI3. Chemical Shift and Anisotropy

In molecules, the electrons which surround nuclei provide a magnetic shielding effect, and differences in the number and orientation of electrons surrounding nuclei will result in chemical groups possessing characteristic resonance frequencies. This magnetic shielding by electrons is called the chemical shift (δ), and is given in ppm in comparison to a reference. These chemical shifts occur because electrons are set in motion by the application of the z-axis magnetic field (B_0), and these electrons also produce secondary magnetic fields, which can either enhance or oppose B_0. It is important to realize that anisotropic electronic charge distribution exists within most molecules, and the shielding of a nucleus can be described by a nuclear shielding tensor with principal components of σ_{xx}, σ_{yy}, and σ_{zz}. With that in mind, the local magnetic field can be summarized in an expression[269], which is written as seen in Equation 5:

$$B_{loc} = (1 - \sigma_{kk})B_0 . \quad (5)$$

In an isotropic liquid, molecules are rapidly reoriented, so the shielding tensor is simply averaged. However, in complex materials such as hydrogels or glass-hydrogel composites, anisotropy is present and the tensor cannot be simply averaged to accurately describe the shielding effect. Instead, the chemical shift anisotropy, which is expressed by Equation 6, can be defined as:

$$\Delta\sigma = \sigma_{zz} - \frac{(\sigma_{xx} + \sigma_{yy})}{2} . \quad (6)$$

AI4. Sources of NMR Signal Broadening in Hydrogel Samples

The line width of an NMR signal is dependent on the internal mobility of specific chemical groups, and the overall tumbling of polymer molecules. The collisions which occur in isotropic liquids lead to the averaging of dipolar couplings of nuclear spins (interactions between polar molecules) and the shielding tensor, resulting in narrow lines appearing in the spectra. However, in systems such as hydrogels or glass-hydrogel composites, the motion of some chemical groups are extremely hindered, which means their dipolar interactions cannot be averaged, and broadening of the lines are observed in the spectra.[270] Luckily, with modern solid-state NMR, we can remove much of the broadening introduced by dipolar couplings and chemical shift anisotropies by the magic angle (54.7º) spinning (MAS) of a sample, with typical rotational frequencies between 2-35 kHz.[271] In a heterogeneous gel or gel composite, a spectrum will be obtained which reveals narrow lines for mobile components of the material, and broader lines for the more rigid components, allowing for assignment of the chemical constituents, and a general sense of the rigidity of different chemical groups present.

AI5. ^{1}H-^{13}C CP/MAS-NMR

In the cross-polarization (CP) method, a characteristic 90º RF pulse on ^{1}H nuclei is immediately followed by simultaneous RF irradiation of ^{1}H and ^{13}C nuclei. In order for this to occur, the Hartmann-Hahn match condition must be fulfilled[272], which is given by Equation 7:

$$\omega_{1C} = (\gamma_C B_1) = (\gamma_H B_1) = \omega_{1H} , \quad (7)$$

where ω_1 = the rotating precession frequencies, and γ = the magnetogyric ratios for protons and carbon. The ^{1}H magnetization is larger than the ^{13}C magnetization, and as a

result, cross-relaxation from protons to carbon will result in the increase of ^{13}C magnetization by a factor of (γ_H/γ_C). This strong polarization of ^{13}C nuclei that can interact with ^{1}H spins results in improved NMR sensitivity, and in typical ^{13}C CP/MAS-NMR experiments using contact pulse times (t_{CP}) of 50-2000 μs, this increase in sensitivity is observed through an increase in signal intensity of carbons directly bound to hydrogen, and in more complex/rigid systems, stronger dipole-dipole coupling resulting in narrower spectral lines. After reviewing the benefits of using ^{13}C CP/MAS-NMR to probe the molecular structure of complex polymer materials, we elected to utilize this technique to analyze our materials to confirm that we had successfully functionalized our polymers, obtained cross-linking within the hydrogels, and also to investigate whether the introduction of glass particles into the system produced any dramatic effects in the molecular structure of the gels.

AII. NCI-H929 Myeloma Viability

AII1. Obtaining Liquid Extracts

To obtain BG extracts, powder samples (n = 3), whose particle size information is displayed in Table 8, were weighed to contain 1 m^2 of glass per incubation sample (Keenan *et al.*[245]), and were then submerged in 10 ml ultrapure water for periods of 1, 7, and 30 days. To obtain BG-hydrogel composite extracts, samples (n = 3) were submerged in 1 ml PBS for periods of 1, 7, and 30 days. After the incubation times were complete, the aqueous solution from each sample was removed and filtered using Amicon® Ultra-4 Centrifugal Filters (Merck KGaA, Darmstadt, Germany).

AII2. Methyl Tetrazolium (MTT) Assays

The established cell line NCI-H929 Myeloma (ATCC®-CRL-9068™) was used in this study. NCI-H929 myeloma cells were cultured in HyClone® RPMI-1640 Medium (Thermo Scientific, MA, USA), which included 25 mM HEPES, L-glutamine, and 0.05 mM mercaptoethanol, and was supplemented with 10 vol% FBS. Cells were maintained on a regular feeding regime in a cell culture incubator at 37˚C, with a 5% CO2/95% air

atmosphere. Cells were then seeded into 96 well plates at a density of 10,000 cells per well and incubated for 24 hours prior to the addition of extracts. The cytotoxicity of glass and glass-hydrogel composite extracts were evaluated using the Methyl Tetrazolium (MTT) assay. 10 µl aliquots of undiluted extract were then added into wells containing cells in culture medium (100 µl), and incubated for an additional 24 hours. 10 µl of the MTT assay was then added to each well and incubated for an additional 4 hours. After 4 hours, the cultures were removed from the incubator, and the resultant formazan crystals were dissolved by first removing all of the aqueous media from each well, and then adding 100 µl of MTT Solubilization Solution (10% Triton x-100 in Acidic Isopropanol. (0.1 n HCI)). Once the crystals were fully dissolved, the absorbance was measured at a wavelength of 570 nm using a µQuant Plate Reader (Bio-Tek Insturments, Inc., VT, USA). 10 µl aliquots of PBS were used as control additions, and cells were assumed to have metabolic activities of 100%. Glass and glass-hydrogel composite extracts in media without cells were also tested, and were found not to interfere with the MTT assay.

AII3. NCI-H929 Myeloma Results

Cell viability analysis was conducted using liquid extracts which were obtained after incubation of glass powder samples in ultrapure water, and glass-hydrogel composites in PBS, for periods of 1, 7, and 30 days. Figure 56 presents the *in vitro* cytotoxicity of the glass extracts towards NCI-H929 Myeloma, and as was seen for the other cancerous cells, MG-63 osteosarcoma, *TGa-2* extracts that were obtained after 30 days of incubation exhibited the largest decrease in NCI-H929 viability, decreasing to 61% viability. The *in vitro* cytotoxicity of extracts obtained from the glass-hydrogel composites was also evaluated, and these results are presented in Figure 57. These results cannot be considered extremely reliable due to the extremely large errors that are present, however, from this data, it appears that composites containing 0.25 m^2 *TGa-1* produced the extracts which were most effective in inhibiting NCI-H929 myeloma viability, decreasing viability to 65% after 30 days of composite incubation. Although the results for the composites do not directly correlate with the results observed for MG-63 osteoblasts, NCI-H929 myeloma viability analysis suggested that for both the glasses and glass-hydrogel composites, the Ga-containing samples were capable of reducing viability

after 30 days of incubation, suggesting that perhaps the Ga^{3+} ions present in these extracts was able to interfere with the Fe-transferrin pathway in both cancer cell lines. Further work should be conducted in order to reduce error, and produce more reliable results which can be statistically analyzed for more accurate determination of extract effects.

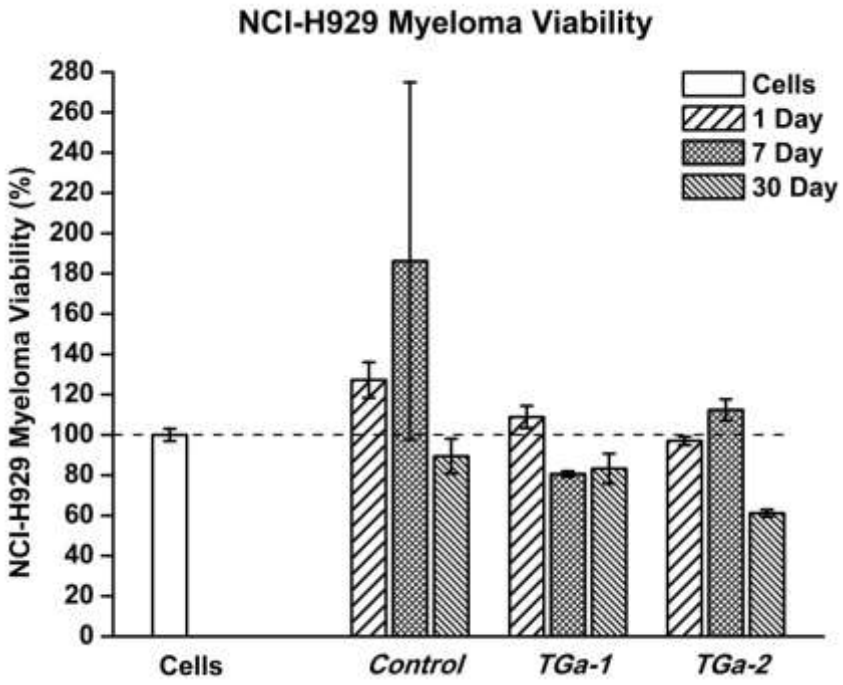

Figure 56. NCI-H929 myeloma viability for extracts obtained from *Control*, *TGa-1*, and *TGa-2* glasses after incubation periods of 1, 7, and 30 days.

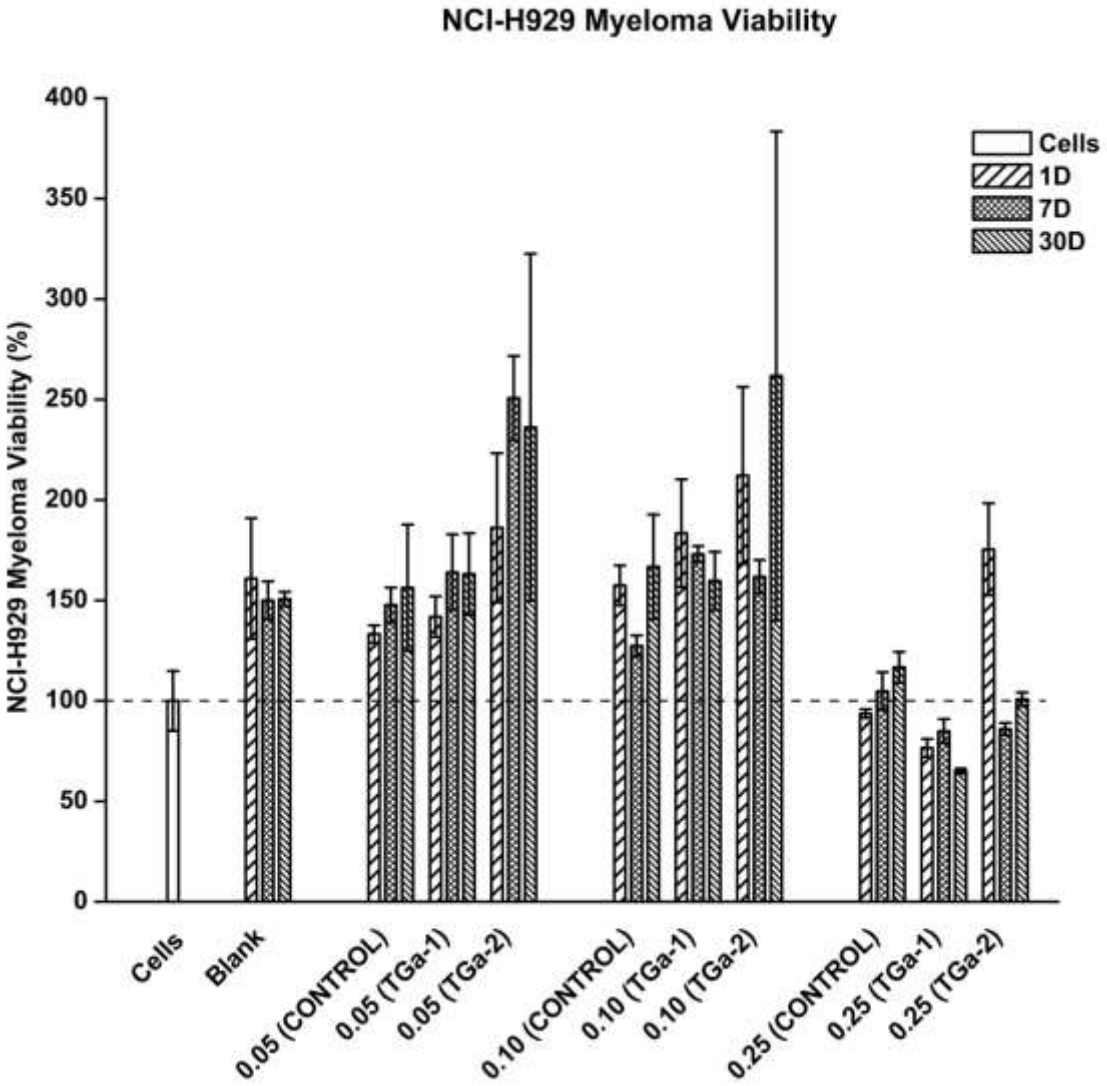

Figure 57. NCI-H929 myeloma viability for extracts obtained from Blank hydrogels and glass-hydrogel composites after incubation periods of 1, 7, and 30 days.

REFERENCES

1. *Definitions in Biomaterials : Proceedings of a Consensus Conference of the European Society for Biomaterials, Chester, England, March 3-5, 1986 / Edited by D.F. Williams*. Edited by D. F. Williams and B. European Society for. Elsevier, Amsterdam ; New York, 1987.

2. S. M. Balaji, *Textbook of Oral and Maxillofacial Surgery*. Elsevier (A Divisionof Reed Elsevier India Pvt. Limited), 2007.

3. P. I. Branemark, "Osseointegration and Its Experimental Background," *J Prosthet Dent*, **50** [3] 399-410 (1983).

4. L. Hench, "The Story of Bioglass®," *J. Mater. Sci. Mater. Med.*, **17** [11] 967-78 (2006).

5. A. S. Hoffman, "The Origins and Evolution Of "Controlled" Drug Delivery Systems," *J Control Release*, **132** [3] 153-63 (2008).

6. F. D. Group, "Amalgam Vs Composite Fillings" (2011) Accessed on: 12/9/2015. Available at <http://www.fraccarodentalgroup.com/fillings.shtml>

7. R. Langer and J. Folkman, "Polymers for the Sustained Release of Proteins and Other Macromolecules," *Nature*, **263** [5580] 797-800 (1976).

8. W. R. Gombotz, M. S. Healy, and L. R. Brown, "Very Low Temperature Casting of Controlled Release Microspheres," Google Patents (1991).

9. F. F. Davis, "The Origin of Pegnology," *Adv. Drug Del. Rev.*, **54** [4] 457-8 (2002).

10. K. Kumar, "Pegylation Technique in Drug Delivery" (2014) Accessed on: 12/9/2015. Available at <http://pharmawiki.in/ppt-pegylation-technique-in-drug-delivery/>

11. H. Ringsdorf, "Structure and Properties of Pharmacologically Active Polymers," *Journal of Polymer Science: Polymer Symposia,* **51** [1] 135-53 (1975).

12. R. Duncan, H. C. Cable, J. B. Lloyd, P. Rejmanová, and J. Kopeček, "Polymers Containing Enzymatically Degradable Bonds, 7. Design of Oligopeptide Side-Chains in Poly[N-(2-Hydroxypropyl)Methacrylamide] Copolymers to Promote Efficient Degradation by Lysosomal Enzymes," *Die Makromolekulare Chemie,* **184** [10] 1997-2008 (1983).

13. L. T. B. Mathe G., and Bernard J., "Effect on Mouse Leukemia 1210 of a Combination by Diazo-Reaction of Amethopterin and Gamma-Globulins from Hamsters Inoculated with Such Leukemia by Heterografts," *Comptes Rendus Hebd Seances Acad. Sci.,* **246** 1626-8 (1958).

14. E. Ruoslahti, "The Rgd Story: A Personal Account," *Matrix Biol.,* **22** [6] 459-65 (2003).

15. K. Iwai, H. Maeda, and T. Konno, "Use of Oily Contrast Medium for Selective Drug Targeting to Tumor: Enhanced Therapeutic Effect and X-Ray Image," *Cancer Res.,* **44** [5] 2115-21 (1984).

16. T. Kashiwagi, Y. Ito, and Y. Imanishi, "Non-Thrombogenicity of Organic Polymers by Blending with Alkylamine-Heparin Complexes," *Biomaterials,* **14** [15] 1145-53 (1993).

17. S. D. Cook, K. A. Thomas, J. F. Kay, and M. Jarcho, "Hydroxyapatite-Coated Titanium for Orthopedic Implant Applications," *Clin. Orthop. Relat. Res.,* **232** 225-43 (1988).

18. L. L. Hench and J. Wilson, "An Introduction to Bioceramics" (1993) World Scientific Publishing Company. Accessed on: Available at <http://public.eblib.com/choice/publicfullrecord.aspx?p=1193572>

19. J. Bergsma, W. De Bruijn, F. Rozema, R. Bos, and G. Boering, "Late Degradation Tissue Response to Poly (L-Lactide) Bone Plates and Screws," *Biomaterials,* **16** [1] 25-31 (1995).

20. I. L. Gore & Associates, "Gore Propaten Vascular Graft" (2012-2015) Accessed on: 12/9/2015. Available at <http://www.goremedical.com/propaten>

21. "Zimmer Hip Replacement Implants" (2015) Healthbase Online Inc. Accessed on: Available at <http://www.healthbase.com/resources/orthopedics/total-hip-replacement-surgery-implants/zimmer-hip-replacement-implant-cemented-cementless-press-fit-india-affordable-medical-tourism_14.html>

22. C. d. M. O. Ltda, "Interference Screw: Biosteon - Cross Pin1a" Accessed on: 12/9/2015. Available at <http://www.cmoortopedia.com.br/produtos/medicina-esportiva/biosteon/?lang=en>

23. B. D. Ratner, *Biomaterials Science: An Introduction to Materials in Medicine*. Academic press, 2004.

24. A. Moss, S. Hamburger, R. Moore, L. Jeng, and L. Howie, "Use of Selected Medical Device Implants in the United States," *Adv. Data*, [191] (1990).

25. C. B. Ma, "Knee Joint Replacement - Series" (2014) Accessed on: 12/9/2015. Available at <https://www.nlm.nih.gov/medlineplus/ency/presentations/100088_4.htm>

26. S. Dumitriu, *Polymeric Biomaterials, Revised and Expanded*. CRC Press, 2001.

27. L. Hench and E. Ethridge, *Biomaterials: An Interfacial Approach;* p. 385. Academic Press, Inc., New York, 1972.

28. L. L. Hench and H. Paschall, "Direct Chemical Bond of Bioactive Glass-Ceramic Materials to Bone and Muscle," *J Biomed Mater Res*, **7** [3] 25-42 (1973).

29. "Novabone Dental Putty" (2009) NovaBone Products, LLC. Accessed on: 12/9/2015. Available at <http://novabone.com/NB/dental.html>

30. F. Driessens, "Formation and Stability of Calcium Phosphates in Relation to the Phase Composition of the Mineral in Calcified Tissues," *Bioceramic of Calcium Phosphate", edited by K. de Groot,* 1-32 (1983).

31. A. Cranin, G. Tobin, and J. Gelbman, "Applications of Hydroxylapatite in Oral and Maxillofacial Surgery. Part Ii: Ridge Augmentation and Repair of Major Oral Defects," *Compendium (Newtown, Pa.),* **8** [5] 334 (1987).

32. Y. Fujishiro, L. Hench, and H. Oonishi, "Quantitative Rates of in Vivo Bone Generation for Bioglass® and Hydroxyapatite Particles as Bone Graft Substitute," *J. Mater. Sci. Mater. Med.,* **8** [11] 649-52 (1997).

33. K. De Groot, R. Geesink, C. Klein, and P. Serekian, "Plasma Sprayed Coatings of Hydroxylapatite," *J. Biomed. Mater. Res.,* **21** [12] 1375-81 (1987).

34. W. J. Van Der Giessen, A. M. Lincoff, R. S. Schwartz, H. M. van Beusekom, P. W. Serruys, D. R. Holmes, S. G. Ellis, and E. J. Topol, "Marked Inflammatory Sequelae to Implantation of Biodegradable and Nonbiodegradable Polymers in Porcine Coronary Arteries," *Circulation*, **94** [7] 1690-7 (1996).

35. M. Gómez-Guillén, B. Giménez, M. a. López-Caballero, and M. Montero, "Functional and Bioactive Properties of Collagen and Gelatin from Alternative Sources: A Review," *Food Hydrocoll.,* **25** [8] 1813-27 (2011).

36. F. O. Schmitt, "Adventures in Molecular Biology," *Annu. Rev. Biophys. Biophys. Chem.,* **14** [1] 1-23 (1985).

37. K. Piez, "Collagen"; pp. 699-727 in Vol. 3, *Encyclopedia of Polymer Science.* Wiley, New York, 1985.

38. I. Yannas, J. Burke, D. Orgill, and E. Skrabut, "Wound Tissue Can Utilize a Polymeric Template to Synthesize a Functional Extension of Skin," *Science*, **215** [4529] 174-6 (1982).

39. C. S. Goude M.C., Brennan A., "Characterization of Collagen-Bioactive Glass Composites for Treating Osteomyelitis."

40. S. Ramakrishna, J. Mayer, E. Wintermantel, and K. W. Leong, "Biomedical Applications of Polymer-Composite Materials: A Review," *Composites Sci. Technol.,* **61** [9] 1189-224 (2001).

41. Q. Liu, J. R. De Wijn, and C. A. Van Blitterswijk, "Nano-Apatite/Polymer Composites: Mechanical and Physicochemical Characteristics," *Biomaterials,* **18** [19] 1263-70 (1997).

42. R. C. Thomson, M. J. Yaszemski, J. M. Powers, and A. G. Mikos, "Hydroxyapatite Fiber Reinforced Poly (< I> A</I>-Hydroxy Ester) Foams for Bone Regeneration," *Biomaterials,* **19** [21] 1935-43 (1998).

43. E. Ural, K. Kesenci, L. Fambri, C. Migliaresi, and E. Piskin, "Poly (D, L-Cactide/< I> E</I>-Caprolactone)/Hydroxyapatite Composites," *Biomaterials,* **21** [21] 2147-54 (2000).

44. T. Yamamuro, L. L. Hench, and J. Wilson, *Crc Handbook of Bioactive Ceramics: Bioactive Glasses and Glass-Ceramics; Vol. 2, Calcium Phosphate and Hydroxylapatite Ceramics*. CRC press, 1990.

45. L. L. Hench, D. L. Wheeler, and D. C. Greenspan, "Molecular Control of Bioactivity in Sol-Gel Glasses," *J. Sol-Gel Sci. Technol.,* **13** [1-3] 245-50 (1998).

46. H. Takadama, H.-M. Kim, T. Kokubo, and T. Nakamura, "Mechanism of Biomineralization of Apatite on a Sodium Silicate Glass: Tem-Edx Study in Vitro," *Chem. Mater.,* **13** [3] 1108-13 (2001).

47. W. Cao and L. L. Hench, "Bioactive Materials," *Ceram. Int.,* **22** [6] 493-507 (1996).

48. A. Balamurugan, G. Balossier, D. Laurent-Maquin, S. Pina, A. Rebelo, J. Faure, and J. Ferreira, "An in Vitro Biological and Anti-Bacterial Study on a Sol–Gel Derived Silver-Incorporated Bioglass System," *Dent. Mater.,* **24** [10] 1343-51 (2008).

49. D. Arcos, D. Greenspan, and M. Vallet-Regí, "A New Quantitative Method to Evaluate the in Vitro Bioactivity of Melt and Sol-Gel-Derived Silicate Glasses," *J. Biomed. Mater. Res. A,* **65** [3] 344-51 (2003).

50. R. Legfros, T. Sakae, C. Bautista, M. Retino, and J. LeGeros, "Magnesium and Carbonate in Enamel and Synthetic Apatites," *Adv. Dental Res.*, **10** [2] 225-31 (1996).

51. M. Kay, R. Young, and A. Posner, "Crystal Structure of Hydroxyapatite," *Nature,* **204** 1050-2 (1964).

52. Z.-h. Zhou, J.-m. Ruan, Z.-c. Zhou, and X.-j. Shen, "Bioactivity of Bioresorbable Composite Based on Bioactive Glass and Poly-L-Lactide," *Transactions of Nonferrous Metals Society of China,* **17** [2] 394-9 (2007).

53. J. Santos, L. J. Jha, and F. Monteiro, "Surface Modifications of Glass-Reinforced Hydroxyapatite Composites," *Biomaterials,* **16** [7] 521-6 (1995).

54. H. H. Lu, S. R. Pollack, and P. Ducheyne, "45s5 Bioactive Glass Surface Charge Variations and the Formation of a Surface Calcium Phosphate Layer in a Solution Containing Fibronectin," *J Biomed Mater Res,* **54** [3] 454-61 (2001).

55. C. NJ, "Glass Bones" (2006) Royal Society of Chemistry. Accessed on: 12/10/2015. Available at <http://www.rsc.org/Education/EiC/issues/2006Nov/GlassBones.asp>

56. I. Xynos, M. Hukkanen, J. Batten, L. Buttery, L. Hench, and J. Polak, "Bioglass® 45s5 Stimulates Osteoblast Turnover and Enhances Bone Formation in Vitro: Implications and Applications for Bone Tissue Engineering," *Calcif. Tissue Int.*, **67** [4] 321-9 (2000).

57. K. Wallace, R. Hill, J. Pembroke, C. Brown, and P. Hatton, "Influence of Sodium Oxide Content on Bioactive Glass Properties," *J. Mater. Sci. Mater. Med.*, **10** [12] 697-701 (1999).

58. C. Turner, A. Robling, R. Duncan, and D. Burr, "Do Bone Cells Behave Like a Neuronal Network?," *Calcif. Tissue Int.,* **70** [6] 435-42 (2002).

59. Y. Gu and S. J. Publicover, "Expression of Functional Metabotropic Glutamate Receptors in Primary Cultured Rat Osteoblasts Cross-Talk with N-Methyl-D-Aspartate Receptors," *J. Biol. Chem.,* **275** [44] 34252-9 (2000).

60. J. Storm-Mathisen, N. Danbolt, F. Rothe, R. Torp, N. Zhang, J. Aas, B. Kanner, I. Langmoen, and O. Ottersen, "Ultrastructural Immunocytochemical Observations on the Localization, Metabolism and Transport of Glutamate in Normal and Ischemic Brain Tissue," *Prog. Brain Res.,* **94** 225 (1992).

61. A. Volterra, P. Bezzi, B. L. Rizzini, D. Trotti, K. Ullensvang, N. C. Danbolt, and G. Racagni, "The Competitive Transport Inhibitor L-Trans-Pyrrolidine-2, 4-Dicarboxylate Triggers Excitotoxicity in Rat Cortical Neuron-Astrocyte Co-Cultures Via Glutamate Release Rather Than Uptake Inhibition," *Eur. J. Neurosci.,* **8** [9] 2019-28 (1996).

62. E. Hinoi, T. Takarada, and Y. Yoneda, "Glutamate Signaling System in Bone," *J Pharmacol Sci*, **94** [3] 215-20 (2004).

63. P. Bhangu, P. Genever, G. Spencer, T. Grewal, and T. Skerry, "Evidence for Targeted Vesicular Glutamate Exocytosis in Osteoblasts," *Bone,* **29** [1] 16-23 (2001).

64. P. Valerio, M. Pereira, A. Goes, and M. F. Leite, "Effects of Extracellular Calcium Concentration on the Glutamate Release by Bioactive Glass (Bg60s) Preincubated Osteoblasts," *Biomed Mater*, **4** [4] 045011 (2009).

65. R. E. Burch, H. K. Hahn, and J. F. Sullivan, "Newer Aspects of the Roles of Zinc, Manganese, and Copper in Human Nutrition," *Clin. Chem.,* **21** [4] 501-20 (1975).

66. A. F. Parisi and B. L. Vallee, "Zinc Metalloenzymes: Characteristics and Significance in Biology and Medicine," *Am. J. Clin. Nutr.,* **22** [9] 1222-39 (1969).

67. M. Stefanidou, C. Maravelias, A. Dona, and C. Spiliopoulou, "Zinc: A Multipurpose Trace Element," *Arch. Toxicol.*, **80** [1] 1-9 (2006).

68. E. Ho, "Zinc Deficiency, DNA Damage and Cancer Risk," *J. Nutr. Biochem.*, **15** [10] 572-8 (2004).

69. A. S. Prasad, "Zinc: An Overview," *Nutrition*, **11** [1 Suppl] 93-9 (1994).

70. A. S. Prasad and O. Kucuk, "Zinc in Cancer Prevention," *Cancer Metastasis Rev.*, **21** [3-4] 291-5 (2002).

71. P. Fraker and D. Lill-Elghanian, "The Many Roles of Apoptosis in Immunity as Modified by Aging and Nutritional Status," *J. Nutr. Health Aging*, **8** [1] 56-63 (2003).

72. R. B. Franklin and L. C. Costello, "The Important Role of the Apoptotic Effects of Zinc in the Development of Cancers," *J. Cell. Biochem.*, **106** [5] 750-7 (2009).

73. M. Provinciali, G. Di Stefano, and N. Fabris, "Dose-Dependent Opposite Effect of Zinc on Apoptosis in Mouse Thymocytes," *Int. J. Immunopharmacol.*, **17** [9] 735-44 (1995).

74. M. Herzberg, J. Foldes, R. Steinberg, and J. Menczel, "Zinc Excretion in Osteoporotic Women," *J. Bone Miner. Res.*, **5** [3] 251-7 (1990).

75. L. S. Hurley, "Teratogenic Aspects of Manganese, Zinc, and Copper Nutrition," *Physiol Rev*, **61** [2] 249-95 (1981).

76. R. da Cunha Ferreira, I. M. Marquiegui, and I. V. Elizaga, "Teratogenicity of Zinc Deficiency in the Rat: Study of the Fetal Skeleton," *Teratology*, **39** [2] 181-94 (1989).

77. J.-Y. Reginster, L. Strause, P. Saltman, and P. Franchimont, "Trace Elements and Postmenopausal Osteoporosis: A Preliminary Report of Decreased Serum Manganese," *Med. Sci. Res.*, **16** (1988).

78. R. Lappalainen, M. Knuuttila, S. Lammi, and E. M. Alhava, "Fluoride Content Related to the Elemental Composition, Mineral Density and Strength of Bone in Healthy and Chronically Diseased Persons," *J Chronic Dis,* **36** [10] 707-13 (1983).

79. B. Staker, "Osteoporosis Awareness Month" (2013) Staker Chiropractic Life Center. Accessed on: 12/9/2015. Available at <http://stakerchiro.com/osteoporosis-awareness-month/>

80. M. Yamaguchi and K. Takahashi, "Role of Zinc as an Activator of Bone Metabolism in Weanling Rats," *Japan Society for Bone and Mineral Research Magazine,* **2** [3] 186-91 (1984).

81. V. Aina, G. Malavasi, A. F. Pla, L. Munaron, and C. Morterra, "Zinc-Containing Bioactive Glasses: Surface Reactivity and Behaviour Towards Endothelial Cells," *Acta Biomater.,* **5** [4] 1211-22 (2009).

82. H.-P. Gerber and N. Ferrara, "Angiogenesis and Bone Growth," *Trends Cardiovasc. Med.,* **10** [5] 223-8 (2000).

83. R. A. Carano and E. H. Filvaroff, "Angiogenesis and Bone Repair," *Drug Discov. Today,* **8** [21] 980-9 (2003).

84. A. L. Sieminski and K. J. Gooch, "Biomaterial–Microvasculature Interactions," *Biomaterials,* **21** [22] 2233-41 (2000).

85. C. Kirkpatrick, M. Otto, T. Van Kooten, V. Krump, J. Kriegsmann, and F. Bittinger, "Endothelial Cell Cultures as a Tool in Biomaterial Research," *J. Mater. Sci. Mater. Med.,* **10** [10-11] 589-94 (1999).

86. L. Courthéoux, J. Lao, J.-M. Nedelec, and E. Jallot, "Controlled Bioactivity in Zinc-Doped Sol− Gel-Derived Binary Bioactive Glasses," *J. Phys. Chem. C Nanomater. Interfaces,* **112** [35] 13663-7 (2008).

87. M. Bini, S. Grandi, D. Capsoni, P. Mustarelli, E. Saino, and L. Visai, "Sio2− P2o5− Cao Glasses and Glass-Ceramics with and without Zno: Relationships among Composition, Microstructure, and Bioactivity," *J. Phys. Chem. C Nanomater. Interfaces,* **113** [20] 8821-8 (2009).

88. G. Lusvardi, G. Makavasi, L. Menabue, M. Menziani, A. Pedone, U. Segre, V. Aina, A. Perardi, C. Morterra, and F. Boccafoschi, "Properties of Zinc Releasing Surfaces for Clinical Applications," *J. Biomater. Appl.*, (2007).

89. M. Yamaguchi, Y. Segawa, N. Shimokawa, N. Tsuzuike, and E. Tagashira, "Inhibitory Effect of B-Alanyl-L-Histidinato Zinc on Bone Resorption in Tissue Culture," *Pharmacology*, **45** [5] 292-300 (1992).

90. S. Kishi and M. Yamaguchi, "Inhibitory Effect of Zinc Compounds on Osteoclast-Like Cell Formation in Mouse Marrow Cultures," *Biochem. Pharmacol.*, **48** [6] 1225-30 (1994).

91. M. Yamaguchi and K. Ozaki, "Aging Affects Cellular Zinc and Protein Synthesis in the Femoral Diaphysis of Rats," *Res Exp Med (Berl)*, **190** [1] 295-300 (1990).

92. M. Yamaguchi, K. Ozaki, and Y. Suketa, "Alteration in Bone Metabolism with Increasing Age: Effects of Zinc and Vitamin D3 in Aged Rats," *J Pharmacobiodyn*, **12** [2] 67-73 (1989).

93. C. R. Chitambar, "Medical Applications and Toxicities of Gallium Compounds," *Int. J. Env. Res. Public Health*, **7** [5] 2337-61 (2010).

94. (IARC), "Gallium Arsenide," *IARC Monogr. Eval. Carcinog. Risks Hum.*, **86** 163-96 (2006).

95. C. L. Edwards and R. Hayes, "Tumor Scanning with 67ga Citrate," Oak Ridge Associated Universities, Tenn., (1969).

96. S. C. King, R. J. Reiman, and L. R. Prosnitz, "Prognostic Importance of Restaging Gallium Scans Following Induction Chemotherapy for Advanced Hodgkin's Disease," *Am. J. Clin. Oncol.*, **12** [2] 306-11 (1994).

97. E. Salloum, D. S. Brandt, V. J. Caride, E. Cornelius, D. Zelterman, W. Schubert, T. Mannino, and D. L. Cooper, "Gallium Scans in the Management of Patients with Hodgkin's Disease: A Study of 101 Patients," *J Clin Oncol*, **15** [2] 518-27 (1997).

98. J. van Amsterdam, J. Kluin-Nelemans, B. van Eck-Smit, and E. Pauwels, "Role of 67ga Scintigraphy in Localization of Lymphoma," *Ann. Hematol.,* **72** [4] 202-7 (1996).

99. M. M. Hart and R. H. Adamson, "Antitumor Activity and Toxicity of Salts of Inorganic Group Iiia Metals: Aluminum, Gallium, Indium, and Thallium," *Proceedings of the National Academy of Sciences,* **68** [7] 1623-6 (1971).

100. R. P. Warrell, C. J. Coonley, D. J. Straus, and C. W. Young, "Treatment of Patients with Advanced Malignant Lymphoma Using Gallium Nitrate Administered as a Seven-Day Continuous Infusion," *Cancer,* **51** [11] 1982-7 (1983).

101. B. Pro, R. Bociek, C. R. Chitambar, S. A. Gregory, J. P. Leonard, S. Smith, and S. Novick, "Phase 2 Multicenter Trial of Gallium Nitrate in Patients with Advanced Non-Hodgkin's Lymphoma (Nhl)"; p. 2487 in ASH annual meeting abstracts, **104,** (2004).

102. R. P. Warrell Jr, L. Danieu, C. J. Coonley, and C. Atkins, "Salvage Chemotherapy of Advanced Lymphoma with Investigational Drugs: Mitoguazone, Gallium Nitrate, and Etoposide," *Cancer Treat. Rep.,* **71** [1] 47-51 (1987).

103. C. R. Chitambar, S. A. Zahir, P. S. Ritch, and T. Anderson, "Evaluation of Continuous-Infusion Gallium Nitrate and Hydroxyurea in Combination for the Treatment of Refractory Non-Hodgkin's Lymphoma," *Am. J. Clin. Oncol.,* **20** [2] 173-8 (1997).

104. S. Smith, K. Wren, P. Stiff, A. Toor, T. Rodriguez, and D. van Gestel, "Gallium, Rituximab, and Dexamethasone for Relapsed Nhl"; p. 8079 in ASCO Annual Meeting Proceedings, **25,** (2007).

105. E. D. Crawford, J. H. Saiers, L. H. Baker, J. H. Costanzi, and R. M. Bukowski, "Gallium Nitrate in Advanced Bladdercarcinoma: Southwest Oncology Group Study," *Urology,* **38** [4] 355-7 (1991).

106. P. A. Seligman and E. D. Crawford, "Treatment of Advanced Transitional Cell Carcinoma of the Bladder with Continuous-Infusion

Gallium Nitrate," *Journal of the National Cancer Institute,* **83** [21] 1582-4 (1991).

107. J. A. McCaffrey, S. Hilton, M. Mazumdar, S. Sadan, M. Heineman, J. Hirsch, W. K. Kelly, H. I. Scher, and D. F. Bajorin, "Phase Ii Randomized Trial of Gallium Nitrate Plus Fluorouracil Versus Methotrexate, Vinblastine, Doxorubicin, and Cisplatin in Patients with Advanced Transitional-Cell Carcinoma," *J Clin Oncol,* **15** [6] 2449-55 (1997).

108. L. H. Einhorn, B. J. Roth, R. Ansari, R. Dreicer, R. Gonin, and P. J. Loehrer, "Phase Ii Trial of Vinblastine, Ifosfamide, and Gallium Combination Chemotherapy in Metastatic Urothelial Carcinoma," *Am. J. Clin. Oncol.,* **12** [11] 2271-6 (1994).

109. R. Dreicer, K. J. Propert, B. J. Roth, L. H. Einhorn, and P. J. Loehrer, "Vinblastine, Ifosfamide, and Gallium Nitrate—an Active New Regimen in Patients with Advanced Carcinoma of the Urothelium," *Cancer,* **79** [1] 110-4 (1997).

110. D. J. Straus, "Gallium Nitrate in the Treatment of Lymphoma"; pp. 25-33 in Seminars in Oncology, **30,** (2003).

111. C. R. Chitambar, W. G. Matthaeus, W. E. Antholine, K. Graff, and W. J. O'Brien, "Inhibition of Leukemic Hl60 Cell Growth by Transferrin-Gallium: Effects on Ribonucleotide Reductase and Demonstration of Drug Synergy with Hydroxyurea [See Comments]," *Blood,* **72** [6] 1930-6 (1988).

112. C. R. Chitambar and J. P. Wereley, "Synergistic Inhibition of T-Lymphoblastic Leukemic Ccrf-Cem Cell Growth by Gallium and Recombinant Human A-Interferon through Action on Cellular Iron Uptake," *Cancer Res.,* **54** [12] 3224-8 (1994).

113. M. S. Myette, H. L. Elford, and C. R. Chitambar, "Interaction of Gallium Nitrate with Other Inhibitors of Ribonucleotide Reductase: Effects on the Proliferation of Human Leukemic Cells," *Cancer Lett.,* **129** [2] 199-204 (1998).

114. K. Ming, "Nuclear Medicine in General Practice," St. Teresa's Hospital, Monthly Self-Study Series, The Hong Kong Medical Association, (2002).

115. L. M. Sherwood, "The Multiple Causes of Hypercalcemia in Malignant Disease," *N Engl J Med,* **303** [24] 1412 (1980).

116. F. Cvitkovic, J.-P. Armand, M. Tubiana-Hulin, J.-F. Rossi, and R. P. Warrell Jr, "Randomized, Double-Blind, Phase Ii Trial of Gallium Nitrate Compared with Pamidronate for Acute Control of Cancer-Related Hypercalcemia," *Cancer J. Sci. Am.,* **12** [1] 47-53 (2006).

117. R. Warrell, W. Murphy, P. Schulman, P. O'Dwyer, and G. Heller, "A Randomized Double-Blind Study of Gallium Nitrate Compared with Etidronate for Acute Control of Cancer-Related Hypercalcemia," *J Clin Oncol,* **9** [8] 1467-75 (1991).

118. R. P. Warrell, R. Israel, M. Frisone, T. Snyder, J. J. Gaynor, and R. S. Bockman, "Gallium Nitrate for Acute Treatment of Cancer-Related Hypercalcemia: A Randomized, Double-Blind Comparison to Calcitonin," *Ann. Intern. Med.,* **108** [5] 669-74 (1988).

119. "Fda Approves Ganite for Hypercalcemia," *Oncol. Times,* **25** [20] 24 (2003).

120. R. Warrell, N. W. Alcock, and R. S. Bockman, "Gallium Nitrate Inhibits Accelerated Bone Turnover in Patients with Bone Metastases," *Journal of Clinical Oncology,* **5** [2] 292-8 (1987).

121. R. Warrell, D. Lovett, F. A. Dilmanian, R. Schneider, and R. T. Heelan, "Low-Dose Gallium Nitrate for Prevention of Osteolysis in Myeloma: Results of a Pilot Randomized Study," *J Clin Oncol,* **11** [12] 2443-50 (1993).

122. E. S. Siris, "Paget's Disease of Bone," *J. Bone Miner. Res.,* **13** [7] 1061-5 (1998).

123. V. Matkovic, G. Apseloff, D. Shepard, and N. Gerber, "Use of Gallium to Treat Paget's Disease of Bone: A Pilot Study," *The Lancet,* **335** [8681] 72-5 (1990).

124. R. S. Bockman, F. Wilhelm, E. Siris, F. Singer, A. Chausmer, R. Bitton, J. Kotler, B. J. Bosco, D. R. Eyre, and D. Levenson, "A Multicenter Trial of Low Dose Gallium Nitrate in Patients with Advanced Paget's Disease of Bone," *The Journal of Clinical Endocrinology & Metabolism,* **80** [2] 595-602 (1995).

125. O. Olakanmi, B. E. Britigan, and L. S. Schlesinger, "Gallium Disrupts Iron Metabolism of Mycobacteria Residing within Human Macrophages," *Infection and immunity,* **68** [10] 5619-27 (2000).

126. Y. Kaneko, M. Thoendel, O. Olakanmi, B. E. Britigan, and P. K. Singh, "The Transition Metal Gallium Disrupts Pseudomonas Aeruginosa Iron Metabolism and Has Antimicrobial and Antibiofilm Activity," *The Journal of clinical investigation,* **117** [4] 877 (2007).

127. K. DeLeon, F. Balldin, C. Watters, A. Hamood, J. Griswold, S. Sreedharan, and K. P. Rumbaugh, "Gallium Maltolate Treatment Eradicates Pseudomonas Aeruginosa Infection in Thermally Injured Mice," *Antimicrob. Agents Chemother.,* **53** [4] 1331-7 (2009).

128. S. R. Vallabhajosula, J. Harwig, and W. Wolf, "The Mechanism of Tumor Localization of Gallium-67 Citrate: Role of Transferrin Binding and Effect of Tumor Ph," *Int J Nucl Med Biol,* **8** [4] 363-70 (1981).

129. J. Habeshaw, T. Lister, A. Stansfeld, and M. Greaves, "Correlation of Transferrin Receptor Expression with Histological Class and Outcome in Non-Hodgkin Lymphoma," *The Lancet,* **321** [8323] 498-501 (1983).

130. I. Basar, A. Ayhan, K. Bircan, and A. Ergen, "Transferrin Receptor Activity as a Marker in Transitional Cell Carcinoma of the Bladder," *Br. J. Urol.,* **67** [2] 165-8 (1991).

131. A. W. Harris and R. G. Sephton, "Transferrin Promotion of 67ga and 59fe Uptake by Cultured Mouse Myeloma Cells," *Cancer Res.,* **37** [10] 3634-8 (1977).

132. C. R. Chitambar and Z. Zivkovic, "Uptake of Gallium-67 by Human Leukemic Cells: Demonstration of Transferrin Receptor-Dependent and Transferrin-Independent Mechanisms," *Cancer Res.*, **47** [15] 3929-34 (1987).

133. C. A. Luttropp, J. A. Jackson, B. J. Jones, and M.-H. Sohn, "Uptake of Gallium-67 in Transfected Cells and Tumors Absent or Enriched in the Transferrin Receptor," *J Nucl Med,* **39** [8] 1405 (1998).

134. W. R. Harris and V. L. Pecoraro, "Thermodynamic Binding Constants for Gallium Transferrin," *Biochemistry (Mosc).* **22** [2] 292-9 (1983).

135. D. P. Kelsen, N. Alcock, S. Yeh, J. Brown, and C. Young, "Pharmacokinetics of Gallium Nitrate in Man," *Cancer,* **46** [9] 2009-13 (1980).

136. I. H. Krakoff, R. A. Newman, and R. S. Goldberg, "Clinical Toxicologic and Pharmacologic Studies of Gallium Nitrate," *Cancer,* **44** [5] 1722-7 (1979).

137. S. M. Larson, J. S. Rasey, D. R. Allen, N. J. Nelson, Z. Grunbaum, G. D. Harp, and D. L. Williams, "Common Pathway for Tumor Cell Uptake of Gallium-67 and Iron-59 Via a Transferrin Receptor," *J. Natl. Cancer Inst.*, **64** [1] 41-53 (1980).

138. C. R. Chitambar and P. A. Seligman, "Effects of Different Transferrin Forms on Transferrin Receptor Expression, Iron Uptake, and Cellular Proliferation of Human Leukemic Hl60 Cells. Mechanisms Responsible for the Specific Cytotoxicity of Transferrin-Gallium," *J. Clin. Invest.*, **78** [6] 1538 (1986).

139. A. Jordan and P. Reichard, "Ribonucleotide Reductases," *Annu. Rev. Biochem.*, **67** [1] 71-98 (1998).

140. J. Narasimhan, W. E. Antholine, and C. R. Chitambar, "Effect of Gallium on the Tyrosyl Radical of the Iron-Dependent M2 Subunit of Ribonucleotide Reductase," *Biochem. Pharmacol.*, **44** [12] 2403-8 (1992).

141. C. R. Chitambar, J. Narasimhan, J. Guy, D. S. Sem, and W. J. O'Brien, "Inhibition of Ribonucleotide Reductase by Gallium in Murine Leukemic L1210 Cells," *Cancer Res.,* **51** [22] 6199-201 (1991).

142. "Iron Metabolism Biochemistry" (2010) Accessed on: 12/9/2015. Available at <http://cardiorespiratorio.blogspot.com/2010/06/bioquimica-metabolismo-de-hierro.html>

143. C. R. Chitambar, J. P. Wereley, and S. Matsuyama, "Gallium-Induced Cell Death in Lymphoma: Role of Transferrin Receptor Cycling, Involvement of Bax and the Mitochondria, and Effects of Proteasome Inhibition," *Mol. Cancer Ther.,* **5** [11] 2834-43 (2006).

144. J. Cai, J. Yang, and D. Jones, "Mitochondrial Control of Apoptosis: The Role of Cytochrome C," *Biochim. Biophys. Acta,* **1366** [1] 139-49 (1998).

145. C. R. Chitambar, D. P. Purpi, J. Woodliff, M. Yang, and J. P. Wereley, "Development of Gallium Compounds for Treatment of Lymphoma: Gallium Maltolate, a Novel Hydroxypyrone Gallium Compound, Induces Apoptosis and Circumvents Lymphoma Cell Resistance to Gallium Nitrate," *J. Pharmacol. Exp. Ther.*, **322** [3] 1228-36 (2007).

146. M. Yang and C. R. Chitambar, "Role of Oxidative Stress in the Induction of Metallothionein-2a and Heme Oxygenase-1 Gene Expression by the Antineoplastic Agent Gallium Nitrate in Human Lymphoma Cells," *Free Radical Biol. Med.,* **45** [6] 763-72 (2008).

147. L. Anghileri, P. Thuvenot, F. Brunotte, C. Marchai, and J. Robert, "Ionic Competition and 67ga in Vivo Accumulation," *Nuklearmedizin,* **21** [3] 114-6 (1982).

148. E. M. Perchellet, J. B. Ladesich, P. Collery, and J.-P. Perchellet, "Microtubule-Disrupting Effects of Gallium Chloride in Vitro," *Anticancer. Drugs,* **10** [5] 477-88 (1999).

149. S. Aharinejad, S. Marks, P. Böck, C. MacKay, E. Larson, A. Tahamtani, A. Mason-Savas, and W. Firbas, "Microvascular Pattern in the Metaphysis During Bone Growth," *Anat. Rec.,* **242** [1] 111-22 (1995).

150. H. Oxlund, M. Barckman, G. Ørtoft, and T. Andreassen, "Reduced Concentrations of Collagen Cross-Links Are Associated with Reduced Strength of Bone," *Bone,* **17** [4] S365-S71 (1995).

151. R. Bockman, "The Effects of Gallium Nitrate on Bone Resorption"; pp. 5-12 in Seminars in Oncology, **30,** (2003).

152. R. S. Bockman, P. T. Guidon, L. C. Pan, R. Salvatori, and A. Kawaguchi, "Gallium Nitrate Increases Type I Collagen and Fibronectin Mrna and Collagen Protein Levels in Bone and Fibroblast Cells," *J. Cell. Biochem.,* **52** [4] 396-403 (1993).

153. S. Novick, T. Julian, S. Majuru, M. Mangelus, B. Brown, B. Mehta, and R. Warrell Jr, "Initial Phase I Clinical and Pharmacokinetic Assessment of G4544, an Oral Gallium-Containing Compound"; p. 8592 in ASCO Annual Meeting Proceedings, **26,** (2008).

154. T. Keenan, "Characterization of Ga2o3-Na2o-Cao-Zno-Sio2 Bioactive Glasses"; M.S. Thesis. Alfred University, 2012.

155. O. Wichterle and D. Lim, "Hydrophilic Gels for Biological Use," *Nature,* **185** 117-8 (1960).

156. J. Cabral and S. C. Moratti, "Hydrogels for Biomedical Applications," *Future Med. Chem.,* **3** [15] 1877-88 (2011).

157. A. S. Hoffman, "Hydrogels for Biomedical Applications," *Adv. Drug Del. Rev.,* **64** 18-23 (2012).

158. D. Campoccia, P. Doherty, M. Radice, P. Brun, G. Abatangelo, and D. F. Williams, "Semisynthetic Resorbable Materials from Hyaluronan Esterification," *Biomaterials,* **19** [23] 2101-27 (1998).

159. P. D. Drumheller and J. A. Hubbell, "Densely Crosslinked Polymer Networks of Poly (Ethylene Glycol) in Trimethylolpropane

Triacrylate for Cell-Adhesion-Resistant Surfaces," *J. Biomed. Mater. Res.*, **29** [2] 207-15 (1995).

160. J. Ullett, J. Schultz, and R. Chartoff, "Novel Liquid Crystal Resins for Stereolithography-Processing Parameters and Mechanical Analysis," *Rapid Prototyp J,* **6** [1] 8-17 (2000).

161. S.-H. Lee and H. Shin, "Matrices and Scaffolds for Delivery of Bioactive Molecules in Bone and Cartilage Tissue Engineering," *Adv. Drug Del. Rev.*, **59** [4] 339-59 (2007).

162. S. P. Hudson, R. Langer, G. R. Fink, and D. S. Kohane, "Injectable in Situ Cross-Linking Hydrogels for Local Antifungal Therapy," *Biomaterials,* **31** [6] 1444-52 (2010).

163. C. E. Carraher, *Polymer Chemistry, Seventh Edition;* p. 776. CRC Press Taylor & Francis Group, Boca Raton, FL, 2007.

164. J. Ma, Y. Xu, B. Fan, and B. Liang, "Preparation and Characterization of Sodium Carboxymethylcellulose/Poly (N-Isopropylacrylamide)/Clay Semi-Ipn Nanocomposite Hydrogels," *Eur. Polym. J.*, **43** [6] 2221-8 (2007).

165. P. Bulpitt and D. Aeschlimann, "New Strategy for Chemical Modification of Hyaluronic Acid: Preparation of Functionalized Derivatives and Their Use in the Formation of Novel Biocompatible Hydrogels," *J. Biomed. Mater. Res.*, **47** [2] 152-69 (1999).

166. S. Kwak and M. Lafleur, "Nmr Self-Diffusion of Molecular and Macromolecular Species in Dextran Solutions and Gels," *Macromolecules,* **36** [9] 3189-95 (2003).

167. Y. Liu and M. B. Chan-Park, "Hydrogel Based on Interpenetrating Polymer Networks of Dextran and Gelatin for Vascular Tissue Engineering," *Biomaterials,* **30** [2] 196-207 (2009).

168. D. Bruneel and E. Schacht, "Chemical Modification of Pullulan: 1. Periodate Oxidation," *Polymer,* **34** [12] 2628-32 (1993).

169. T. Soderberg, "Section 11.6: Imine (Schiff Base) Formation" Accessed on: 12/9/2015. Available at <http://chemwiki.ucdavis.edu/Organic_Chemistry/Organic_Chemistry_With_a_Biological_Emphasis/Chapter_11%3A_Nucleophilic_carbonyl_addition_reactions/Section_11.6%3A_Imine_(Schiff_base)_formation>

170. K. C. Pappas PG, Andes D, Benjamin Jr DK, Calandra TF, Edwards Jr JE, et al., "Clinical Practice Guidelines for the Management of Candidiasis: 2009 Update by the Infectious Diseases Society of America," *Clin. Infect. Dis.*, **48** [5] 503-35 (2009).

171. X. Yang, W. Yang, Q. Wang, H. Li, K. Wang, L. Yang, and W. Liu, "Atomic Force Microscopy Investigation of the Characteristic Effects of Silver Ions on Escherichia Coli and Staphylococcus Epidermidis," *Talanta*, **81** [4] 1508-12 (2010).

172. T. Yamamuro, L. L. Hench, and J. Wilson, *Crc Handbook of Bioactive Ceramics: Calcium Phosphate and Hydroxylapatite Ceramics*. CRC Press, 1990.

173. L. L. Hench, "Genetic Design of Bioactive Glass," *J. Eur. Ceram. Soc.*, **29** [7] 1257-65 (2009).

174. W. Holloway, F. Collier, R. Herbst, J. Hodge, and G. Nicholson, "Osteoblast-Mediated Effects of Zinc on Isolated Rat Osteoclasts: Inhibition of Bone Resorption and Enhancement of Osteoclast Number," *Bone*, **19** [2] 137-42 (1996).

175. M. Yamaguchi, A. Mochizuki, and S. Okada, "Stimulatory Effect of Zinc on Bone Growth in Weanling Rats," *J Pharmacobiodyn*, **5** [8] 619-26 (1982).

176. W. Peters, R. Jackson, K. Iwano, and D. Smith, "The Biological Response to Zinc Polyacrylate Cement," *Clinical orthopaedics and related research*, **88** 228-33 (1972).

177. A. M. Deliormanlı, "Synthesis and Characterization of Cerium-and Gallium-Containing Borate Bioactive Glass Scaffolds for Bone Tissue Engineering," *J. Mater. Sci. Mater. Med.*, **26** [2] 1-13 (2015).

178. S. Shruti, A. J. Salinas, G. Malavasi, G. Lusvardi, L. Menabue, C. Ferrara, P. Mustarelli, and M. Vallet-Regì, "Structural and in Vitro Study of Cerium, Gallium and Zinc Containing Sol–Gel Bioactive Glasses," *J. Mater. Chem.,* **22** [27] 13698-706 (2012).

179. A. Salinas, S. Shruti, G. Malavasi, L. Menabue, and M. Vallet-Regi, "Substitutions of Cerium, Gallium and Zinc in Ordered Mesoporous Bioactive Glasses," *Acta Biomater.,* **7** [9] 3452-8 (2011).

180. J. A. McCaffrey, S. Hilton, M. Mazumdar, S. Sadan, M. Heineman, J. Hirsch, W. K. Kelly, H. I. Scher, and D. F. Bajorin, "Phase Ii Randomized Trial of Gallium Nitrate Plus Fluorouracil Versus Methotrexate, Vinblastine, Doxorubicin, and Cisplatin in Patients with Advanced Transitional-Cell Carcinoma," *Journal of clinical oncology,* **15** [6] 2449-55 (1997).

181. F. Cvitkovic, J.-P. Armand, M. Tubiana-Hulin, J.-F. Rossi, and R. P. Warrell Jr, "Randomized, Double-Blind, Phase Ii Trial of Gallium Nitrate Compared with Pamidronate for Acute Control of Cancer-Related Hypercalcemia," *The Cancer Journal,* **12** [1] 47-53 (2006).

182. R. Warrell, W. Murphy, P. Schulman, P. O'Dwyer, and G. Heller, "A Randomized Double-Blind Study of Gallium Nitrate Compared with Etidronate for Acute Control of Cancer-Related Hypercalcemia," *Journal of clinical oncology,* **9** [8] 1467-75 (1991).

183. A. Wren, T. Keenan, A. Coughlan, F. Laffir, D. Boyd, M. Towler, and M. Hall, "Characterisation of Ga2o3–Na2o–Cao–Zno–Sio2 Bioactive Glasses," *Journal of Materials Science,* **48** [11] 3999-4007 (2013).

184. D. R. Baker, "Diffusion of Silicon and Gallium (as an Analogue for Aluminum) Network-Forming Cations and Their Relationship to Viscosity in Albite Melt," *Geochim. Cosmochim. Acta,* **59** [17] 3561-71 (1995).

185. T. Kokubo, H. Kushitani, C. Ohtsuki, S. Sakka, and T. Yamamuro, "Chemical Reaction of Bioactive Glass and Glass-Ceramics with a Simulated Body Fluid," *J. Mater. Sci. Mater. Med.,* **3** [2] 79-83 (1992).

186. "International Standard 10993-5 "Biological Evaluation of Medical Devices Part 5: Tests for in Vitro Cytotoxicity"," **Case Postale 56** [CH-1211] (1999).

187. M. G. Gandolfi, P. Taddei, A. Tinti, E. D. S. Dorigo, P. L. Rossi, and C. Prati, "Kinetics of Apatite Formation on a Calcium-Silicate Cement for Root-End Filling During Ageing in Physiological-Like Phosphate Solutions," *Clin. Oral Investig.*, **14** [6] 659-68 (2010).

188. D. Boyd, M. Towler, A. Wren, and O. Clarkin, "Comparison of an Experimental Bone Cement with Surgical Simplex® P, Spineplex® and Cortoss®," *J. Mater. Sci. Mater. Med.*, **19** [4] 1745-52 (2008).

189. U. M. Gross and V. Strunz, "The Anchoring of Glass Ceramics of Different Solubility in the Femur of the Rat," *J Biomed Mater Res*, **14** [5] 607-18 (1980).

190. I. Ahmed, M. Lewis, I. Olsen, and J. Knowles, "Phosphate Glasses for Tissue Engineering: Part 2. Processing and Characterisation of a Ternary-Based P 2 O 5–Cao–Na 2 O Glass Fibre System," *Biomaterials*, **25** [3] 501-7 (2004).

191. R. Hill, "An Alternative View of the Degradation of Bioglass," *J. Mater. Sci. Lett.*, **15** [13] 1122-5 (1996).

192. J. Oliveira, R. Correia, and M. Fernandes, "Effects of Si Speciation on the in Vitro Bioactivity of Glasses," *Biomaterials*, **23** [2] 371-9 (2002).

193. M. Cerruti, D. Greenspan, and K. Powers, "Effect of Ph and Ionic Strength on the Reactivity of Bioglass® 45s5," *Biomaterials*, **26** [14] 1665-74 (2005).

194. A. Schedle, P. Samorapoompichit, X. Rausch-Fan, A. Franz, W. Füreder, W. Sperr, W. Sperr, A. Ellinger, R. Slavicek, and G. Boltz-Nitulescu, "Response of L-929 Fibroblasts, Human Gingival Fibroblasts, and Human Tissue Mast Cells to Various Metal Cations," *Journal of dental research*, **74** [8] 1513-20 (1995).

195. J. Li and A. Eastman, "Apoptosis in an Interleukin-2-Dependent Cytotoxic T Lymphocyte Cell Line Is Associated with Intracellular Acidification Role of the Na/H-Antiport," *J. Biol. Chem.,* **270** [7] 3203-11 (1995).

196. I. J. Furlong, R. Ascaso, A. L. Rivas, and M. Collins, "Intracellular Acidification Induces Apoptosis by Stimulating Ice-Like Protease Activity," *J. Cell Sci.,* **110** [5] 653-61 (1997).

197. K. K. Kaysinger and W. K. Ramp, "Extracellular Ph Modulates the Activity of Cultured Human Osteoblasts," *J. Cell. Biochem.,* **68** [1] 83-9 (1998).

198. J. A. Killion, S. Kehoe, L. M. Geever, D. M. Devine, E. Sheehan, D. Boyd, and C. L. Higginbotham, "Hydrogel/Bioactive Glass Composites for Bone Regeneration Applications: Synthesis and Characterisation," *Materials Science and Engineering: C,* **33** [7] 4203-12 (2013).

199. S.-C. Lee, J.-F. Chen, C.-T. Wu, and S.-T. Lee, "In Situ Local Autograft for Instrumented Lower Lumbar or Lumbosacral Posterolateral Fusion," *J Clin Neurosci,* **16** [1] 37-43 (2009).

200. G. Calori, E. Mazza, M. Colombo, and C. Ripamonti, "The Use of Bone-Graft Substitutes in Large Bone Defects: Any Specific Needs?," *Injury,* **42** S56-S63 (2011).

201. L. L. Hench and H. Paschall, "Direct Chemical Bond of Bioactive Glass-Ceramic Materials to Bone and Muscle," *Journal of biomedical materials research,* **7** [3] 25-42 (1973).

202. I. D. Xynos, A. J. Edgar, L. D. Buttery, L. L. Hench, and J. M. Polak, "Gene-Expression Profiling of Human Osteoblasts Following Treatment with the Ionic Products of Bioglass® 45s5 Dissolution," *Journal of biomedical materials research,* **55** [2] 151-7 (2001).

203. M. Bellantone, H. D. Williams, and L. L. Hench, "Broad-Spectrum Bactericidal Activity of Ag2o-Doped Bioactive Glass," *Antimicrobial agents and chemotherapy,* **46** [6] 1940-5 (2002).

204. M. Kawashita, S. Tsuneyama, F. Miyaji, T. Kokubo, H. Kozuka, and K. Yamamoto, "Antibacterial Silver-Containing Silica Glass Prepared by Sol–Gel Method," *Biomaterials,* **21** [4] 393-8 (2000).

205. E. M. Carlisle, "Silicon: A Requirement in Bone Formation Independent of Vitamin D1," *Calcified tissue international,* **33** [1] 27-34 (1981).

206. E. M. Carlisle, "Silicon: A Possible Factor in Bone Calcification," *Science,* **167** [3916] 279-80 (1970).

207. J. Damen and J. Ten Cate, "Silica-Induced Precipitation of Calcium Phosphate in the Presence of Inhibitors of Hydroxyapatite Formation," *J. Dent. Res.,* **71** [3] 453-7 (1992).

208. L. L. Hench, "Bioceramics: From Concept to Clinic," *Journal of the American Ceramic Society,* **74** [7] 1487-510 (1991).

209. P. J. Marie, "The Calcium-Sensing Receptor in Bone Cells: A Potential Therapeutic Target in Osteoporosis," *Bone,* **46** [3] 571-6 (2010).

210. M. Valiathan and V. Krishnan, "Biomaterials: An Overview," (1999).

211. S. Deb, R. Mandegaran, and L. Di Silvio, "A Porous Scaffold for Bone Tissue Engineering/45s5 Bioglass® Derived Porous Scaffolds for Co-Culturing Osteoblasts and Endothelial Cells," *Journal of Materials Science: Materials in Medicine,* **21** [3] 893-905 (2010).

212. M. Handel, T. R. Hammer, P. Nooeaid, A. R. Boccaccini, and D. Hoefer, "45s5-Bioglass®-Based 3d-Scaffolds Seeded with Human Adipose Tissue-Derived Stem Cells Induce in Vivo Vascularization in the Cam Angiogenesis Assay," *Tissue Engineering Part A,* **19** [23-24] 2703-12 (2013).

213. D. Boyd and M. Towler, "The Processing, Mechanical Properties and Bioactivity of Zinc Based Glass Ionomer Cements," *Journal of Materials Science: Materials in Medicine,* **16** [9] 843-50 (2005).

214. D. Boyd, O. Clarkin, A. Wren, and M. Towler, "Zinc-Based Glass Polyalkenoate Cements with Improved Setting Times and Mechanical Properties," *Acta biomaterialia*, **4** [2] 425-31 (2008).

215. A. Wren, D. Boyd, and M. Towler, "The Processing, Mechanical Properties and Bioactivity of Strontium Based Glass Polyalkenoate Cements," *Journal of Materials Science: Materials in Medicine*, **19** [4] 1737-43 (2008).

216. A. Wren, A. Coughlan, L. Placek, and M. Towler, "Gallium Containing Glass Polyalkenoate Anti-Cancerous Bone Cements: Glass Characterization and Physical Properties," *Journal of Materials Science: Materials in Medicine*, **23** [8] 1823-33 (2012).

217. B. S. Ber, J. F. Hatton, and G. P. Stewart, "Chemical Modification of Proroot Mta to Improve Handling Characteristics and Decrease Setting Time," *Journal of endodontics*, **33** [10] 1231-4 (2007).

218. L. Jonck and C. Grobbelaar, "Ionos Bone Cement (Glass-Ionomer): An Experimental and Clinical Evaluation in Joint Replacement," *Clinical materials*, **6** [4] 323-59 (1990).

219. J. Cabral and S. C. Moratti, "Hydrogels for Biomedical Applications," *Future medicinal chemistry*, **3** [15] 1877-88 (2011).

220. S. Wakitani, T. Goto, S. J. Pineda, R. G. Young, J. M. Mansour, A. I. Caplan, and V. M. Goldberg, "Mesenchymal Cell-Based Repair of Large, Full-Thickness Defects of Articular Cartilage," *J Bone Joint Surg Am*, **76** [4] 579-92 (1994).

221. J. Y. Kang, C. W. Chung, J.-H. Sung, B.-S. Park, J.-Y. Choi, S. J. Lee, B.-C. Choi, C.-K. Shim, S.-J. Chung, and D.-D. Kim, "Novel Porous Matrix of Hyaluronic Acid for the Three-Dimensional Culture of Chondrocytes," *Int. J. Pharm.*, **369** [1] 114-20 (2009).

222. X. Z. Shu, Y. Liu, F. Palumbo, and G. D. Prestwich, "Disulfide-Crosslinked Hyaluronan-Gelatin Hydrogel Films: A Covalent Mimic of the Extracellular Matrix for in Vitro Cell Growth," *Biomaterials*, **24** [21] 3825-34 (2003).

223. B. Fang, Y.-Z. Wan, T.-T. Tang, C. Gao, and K.-R. Dai, "Proliferation and Osteoblastic Differentiation of Human Bone Marrow Stromal Cells on Hydroxyapatite/Bacterial Cellulose Nanocomposite Scaffolds," *Tissue Engineering Part A,* **15** [5] 1091-8 (2009).

224. F.-M. Chen, Y.-M. Zhao, R. Zhang, T. Jin, H.-H. Sun, Z.-F. Wu, and Y. Jin, "Periodontal Regeneration Using Novel Glycidyl Methacrylated Dextran (Dex-Gma)/Gelatin Scaffolds Containing Microspheres Loaded with Bone Morphogenetic Proteins," *Journal of controlled release*, **121** [1] 81-90 (2007).

225. P. Bulpitt and D. Aeschlimann, "New Strategy for Chemical Modification of Hyaluronic Acid: Preparation of Functionalized Derivatives and Their Use in the Formation of Novel Biocompatible Hydrogels," *Journal of biomedical materials research,* **47** [2] 152-69 (1999).

226. "International Standard 10993-5 "Biological Evaluation of Medical Devices Part 5: Tests for in Vitro Cytotoxicity"," Geneve, Switzerland (1999).

227. B. V. Slaughter, S. S. Khurshid, O. Z. Fisher, A. Khademhosseini, and N. A. Peppas, "Hydrogels in Regenerative Medicine," *Adv Mater,* **21** [32-33] 3307-29 (2009).

228. J. L. West and J. A. Hubbell, "Photopolymerized Hydrogel Materials for Drug Delivery Applications," *Reactive Polymers,* **25** [2] 139-47 (1995).

229. M. Kosmulski, *Chemical Properties of Material Surfaces*, Vol. 102. CRC press, 2001.

230. S. Maeno, Y. Niki, H. Matsumoto, H. Morioka, T. Yatabe, A. Funayama, Y. Toyama, T. Taguchi, and J. Tanaka, "The Effect of Calcium Ion Concentration on Osteoblast Viability, Proliferation and Differentiation in Monolayer and 3d Culture," *Biomaterials,* **26** [23] 4847-55 (2005).

231. V. Aina, A. Perardi, L. Bergandi, G. Malavasi, L. Menabue, C. Morterra, and D. Ghigo, "Cytotoxicity of Zinc-Containing Bioactive

Glasses in Contact with Human Osteoblasts," *Chem.-Biol. Interact.,* **167** [3] 207-18 (2007).

232. L. G. Harris and R. G. Richards, "Staphylococci and Implant Surfaces: A Review," *Injury,* **37** [2] S3-S14 (2006).

233. D. A. Talan, "Mrsa: Deadly Super Bug or Just Another Staph?," *Ann. Emergency Med.,* **51** [3] 299-302 (2008).

234. J. S. Moya, L. Esteban-Tejeda, C. Pecharroman, S. R. Mello-Castanho, A. C. Da Silva, and F. Malpartida, "Glass Powders with a High Content of Calcium Oxide: A Step Towards a “Green” Universal Biocide," *Advanced Engineering Materials,* **13** [6] B256-B60 (2011).

235. S. Hu, J. Chang, M. Liu, and C. Ning, "Study on Antibacterial Effect of 45s5 Bioglass®," *Journal of Materials Science: Materials in Medicine,* **20** [1] 281-6 (2009).

236. A. W. Wren, P. Hassanzadeh, L. M. Placek, T. J. Keenan, A. Coughlan, L. R. Boutelle, and M. R. Towler, "Silver Nanoparticle Coated Bioactive Glasses–Composites with Dex/Cmc Hydrogels: Characterization, Solubility, and in Vitro Biological Studies," *Macromol. Biosci.,* (2015).

237. H. Yli-Urpo, T. Närhi, and E. Söderling, "Antimicrobial Effects of Glass Ionomer Cements Containing Bioactive Glass (S53p4) on Oral Micro-Organisms in Vitro," *Acta Odontol. Scand.,* **61** [4] 241-6 (2003).

238. C. Chang, L. Zhang, J. Zhou, L. Zhang, and J. F. Kennedy, "Structure and Properties of Hydrogels Prepared from Cellulose in Naoh/Urea Aqueous Solutions," *Carbohydrate Polymers,* **82** [1] 122-7 (2010).

239. P. Calvert, "Hydrogels for Soft Machines," *Adv. Mater,* **21** [7] 743-56 (2009).

240. C. Chang, B. Duan, J. Cai, and L. Zhang, "Superabsorbent Hydrogels Based on Cellulose for Smart Swelling and Controllable Delivery," *European Polymer Journal,* **46** [1] 92-100 (2010).

241. A. W. Chan, R. A. Whitney, and R. J. Neufeld, "Semisynthesis of a Controlled Stimuli-Responsive Alginate Hydrogel," *Biomacromolecules,* **10** [3] 609-16 (2009).

242. M. Yamamoto, Y. Takahashi, and Y. Tabata, "Controlled Release by Biodegradable Hydrogels Enhances the Ectopic Bone Formation of Bone Morphogenetic Protein," *Biomaterials,* **24** [24] 4375-83 (2003).

243. T. Keenan, L. Placek, T. McGinnity, M. Towler, M. Hall, and A. Wren, "Relating Ion Release and Ph to in Vitro Cell Viability for Gallium-Inclusive Bioactive Glasses," *Journal of Materials Science,* (2015).

244. X. Cai, G.-J. Dai, S.-Z. Tan, Y. Ouyang, Y.-S. Ouyang, and Q.-S. Shi, "Synergistic Antibacterial Zinc Ions and Cerium Ions Loaded A-Zirconium Phosphate," *Materials Letters,* **67** [1] 199-201 (2012).

245. T. J. Keenan, L. Placek, T. McGinnity, M. Towler, M. Hall, and A. Wren, "Relating Ion Release and Ph to in Vitro Cell Viability for Gallium-Inclusive Bioactive Glasses," *J Mater Sci,* **51** [2] 1107-20 (2016).

246. Y.-Y. Liu and X.-D. Fan, "Synthesis, Properties and Controlled Release Behaviors of Hydrogel Networks Using Cyclodextrin as Pendant Groups," *Biomaterials*, **26** [32] 6367-74 (2005).

247. F. Cavalieri, E. Chiessi, I. Finelli, F. Natali, G. Paradossi, and M. F. Telling, "Water, Solute, and Segmental Dynamics in Polysaccharide Hydrogels," *Macromol. Biosci.,* **6** [8] 579-89 (2006).

248. M. Prabaharan and J. F. Mano, "Stimuli-Responsive Hydrogels Based on Polysaccharides Incorporated with Thermo-Responsive Polymers as Novel Biomaterials," *Macromol. Biosci.,* **6** [12] 991-1008 (2006).

249. H. Yu, J. Lu, and C. Xiao, "Preparation and Properties of Novel Hydrogels from Oxidized Konjac Glucomannan Cross-Linked Chitosan for in Vitro Drug Delivery," *Macromol. Biosci.,* **7** [9-10] 1100-11 (2007).

250. M. Zhai, F. Yoshii, T. Kume, and K. Hashim, "Syntheses of Pva/Starch Grafted Hydrogels by Irradiation," *Carbohydr. Polym.*, **50** [3] 295-303 (2002).

251. D. Klemm, B. Heublein, H. P. Fink, and A. Bohn, "Cellulose: Fascinating Biopolymer and Sustainable Raw Material," *Angew. Chem. Int. Ed.*, **44** [22] 3358-93 (2005).

252. R. Crawford, *Lignin Biodegradation and Transformation*. John Wiley & Sons Inc, 1981.

253. D. M. Updegraff, "Semimicro Determination of Cellulose Inbiological Materials," *Anal. Biochem.*, **32** [3] 420-4 (1969).

254. K. Gekko, "Thermal Analysis of Low Molecular Weight Dextran," *Agric. Biol. Chem.*, **42** [6] 1287-8 (1978).

255. K. M. Holtman, N. Chen, M. A. Chappell, J. F. Kadla, L. Xu, and J. Mao, "Chemical Structure and Heterogeneity Differences of Two Lignins from Loblolly Pine as Investigated by Advanced Solid-State Nmr Spectroscopy," *J. Agric. Food Chem.*, **58** [18] 9882-92 (2010).

256. G. E. Maciel, "High-Resolution Nuclear Magnetic Resonance of Solids," *Science*, **226** [4672] 282-8 (1984).

257. S. Hartmann and E. Hahn, "Nuclear Double Resonance in the Rotating Frame," *Phys Rev*, **128** [5] 2042 (1962).

258. N. P. Wickramasinghe and Y. Ishii, "Sensitivity Enhancement, Assignment, and Distance Measurement in 13 C Solid-State Nmr Spectroscopy for Paramagnetic Systems under Fast Magic Angle Spinning," *J Magn Reson*, **181** [2] 233-43 (2006).

259. E. Stejskal, J. Schaefer, and J. Waugh, "Magic-Angle Spinning and Polarization Transfer in Proton-Enhanced Nmr," *J Magn Reson*, **28** [1] 105-12 (1977).

260. R. A. Hall, A. Jurkiewicz, and G. E. Maciel, "A Bicyclic Ketone as a Solid-State Carbon-13 Nmr Intensity Reference," *Anal. Chem.*, **65** [5] 534-8 (1993).

261. A. E. de Nooy, D. Capitani, G. Masci, and V. Crescenzi, "Ionic Polysaccharide Hydrogels Via the Passerini and Ugi Multicomponent Condensations: Synthesis, Behavior and Solid-State Nmr Characterization," *Biomacromolecules*, **1** [2] 259-67 (2000).

262. T. Heinze and A. Koschella, "Carboxymethyl Ethers of Cellulose and Starch: A Review"; pp. 13-40 in Macromolecular Symposia, **223,** Wiley Online Library (2005).

263. H. Reich, "University of Wisconsin C-13 Chemical Shifts Database" (2004) Accessed on: Available at <http://www.chem.wisc.edu/areas/reich/handouts/nmr-c13/cdata.htm>

264. H. Cheng and T. G. Neiss, "Solution Nmr Spectroscopy of Food Polysaccharides," *Polym. Rev.*, **52** [2] 81-114 (2012).

265. A. Synytsya and M. Novak, "Structural Analysis of Glucans," *Ann Transl Med*, **2** [2] (2014).

266. Y. E. Shapiro, "Structure and Dynamics of Hydrogels and Organogels: An Nmr Spectroscopy Approach," *Prog. Polym. Sci.*, **36** [9] 1184-253 (2011).

267. N. Shterman, B. Kupfer, and C. Moroz, "Comparison of Transferrin Receptors, Iron Content and Isoferritin Profile in Normal and Malignant Human Breast Cell Lines," *Pathobiology*, **59** [1] 19-25 (1991).

268. R. R. Ernst, G. Bodenhausen, and A. Wokaun, *Principles of Nuclear Magnetic Resonance in One and Two Dimensions*, Vol. 14. Clarendon Press Oxford, 1987.

269. J. Sanders and B. Hunter, *Modern NMR Spectroscopy. A Guide for Chemists.* University Press, Oxford, UK p.(a), 1987.

270. D. C. Duncan and D. G. Whitten, "1h Nmr Investigation of the Composition, Structure, and Dynamics of Cholesterol-Stilbene Tethered Dyad Organogels," *Langmuir*, **16** [16] 6445-52 (2000).

271. S. Hafner and H. W. Spiess, "Advanced Solid-State Nmr Spectroscopy of Strongly Dipolar Coupled Spins under Fast Magic Angle Spinning," *Concepts Magn Reson*, **10** [2] 99-128 (1998).

272. M. Mehring, *Principles of High Resolution NMR in Solids*. Springer Science & Business Media, 2012.